NASA
CR
3312
c.1

# NASA Contractor Report 3312

# Pilot/Vehicle Model Analysis of Visual and Motion Cue Requirements in Flight Simulation

Sheldon Baron, Roy Lancraft, and Greg Zacharias

NASA

NASA Contractor Report 3312

# Pilot/Vehicle Model Analysis of Visual and Motion Cue Requirements in Flight Simulation

Sheldon Baron, Roy Lancraft,
and Greg Zacharias
*Bolt, Beranek and Newman, Inc.*
*Cambridge, Massachusetts*

**NASA**
National Aeronautics
and Space Administration

**Scientific and Technical**
**Information Branch**

1980

TABLE OF CONTENTS

# LIST OF FIGURES

ACKNOWLEDGEMENT

# 1. INTRODUCTION

As flight control and management tasks become more complex so, too, do the simulators used to investigate these tasks. The designers of simulations are confronted with difficult choices between requirements for simulation fidelity and the needs for cost-effective methods of simulation. The latter demands have resulted in a trend toward the use of digital equipment in simulation both in modeling the vehicle and in generating visual cues (CGI systems) for the pilot of the simulator. These digital simulations can have characteristics that are significantly different from those desired. In particular, unwanted delays frequently result in such a simulation. When motion cues are also needed, the problems can be aggravated further both by delays in generating motion cues (even with analog hardware) and by the potential lack of correlation between visual and motion cues. The significance of these problems has been amply demonstrated in recent studies (Gum and Albery (1977), Queijo and Riley (1975)).

Unfortunately, the specification of fidelity requirements for the generation of visual and motion cues is very difficult for several reasons. The requirements are governed by the purpose of the simulation: training simulators have different needs than research simulators. They are also problem dependent (e.g., the need for motion cues in the analysis of aircraft control in a gusty

environment will depend on the gust response of the aircraft.) Finally, it is difficult because it involves complex psychological as well as engineering factors. Not only is there a need to understand and account for the perceptual capabilities of a human operator, but also one must account for the fact that the adaptive human pilot may be able to compensate for simulator shortcomings and maintain system performance at the expense of workload (assuming the real cues are helpful, an assumption that is not always valid). In such a situation, the pilot could give a degraded evaluation of the system that would be unwarranted.

"Rules of thumb", open loop response measurements, and subjective feedback from pilots are all helpful in developing the cue requirements for simulators. For simulations in which the pilot's principal task is flight control, a pilot/vehicle model that accounts for perceptual limitations of the pilot/environment interface can be very helpful in defining the cue generation requirements. An appropriate model can provide the designer with a tool to examine potential performance penalties and performance/workload tradeoffs in the mission context of interest. Thus, it can aid the designer greatly in defining the requirements for the particular simulation of interest.

In this report, such a pilot/vehicle model is used to investigate the closed-loop consequences of the performance

limitations associated with a computer generated image (CGI) visual system and a six degree-of-freedom motion simulator (VMS) in a helicopter hover task. In particular, the performance/workload effects of these simulation elements are analyzed using the optimal control model (OCM) for the pilot/vehicle system. (Baron and Kleinman (1968), Kleinman et al (1970, 1971)). To accomplish this, the basic OCM is elaborated to include sensory perception of both CGI-generated external visual cues and VMS-generated motion cues.

## 2. OPTIMAL CONTROL MODEL

The closed-loop helicopter hover task which was the object of this study is illustrated in block diagram form in figure 2.1a. The pilot's task is to hover over a fixed point at a fixed altitude, in the presence of disturbances generated by air turbulence. Control is to be maintained by relying on extra-cockpit visual cues obtained from an out-the-window view and by motion cues associated with helicopter rotation and translation.

Figure 2.1b is a similar block diagram showing how the task is assumed to be implemented on the simulator. Visual cueing is provided by a computer generated image (CGI) system, and motion cueing is provided by a vertical motion simulator (VMS).* The problem addressed in this study was to determine the potential effects of CGI and VMS system characteristics on closed-loop hover performance and pilot workload, and to evaluate these effects in light of performance/workload levels we might expect to see in the actual flight situation.

Our objective in this chapter is to describe how this task is modelled in the context of the Optimal Control Model (OCM) of the pilot. Inasmuch as the model has been documented extensively

---

* In spite of its name, the VMS is not restricted to vertical motion cues; it is a six degree-of-freedom cueing system.
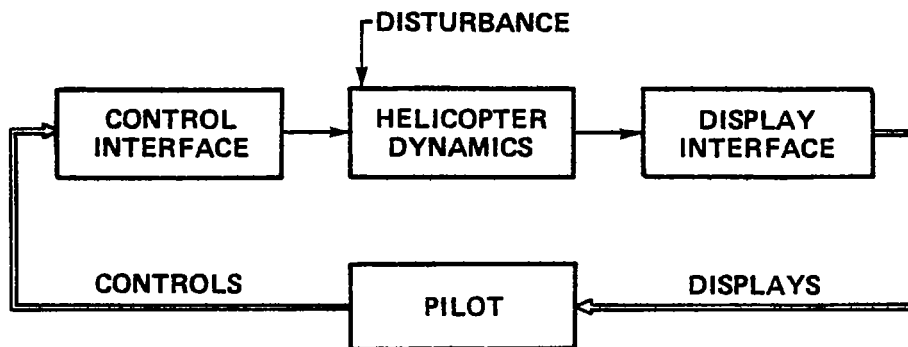
Figure 2.1a:  Closed-Loop Helicopter Hover Task
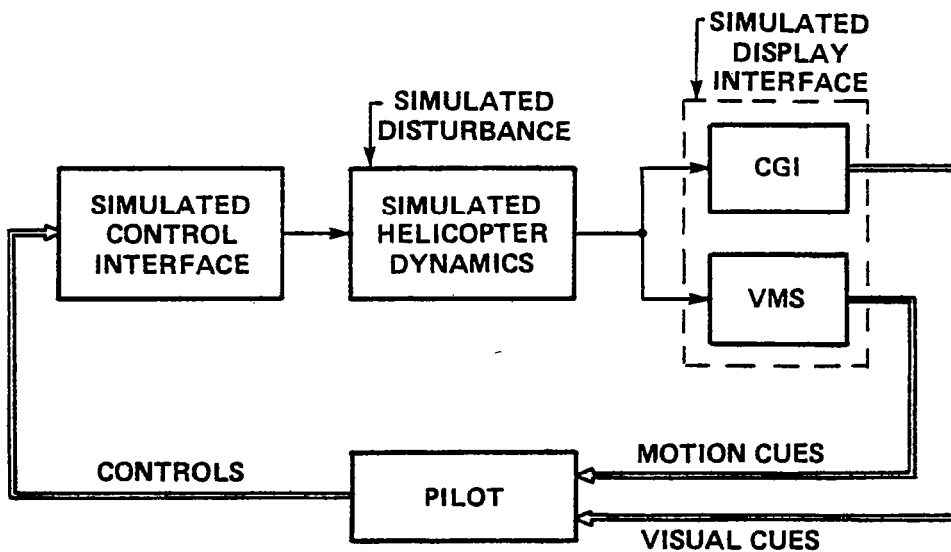


Figure 2.1b:  Simulated Helicopter Hover Task

(Baron and Kleinman (1968), Kleinman et al (1970, 1971)), the discussion will be brief, with emphasis on those aspects of the model that are of special relevance to this study. First, however, we will give a general description of the system under study, in section 2.1, to provide a background for the pilot model description given in section 2.2. We will defer a detailed description of the "perceptual" portion of this model to chapter 3; likewise, we will defer a complete specification of the task and system dynamics to chapter 4.

## 2.1 General System Description

A detailed block diagram of both the system and the OCM pilot model is given in figure 2.2. The system portion (outside the dashed box) provides for representations of control stick dynamics, vehicle dynamics, and the dynamics associated with the simulator drive logic (e.g., a motion base washout filter) and its hardware (e.g., the VMS servo drives). As shown, the two inputs to the system are the set of controls generated by the pilot ($\underline{u}$), and the system disturbances which perturb the vehicle dynamics ($\underline{d}$). The set of system outputs is the cue set provided by the simulator to the pilot's various sensory systems.*

---

* Although an instrument "channel" is shown in the diagram for generality, the present study presumed that no such informational cues were available to the pilot.
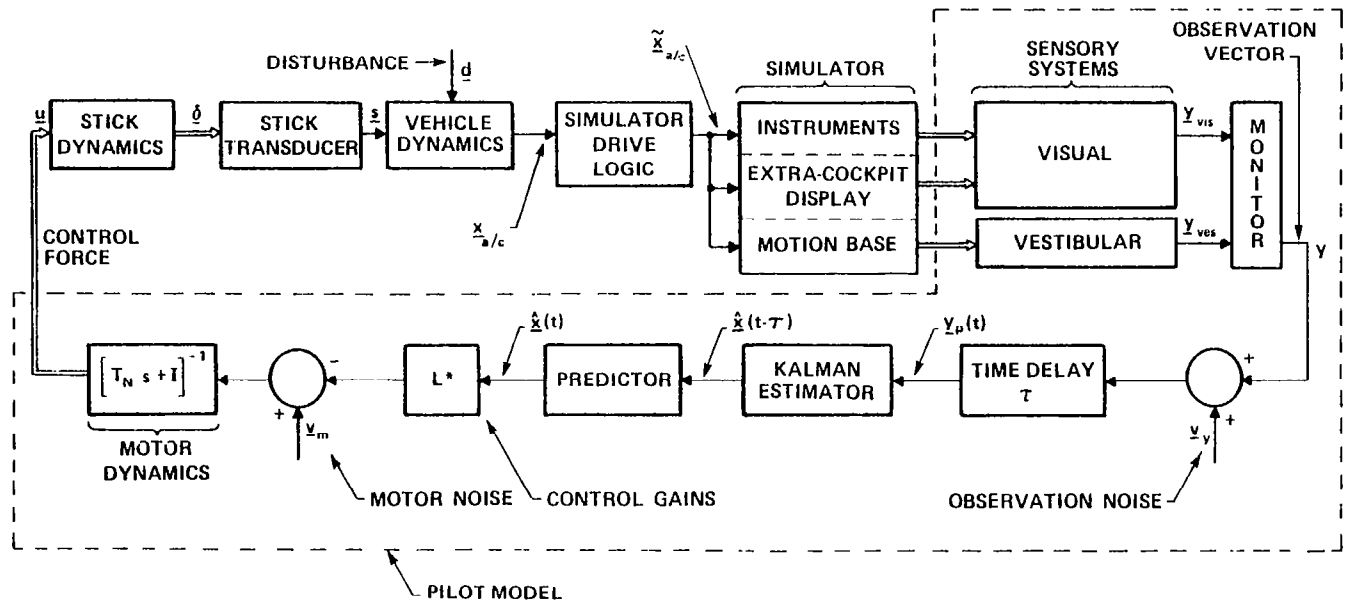
Figure 2.2: Overall Pilot/Vehicle System

As we noted earlier, the detailed descriptions of these subsystems will be given later in chapter 4. Here, however, it suffices to note that our system modelling approach involves: a) a linearization of the relevant dynamics associated with each of the subsystems; and b), the construction of a state-variable representation of the combined system dynamics. The resulting vector- matrix state equation has the following form:

$$\dot{\underline{x}}(t) = \underline{A}\underline{x}(t) + \underline{B}\underline{u}(t) + \underline{E}\underline{w}(t) \qquad (2.1)$$

where $\underline{x}(t)$ is the n-vector which describes the state of the simulator system, $\underline{u}(t)$ the r-vector of pilot control inputs, and $\underline{w}(t)$ a vector of white driving noise processes, the latter included to model the system disturbances. In general, the matrices $\underline{A}$, $\underline{B}$, and $\underline{E}$ may all be time-varying (piece-wise constant) to reflect changes due to differing flight conditions; in our application, however, they are fixed for a specific hover condition and vehicle configuration.

As noted, the above system model includes all of the dynamics associated with all of the subsystems comprising the simulator. In general, however, the system model will include additional dynamics associated with three other aspects of the closed-loop control task: a) the disturbance or gust model; b) the dynamics which characterize the pilot's sensory capabilities; and c) any dynamics

which might be used to approximate other system characteristics which cannot be expressed directly in terms of linear first-order vector-matrix equations. We discuss these points in the following paragraphs.

Insofar as gust models can be represented by rational noise spectra, they can be incorporated in the system model by first determining the appropriate shaping filter, which, when acting on white noise, generates the desired gust spectrum. By expressing this shaping filter in state-variable format, the system (2.1) may then be augmented to generate appropriate gust states which are driven by the white noise process vector $\underline{w}(t)$, through the disturbance input matrix $\underline{E}$.

If the pilot's sensory dynamics are deemed relevant to understanding closed-loop performance in the given task, the dynamics may be expressed in state variable form, and used to augment the system dynamics of (2.1). We will discuss this at greater length in the next section, in our description of the pilot portion of the closed-loop system.

System dynamics which, after linearization, are not directly expressible in the form of (2.1) may be included in the system description by first finding a suitable state-variable approximation and then augmenting (2.1) with this approximation.

Pure time delays, in particular, are conveniently handled by this approach. An appropriate Pade filter approximation is found, and the associated state variable dynamics are used to augment the system dynamics of (2.1).

In summary, the system (2.1) not only includes the explicit dynamics of the various simulator subsystems, but also the implicit dynamics associated with the disturbance spectra, the relevant sensory dynamics of the pilot, and any additional approximations deemed necessary for accurate system modelling.

## 2.2    Overview of the Pilot Model

The basic assumption underlying the optimal control model for the pilot is that the well-trained, well-motivated human controller will act in a near optimal manner subject to certain internal constraints that limit the range of his behavior and also subject to the extent to which he understands the objectives of the task. When this assumption is incorporated in the optimal control framework and when appropriate limitations on the human are imposed, the structure shown within the dashed lines of of Figure 2.2 results. In discussing this structure it is convenient and meaningful to view this model as being comprised of the following: (i) a display interface which converts system state variables and pilot control outputs into a set of "displayed" variables $y(t)$;

(ii) an "equivalent" perceptual model that translates these variables into noisy, delayed "perceived" variables denoted by $\underline{y}_p(t)$; (iii) an information processor, consisting of an optimal (Kalman) estimator and predictor that generates the minimum-variance estimate $\hat{\underline{x}}(t)$ of $\underline{x}(t)$; (iv) a set of "optimal gains", $\underline{L}^*$, chosen to minimize a quadratic cost functional that expresses task requirements; and (v) an equivalent "motor" or output model that accounts for "bandwidth" limitations (frequently associated with neuromotor dynamics) of the human and his inability to generate noisefree controls. We now discuss these model components in greater detail.

2.2.1 Display Interface

The display interface provides a means for transforming the system state variables and the pilot's control actions into a display "vector" which represents that set of all information available to the pilot. The components of the display vector are assumed to be linear combinations of the state and control variables, and are defined by the following m-dimensional vector equation:

$$\underline{y}(t) = \underline{C}\underline{x}(t) + \underline{D}\underline{u}(t) \tag{2.2}$$

where $\underline{C}$ and $\underline{D}$ may be time-varying (piece-wise constant) to account for changes in the quantities being displayed or "observed".

In the present task, we assume that the only information available to the pilot is that which he obtains via his visual and vestibular sensory systems. As shown in the figure then, the display vector $\underline{y}$ can be partitioned as follows:

$$\underline{y} = (\underline{y}_{VIS}, \underline{y}_{VES})^T \tag{2.3}$$

where $\underline{y}_{vis}$ and $\underline{y}_{ves}$ are the outputs of the two sensory systems. In the more general situation, the display vector could include "displays" from other sensory modalities, such as proprioceptive, tactile, or auditory cues. In addition, the individual display vectors associated with a particular modality (e.g., $\underline{y}_{vis}$, $\underline{y}_{ves}$, etc.) can be expanded to account for information provided by other cueing systems which impinge on that same modality. Thus, in the current study, we have assumed that $\underline{y}_{vis}$ reflects the pilot's reliance on only out-the-window (visual) cues; if he were to have available additional instrument (visual) cues, we would augment $\underline{y}_{vis}$ to account for the information provided by this additional (same-modality) cueing system.

In general, the processing provided by the pilot's sensory systems requires a model which involves not only a linear transformation of the system state (as in (2.2)), but also a dynamic transformation which accounts for any important sensory processing dynamics (e.g., vestibular dynamics). As we noted

earlier, this latter modelling requirement is implemented by assigning the sensory dynamics to the set of overall system dynamics, and appropriately augmenting the state equation of (2.1).

## 2.2.2 Perceptual Model

Limitations on the pilot's ability to process information "displayed" to him are accounted for in the "equivalent" perceptual model. This model translates the displayed variables $\underline{y}$ into delayed, "noisy" perceived variables $\underline{y}_p$ via the relation

$$\underline{y}_p(t) = \underline{y}(t-\tau) + \underline{v}_y(t-\tau) \qquad (2.4)$$

where $\tau$ is an "equivalent" perceptual delay and $\underline{v}_y$ is an "equivalent" observation noise vector.*

The various internal time delays associated with visual, vestibular, central processing and neuro-motor pathways are combined and conveniently represented by this lumped equivalent perceptual time delay $\tau$ . Typical values for this delay are $0.2 \pm .05$ sec. (Kleinman et al (1971)).

---

* The use of the word equivalent in this context is to emphasize that the parameters may be lumped representations of a variety of limitations that can not be "identified" separately by existing measurement techniques.

The observation noise $\underline{v}_y$ is included to account for the pilot's inherent randomness, due to random perturbations in human response characteristics, errors in observing displayed variables, and attention-sharing effects which limit the pilot's ability to accurately process all the cues simultaneously available to him. In combination with the motor noise model (described below in section 2.2.4), the observation noise model provides a convenient and accurate means of modelling pilot remnant and thus accounting for random control actions.

For manual control situations in which the displayed signal is large enough to negate the effects of visual resolution ("threshold") limitations, the autocovariance of each observation noise component appears to vary proportionally with mean-squared signal level. In this situation, the autocovariance may be represented as

$$V_i(t) = \pi P_i \sigma^2_{y_i}(t) \qquad (2.5)$$

where $\sigma^2_{yi}$ is the variance of the $i^{th}$ output, $P_i$ is the "noise/signal ratio" for the $i^{th}$ display variable, and has units of normalized power per rad/sec. Numerical values for $P_i$ of 0.01 (i.e., -20 dB) have been found to be typical of single-variable control situations (Levison et al (1969), Kleinman et al (1970)).

The perceptual model defined by (2.4) and (2.5) applies to "ideal" display conditions, in which the signal levels are large with respect to both system-imposed and pilot-associated thresholds. To account for threshold effects we let the autocovariance for each observation noise process be

$$V_i(t) = P_i \left( \frac{\sigma_i^2}{K_i^2(\sigma_i, a_i)} \right) \tag{2.6}$$

where the subscript $i$ refers to the $i^{th}$ display variable. The quantity $K(\sigma_i, a_i)$ is the describing function gain associated with a threshold device

$$K(\sigma, a) = \frac{2}{\sqrt{\pi}} \int_{-\infty}^{-\frac{a}{\sigma\sqrt{2}}} e^{-x^2} dx \tag{2.7}$$

where "a" is the threshold and $\sigma$ is the standard deviation of the "input" to the threshold device.* The net result of this type of describing function model is to increase the observation noise covariance as the display signal variance becomes smaller relative to the threshold.

The sources of these threshold effects depend on the particular task being modelled. They may be associated with the system display implementation, for example, due to resolution limitations on a display screen. Or, they may be associated with

---

* For non-zero mean signals this expression must be modified (see (Baron and Levison (1973)).

the pilot's sensory limitations, such as one might identify with visual acuity thresholds. In the hover task both types of threshold effects enter into the analysis, and will be discussed in greater detail in chapter 3.

One additional factor which tends to increase the observation noise (present on any given display variable) is the pilot's attention-sharing limitations. Because the numerical value associated with the pilot's noise/signal ratio (P) has been found to be relatively invariant with respect to system dynamics and display characteristics, we associate this parameter with limitations in the pilot's overall information-processing capability. This forms the basis for a model for pilot attention-sharing where the amount of attention paid to a particular display is reflected in the noise/signal ratio associated with information obtained from that display (Levison et al (1971), Baron and Levison (1973)). Specifically, the effects of attention-sharing are represented as

$$P_i = P_o/f_i \qquad (2.8)$$

where $P_i$ is the noise/signal ratio associated with the $i^{th}$ display. When attention is shared among two or more displays, $f_i$ is the fraction of attention allocated to the $i^{th}$ display, and $P_o$ is the noise/signal ratio associated with full attention to the task. A

detailed description of task-specific attention allocation levels is deferred to chapters 3 and 5, where we discuss the perceptual modelling and specific task components in more detail.

## 2.2.3 Estimation and Control Models

The optimal predictor, optimal estimator, and optimal gain matrix represent the set of "adjustments" or "adaptations" by which the pilot tries to optimize his behavior. The general expressions for these model elements are determined by system dynamics and task objectives according to well-defined mathematical rules that are derived in (Kleinman et al (1971)). The controller is assumed to adopt a response strategy to minimize a weighted sum of averaged output and control variances as expressed in the cost functional:

$$J(\underline{u}) = E[\underline{y}^T(t)\underline{Q}_y\underline{y}(t) + \underline{u}^T(t)\underline{Q}_u\underline{u}(t) + \underline{\dot{u}}^T(t)\underline{R}_u\underline{\dot{u}}(t)] \qquad (2.9)$$

where $J(\underline{u})$ is conditioned on the perceived information $\underline{y}_p$.*

The selection of the weightings $\underline{Q}_y = \text{diag}[q_{y_i}]$, $\underline{Q}_u = \text{diag}[q_{u_i}]$ and $\underline{R} = \text{diag}[r_i]$ in $J(\underline{u})$ is a non-trivial step in applying the OCM. The most commonly used method for selecting reasonable a priori estimates for the output weightings is to associate them with allowable deviations in the system variables, and has been described in several recent applications of the OCM (see, for

_____

* The cost functional can also include a term that is quadratic in the state.

example, Kleinman (1976)). The control related weightings may be chosen in a similar fashion or they may be picked to yield a desired value of $\underline{T}_N$, as discussed below. This method of choosing weightings has several advantages. Maximum or limiting values of system quantities are often easy to specify or elicit from pilots. In addition, with this normalization, the contribution of each term to the total cost depends on how close that quantity is to its maximum value; the penalty is relatively small when the variable is within limits but increases rapidly as the variable exceeds its limit.

As noted above, the tandem of predictor and estimator generate a minimum variance estimate of the system state. As such, they (linearly) compensate for any time delays or noises introduced by the system and/or the operator. These elements incorporate "perfect" models of the simulation environment including models of the CGI and VMS systems.* Thus, the model predictions are appropriate for pilots that are well trained on the simulator.

### 2.2.4 Motor Model

Limitations on the pilot's ability to execute appropriate control actions are accounted for in the motor model, which is

---

* Indeed, they also include models of the pilot's own sensory limitations.

composed of a white motor noise source and a first-order lag matrix. This model translates "commanded" controls, $\underline{u}_c$, into the output control actions $\underline{u}$ via the following relation:

$$\underline{T}_N\dot{\underline{u}} + \underline{u} = \underline{u}_c + \underline{v}_M \tag{2.10}$$

where $\underline{T}_N$ is an "equivalent" lag matrix and $\underline{v}_M$ is an "equivalent" motor-noise vector.

In laboratory tracking tasks with optimized control sticks, the motor lag parameters have been associated with the operator's neuro-motor time constant; accordingly, the lag values of the $T_N$ matrix have been set to a value of about 0.1 second. For more realistic flight control situations, however, this bandwidth limitation may be overshadowed by the system dynamics and flight control objectives, so that the 0.1 second value may lead to model predictions of control activity which exceed that observed in actual flight situations. In these cases, it is more reasonable to choose lag values by a model trade-off analysis in the following manner: choose a lag value such that if a larger value is chosen, substantial increases in tracking error will result, whereas if a smaller value is chosen, only marginal improvements in tracking performance will result. This method of choosing the motor lag at the "knee" of the cost vs. lag value curve was used for the study described here; the numerical results are given in section 4.1.

The neuro-motor noise vector of (2.10) is provided to account for random errors in executing intended control movements, and, in addition, to account for the fact that the pilot may not have perfect knowledge of his own control activity. The motor noise is assumed to be a white noise, with autocovariance that scales with the control variance, i.e.,

$$V_{m_i}(t) = P_{m_i} \sigma_{u_i}^2(t) \qquad (2.11)$$

Previous studies (Kleinman et al (1970)) have found, typically, that a value for $P_m$ of .003 (i.e., a "motor noise ratio" of -25 dB) yields good agreement with experimental results. Throughout this study the motor-noise ratio was set to approximately -25 dB.

This then concludes our general description of the pilot model. We now proceed to describe the perceptual portion of this model in more detail, since it is central to our evaluation of CGI and VMS cueing system specifications.

# 3. VISUAL AND VESTIBULAR PERCEPTUAL MODELS

The previous chapter described the general characteristics of the perceptual portion of the optimal control model. Here, we provide more detail concerning the perceptual models for the two modalities considered most relevant to the hover task being studied: the out-the-window visual perception model, and the vestibular motion-sensing model. We also provide a brief discussion of the model for attention-sharing among the cues provided by these two modalities.

## 3.1 Visual Perception Model

In contrast to the relatively well-defined set of visual cues provided by within-cockpit instrumentation, the extra-cockpit visual scene can provide the pilot with an exceptionally rich stimulus environment, even for a relatively simple display. Attempting to describe and quantify this stimulus environment has been the object of many studies. For example, Brown (1973) discussed five "dimensions" of the visual world: field-of-view, range of luminance, color, spectral resolution, and visual motion. Staples (1970) listed fifteen factors that are present in the visual scene which can be of importance to the pilot, and noted that this list was incomplete. Gibson (1950,1955) concentrated on geometric and textural cues, but also noted the potential utility

of the "traditional" cues for depth perception (i.e., lens accommodation, binocular convergence, and retinal disparity).

The literature on scene attributes is extensive, and it became clear to us that some narrowing of focus was called for, if a successful attempt was to be made in the area of modelling this type of cue processing.

Matheny, et. al. (1971) present a taxonomy of cues that is helpful in structuring and limiting the problem. They define relevant cues as cues which are directly useful for controlling the aircraft or for making decisions. The non-relevant cues are those that are not essential to the successful operation of the aircraft, but which may add realism or face-validity to the task. Within the domain of relevant cues are subsets of primary, secondary, complementary and conflicting cues. This assumes that the operator has, for a given situation, a hierarchy of preferred cues and that he seeks a primary cue from a set of cues that are available. Cues that tend to reinforce his primary cues are called secondary if from the same modality, and complementary if from a different modality. Finally, cues that are in opposition in terms of the information they present are called conflicting (additional discussion can be found in Thielges and Matheny (1971)).

## 3.1.1 Visual Cueing Geometry

It seems clear that in extending the optimal control model to account for perception of the visual scene, our first concern should be the relevant cues. Thus, for example, color can be neglected in our hover task, since adequate foreground-background separation can be provided by a sufficiently large contrast differential. Similarly, range of luminance might be neglected if adequate surface definition is provided by the display hardware. Other "non-geometric" visual cue factors can be similarly neglected, at least for an initial analysis, so that modeling can concentrate on the basic geometric characteristics of the visual scene. These were identified by Gibson (1950) in his analysis of visual scene processing: table 3.1 lists these "geometric" cues and the corresponding type of information they provide.

Table 3.1: Geometric Visual Cues

| Cue | Information |
|---|---|
| Field Orientation | Attitude, Attitude Rate |
| Linear Perspective | Position |
| Motion Parallax | Linear Velocity |
| Apparent Size/ Size Constancy | Position |
| Occultation | Position |

Field orientation provides the pilot with attitude cues: assuming that the visual world is inertially fixed, then any rotation of the scene elements, measured with respect to the vehicle (or pilot) frame of reference, must be due to self-rotation of the vehicle (and pilot). Linear perspective changes with the location of the vehicle; thus, these cues provide the pilot with positional information. Motion parallax is effectively a rate of change of linear perspective, and thus provides the pilot cues for inferring linear self-velocity. The apparent size of an object (combined the pilot's perceptual set which ensures size constancy) provides a "looming" or range cue which can be used to infer relative distances, and hence position. Finally, occultation of one object by another provides an angular "line-of-position" cue similar to a navigation "fix", and, hence, also provides a means of inferring position.

To illustrate how the use of these cues might be analyzed in a quantitative manner, we briefly summarize a study conducted by Wewerinke (1978). He concentrated on the pilot's use of field orientation, linear perspective, and motion parallax cues during a VFR landing approach. By use of elementary perspective geometry, he related rotational and translational vehicle movements to changes in orientation of line segments comprising the extra-cockpit visual scene. For example, he showed that small

changes in the perceived orientation of the runway centerline, with respect to the aircraft's longitudinal plane of symmetry, is given by

$$w = C_h h + C_y y + \phi$$

where w is the runway centerline deviation, $C_h$ and $C_y$ are trajectory dependent constants,* and h, y, and $\phi$ are small deviations in altitude, localizer error, and roll attitude, respectively. Similar expressions were derived for orientational changes in other line elements comprising the visual scene, and corresponding expressions were derived for their rates of change.

To model pilot processing of these cues, Wewerinke (1978) followed the suggestion of Baron and Berliner (1975) and used the optimal control model and its "display vector" capability. Specifically, he recognized that each $w_i$ associated with a scene line element was linearly related to the vehicle state vector $\underline{x}$, in the form

$$w_i = \underline{c}_i^T \underline{x} \qquad (3.1)$$

where $\underline{c}_i$ is the "display gain" associated with the $i^{th}$ line

---

* This assumes there are no significant changes in vehicle position along the approach path, a condition which was satisfied in Wewerinke's study.

element. If the pilot's display vector $\underline{y}$ is composed of N extra-cockpit geometric cues, then

$$\underline{y} = \underline{C}\underline{x} \qquad (3.2a)$$

where

$$\underline{C} = [\underline{c}_1, \ \underline{c}_2, \ldots, \underline{c}_N]^T \qquad (3.2b)$$

so that the display matrix $\underline{C}$ is completely defined for the purposes of model analysis.

To test this hypothesis of visual cue processing, Wewerinke conducted a model analysis of experimental data obtained from a simulated VFR approach and found that the data could be closely matched by assuming: a) "nominal" pilot-related model parameters (except for a motor time constant of 0.25); b) optimal attention allocation between display vector elements (as described later in section 3.3; and c) individual display thresholds which were consistent with visual perception thresholds found in related psychophysical experiments. In short, the modeling approach toward visual cue processing was well-supported by the experimental data.

Since a pilot's perspective of the runway is by far the most useful visual cue in a conventional VFR approach and landing, Wewerinke (1978) was able to use a highly schematized line drawing of the runway environment. As a consequence, there were a limited

number of well-defined cue elements comprising the visual scene, and thus the construction of the display matrix C was a relatively straightforward exercise. In the hover task, however, no single object is important. Instead, a pilot can use various portions of his visual field, and any number of objects or parts of objects to maintain his hover position and attitude. As a consequence, we have assumed that a relatively "realistic" visual scene is always available to the pilot. Since such a scene is typically comprised of thousands (or perhaps tens of thousands) of discriminable line elements (and hence cues), the display analysis outlined above is not appropriate here.

Our approach, instead, was to take a much simplified view of visual cue processing, based on the following notion. Each of the cues listed in table 3.1 involve changes in the location, length, and/or orientation of the various line elements comprising the visual scene. These changes, in turn, can be expressed in terms of changes to four parameters which specify the line element itself: the four angular coordinates associated with the line element endpoints, two coordinates per point. For our study, we have taken these two coordinates to be the azimuth and elevation angles associated with the line-of-sight (LOS) to the particular line element endpoint.

Changes in these LOS angles are due to changes in vehicle state (position and attitude). Assuming small changes, we can use the linearized relation we introduced earlier, so that

$$\psi_{vis} = \underline{c}_\psi^T \underline{x}$$
$$\theta_{vis} = \underline{c}_\theta^T \underline{x}$$

(3.3)

where $\psi_{vis}$ and $\theta_{vis}$ are the azimuth and elevation LOS angles, $\underline{c}_\psi$ and $\underline{c}_\theta$ are the display "gains", and it is understood that the above relation holds (with different gains) for each specific point in the visual scene. Thus, we would expect to have two such equation sets for each line element in the scene, with perhaps thousands of these set pairs associated with any given "realistic" scene. Naturally, all of these equations would be dependent on the specifics of the particular scene being analyzed.

Rather than attempt to specify, and then solve, this large number of simultaneous equations in the state $\underline{x}$, we chose to take an approach which effectively idealizes the scene content. We assumed, for each vehicle state the pilot was trying to estimate, that the pilot chose one particular point in the visual scene to provide the most appropriate visual cue. Thus, if the vehicle state is comprised of three rotational coordinates and three translational coordinates, then, in general, there would be six specific points in the visual scene the pilot would use for inferring changes in vehicle state.

This is illustrated in figures 3.1 and 3.2, which show how specific vehicle rotations and translations result in changes in the azimuth and elevation angles associated with the line-of-sight to a specific point in the visual scene.

Figure 3.1 shows the effect of vehicle (pilot) rotations. For both yaw ($\psi$) and pitch ($\theta$) motion, we assume the presence of an object (or an identifiable part of an object) located along the forward (x) axis of the vehicle.* In yaw, this might be achieved through the presence of a sufficiently tall vertical reference (e.g., a tree or telephone pole); in pitch, via a sufficiently wide horizontal reference (e.g., a roof line or the horizon line). In either case, the figures show that the observed change in the LOS angle will be equal and opposite to the change in the corresponding vehicle attitude angle:

$$\psi_{vis} = -\psi \qquad (3.4a)$$
$$\theta_{vis} = -\theta \qquad (3.4b)$$

Figure 3.1 also shows the effect of roll motion. We assume the presence of an object located on the horizon, and just within the lateral field-of-view of the pilot ($\psi_{FOV}$). If small roll angles are assumed, then it is a direct matter to show that the

---

* For this cueing analysis, we also assume the origin of the vehicle body axis to coincide with the location of the pilot's eyes.
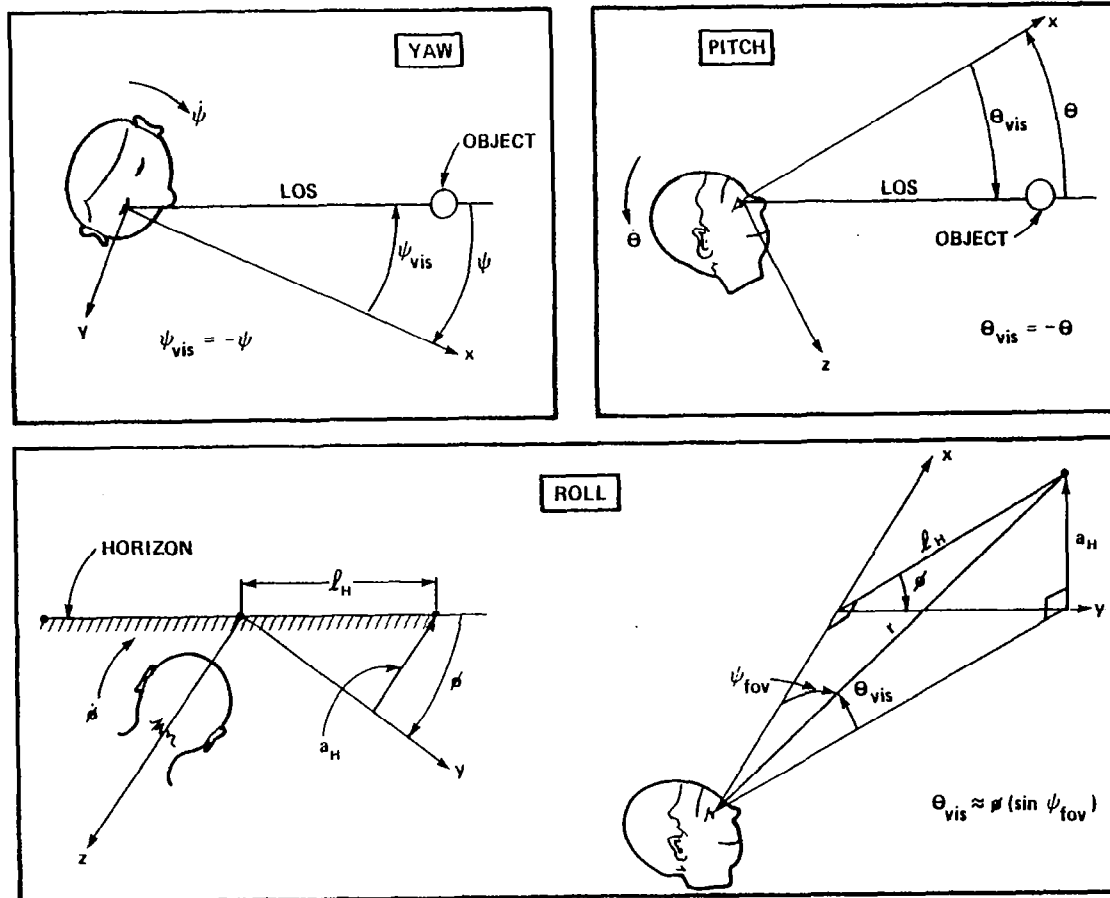
Figure 3.1: Line-of-Sight Changes Due to Vehicle/Pilot Rotations

$$\theta_{vis} \approx -(x/h_o) \sin^2 \theta_o$$

SURGE

OBJECT IN
x-z PLANE

GROUND PLANE

$$\psi_{vis} \approx -(y/\ell_o) \cos \psi_o$$

SWAY

OBJECT IN
x-y PLANE

$$\theta_{vis} \approx -(h/h_o) \cos \theta_o \sin \theta_o$$

HEAVE

OBJECT IN
x-z PLANE

GROUND PLANE
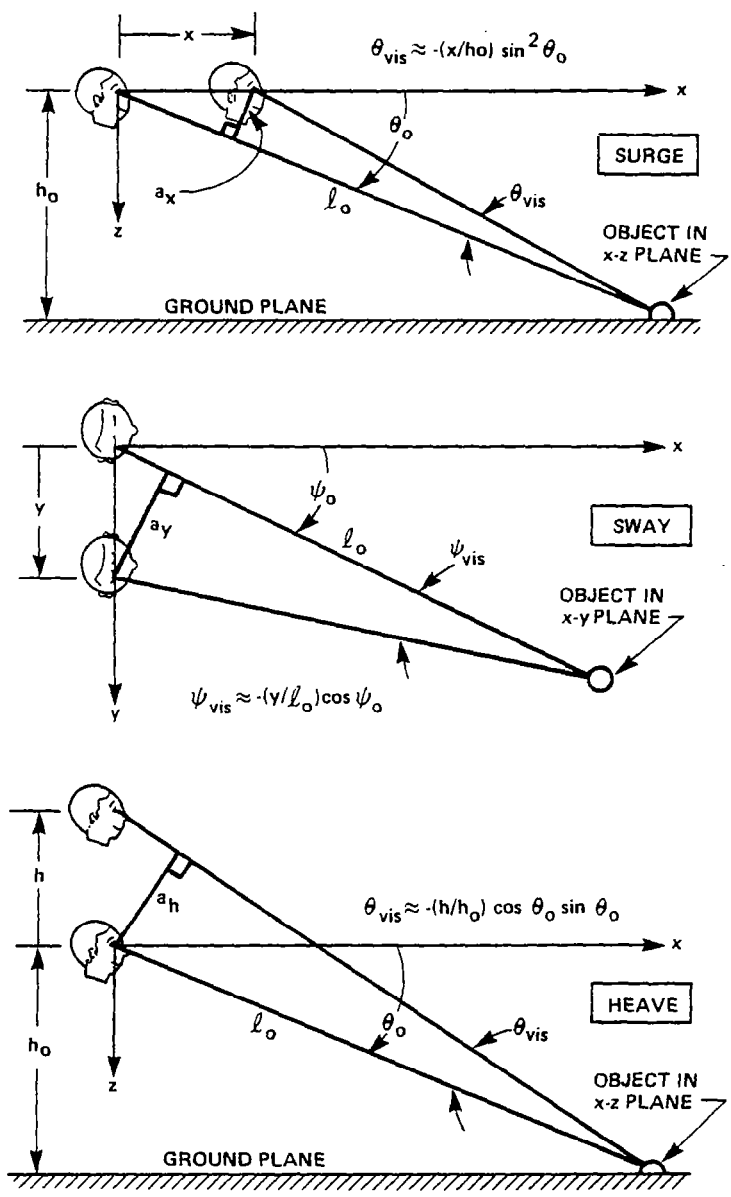
GL2159

Figure 3.2:   Line-of-Sight Changes Due to
Vehicle/Pilot Translations

observed change in the LOS elevation angle is given by:

$$\theta_{vis} = \phi(\sin\psi_{FOV}) \qquad (3.4c)$$

Since the roll angle is assumed small, it is also a direct matter to show that the resulting change in the LOS azimuth angle $(\psi_{vis})$ is negligible. Thus, it can be neglected as a cue to inferring roll angle.

Figure 3.2 shows the effect of vehicle (pilot) translations. For both surge (x) and heave (z) motion, we assume the presence of an object located in the vehicle's longitudinal plane of symmetry (the x-z plane), at ground level. This might be achieved through the presence of a small object ideally located in the forward viewing plane, or via a horizontal reference line on the ground plane (e.g., a painted stripe on a helicopter landing pad). As shown in the figure, surge or heave motion results in a change in the LOS elevation angle. Assuming that the nominal hover altitude is $h_o$, and that the nominal LOS depression angle* is $\theta_o$, then it can be shown that

$$(\text{x-axis}) \qquad \theta_{vis} = -(x/h_o)\sin^2\theta_o \qquad (3.4d)$$

--------

* The depression angle is merely the negative of the elevation angle.

$$(z\text{-axis}) \quad \theta_{vis} = -(h/h_o)\cos\theta_o\sin\theta_o \qquad (3.4e)$$

where, consistent with our earlier assumptions, we assume small displacements x and h, relative to the sighted object distance $l_o$.

Figure 3.2 also shows the effect of a lateral displacement along the vehicle y-axis We assume the presence of an object in the horizontal plane containing the vehicle origin (the x-y plane) and located off the longitudinal axis an angular distance $\psi_o$. As in the yaw-axis case, this might be due to the presence of a sufficiently tall vertical reference such as a telephone pole or tree. Assuming a nominal object distance $l_o$, it follows that the change in the LOS azimuth angle will be given by:

$$\psi_{vis} = -(y/l_o)\cos\psi_o \qquad (3.4f)$$

where, as before, we assume that the vehicle translation y is small with respect to the sighted object distance $l_o$.

To this point, we have shown, for a given object in the visual scene, how the LOS azimuth and elevation angles will change due to vehicle motion. It should be clear that this is a many-on-two mapping, since quite different vehicle motions can result in identical changes in the LOS angle. For example, it can be shown from (3.4a) and (3.4f) that a yaw rotation $\psi$ and a lateral displacement y cannot be differentiated on the basis of a single LOS observation, if we choose

$$y = l_o\psi/\cos\psi_o$$

where $l_o$ and $\psi_o$ are as defined previously. However, it should also be clear that if we had two such observations, associated with two different objects in the visual field, then we would be able to differentiate between the motions.

In the actual hover task, we have six distinct motions which must be differentiated; but with a "realistic" scene available, the pilot should have thousands of LOS "measurements" available to him. Thus, it seems safe to presume that the pilot can effectively "decouple" the many-on-two mapping, and correctly infer the vehicle motion from the given cue set of azimuth and elevation LOS angle changes.

To avoid the necessity of postulating a cue decoupling model for the pilot, we have chosen to assume that the pilot can directly invert the equations given above, to correctly infer the vehicle motion from the observed LOS visual cue. For example, if the pilot observes an azimuth change ($\psi_{vis}$) in the LOS to a specific object, and this has been caused by a y-axis translation, then we presume that he correctly infers this y-axis motion by inverting (3.4f):

$$\tilde{y} = -(l_o/\cos\psi_o)\,\psi_{vis}$$

where y is his inference from the observation $\psi_{vis}$, and his knowledge of the nominal geometry $(l_o, \psi_o)$.

Subject to the limitations described immediately below, this then is our basic model of visual cue processing. The azimuth and elevation LOS angles are the available cues. By choosing and inverting the appropriate equation in equation set (3.4), the correct vehicle motion can be inferred. It should be recognized that (3.4) presumes a specific cueing geometry (as described earlier) and thus is not cast in the most general form possible. However, it should be clear that any other cueing geometry choice will result in a similar set of six equations, which, under the modelling assumptions just given, could be similarly inverted to infer changes in vehicle attitude and position.

3.1.2  Visual Thresholds

It is now appropriate to consider the fact that the pilot will be limited in his ability to detect changes in the LOS angle cues available to him. This limitation will be due either to his own inherent sensory/perceptual limitations, or, in the simulator situation, possibly due to CGI-imposed resolution limits. The effective visual cue threshold will be the greater of the two thresholds associated with the pilot and the display hardware, and will ultimately limit the pilot's ability to infer vehicular state

changes from changes in the visual scene.* Naturally, if display hardware is not involved (as in the actual helicopter environment), then the effective threshold will be determined solely by the pilot's visual limitations.

Turning first to the pilot's visual limitations, we make a distinction between angular resolution threshold ($\alpha_R$) and angular discrimination threshold ($\alpha_D$). The former refers to his visual acuity, and his ability to resolve small angular differences in the LOS angle, when given a visual reference which, in angular distance, is very close to the object being sighted. The latter refers to the pilot's ability to discriminate between two large visual angles, and thus his ability to identify a small angular difference in the LOS angle, when given a visual reference which, in angular distance, is relatively far from the object being sighted.

The angular resolution threshold ($\alpha_R$) might be chosen on the basis of measured human visual acuity, which appears to be on the order of one minute of arc (Riggs (1965)). However, we chose to

---

* Strictly speaking, we should restrict our attention to pilot-related visual thresholds in this section, since we are attempting to define the perceptual submodel of the pilot. However, since display-related visual thresholds will act in a functionally equivalent manner, it is appropriate to consider both types of limitations at the same time, and define an overall "effective" pilot/simulator visual threshold.

set it at a slightly higher level, based on an earlier analysis of the data obtained from dynamic tracking experiments (Levison (1971)):

$$\alpha_R = 0.05 \text{ deg} \qquad (3.5a)$$

The angular discrimination threshold ($\alpha_D$) was chosen in accordance with the Weber-Flechner law (Luce and Galanter (1963)), and set at a fixed fraction of the total angle being viewed:

$$\alpha_D = \alpha_O/30 \qquad (3.5b)$$

where $\alpha_O$ is the total angle being viewed.

We now define the pilot-associated visual threshold as the maximum of the resolution and discrimination thresholds:

$$\alpha = \text{MAX}(\alpha_R, \alpha_D) \qquad (3.5c)$$

To determine which of these two thresholds will dominate, we turn to the cueing geometry illustrated earlier in figures 3.1 and 3.2. Figure 3.1 shows that the nominal LOS angles for attitude cues is zero; thus $\alpha_D$ is zero, and $\alpha$ is determined by the resolution threshold $\alpha_R$. Figure 3.2 shows that the nominal LOS angle for a sway cue is $\psi_O$. If we specify this to be zero (i.e., a straight-ahead target), then the threshold associated with sway motion will also be determined by the resolution threshold.

Finally, if we assume reasonable values for hover height $h_O$ and object distance $l_O$, say:

$$h_O = 10 \text{ ft.}$$

$$l_O = 50 \text{ ft.} \qquad (3.6)$$

then the LOS depression angle associated with a surge or heave cue will be on the order of 10 degrees. The discrimination threshold will therefore be on the order of 0.3 degrees. This determines the pilot-related threshold for these two types of visual motion cues.

We now turn to the potential effects of CGI-imposed resolution thresholds. If the CGI has associated with it an average angular resolution $\beta$, then the overall pilot/simulator visual threshold will be given by*

$$\gamma = \text{MAX}(\alpha, \beta) \qquad (3.7)$$

We will reserve discussion of particular values of $\beta$ associated with specific CGI configurations until Chapter 4, where we discuss the system characteristics in more detail. However, it suffices to note that $\beta$ is on the order of the pilot's resolution threshold $\alpha_R$. Thus, if the pilot-associated threshold for a given cue is determined by the discrimination threshold $\alpha_D$, then the overall

---

* Note that will be zero in the case of the "infinite resolution" display available from a true out-the-window scene in the actual helicopter.

pilot/system threshold will likewise be determined by $\alpha_D$. From the discussion given above, we therefore expect the overall threshold for surge and heave cues to be determined by $\alpha_D$. Thresholds for the other axes will depend on the relative magnitudes of the pilot-associated $\alpha_R$ and the system-associated $\beta$.

The discussion to this point has concentrated on static "position" thresholds. To determine dynamic "velocity" thresholds associated with visual cueing, one might attempt to assign a value on the basis of past psychophysical motion detection/discrimination experiments. However, a review of the subject by Graham (1965) shows that a wide range of values can be assigned, depending on the particular experimental situation and empirical measures used. We chose to assign a value on the basis of earlier dynamic tracking experiments. In his manual tracking study and model analysis of visual threshold effects. Levison (1971) found that the data could be best matched in terms of OCM parameters by choosing visual position and rate thresholds as follows:

$$\gamma_{TH} = 0.071 \text{ deg}$$

$$\dot{\gamma}_{TH} = 0.24 \text{ deg/sec}$$

resulting in a ratio of $\dot{\gamma}_{TH}/\gamma_{TH}$ of approximately 3.4. In a subsequent study of tracking, with a quantized visual display (Levison et al (1972)), a similar model match was obtained by

setting $\dot{\gamma}_{TH}$ equal to the display quantization level, and adjusting $\gamma_{TH}$ to provide the best fit to the data. This resulted in

$$\gamma_{TH} = 0.25 \text{ deg}$$

$$\dot{\gamma}_{TH} = 1.1 \text{ deg/sec}$$

yielding a $\dot{\gamma}_{TH}/\gamma_{TH}$ ratio of approximately 4.4. Other studies have shown similar ratios between velocity and position thresholds, and thus we chose for this study to specify the visual velocity threshold according to:

$$\dot{\gamma} = 4\gamma \qquad\qquad (3.8)$$

where, if $\gamma$ is given in degrees, $\dot{\gamma}$ is given in degrees/sec. Hence, we tie the rate threshold to the position threshold, which, in turn, depends on the pilot-associated and display-associated resolution limitations.

3.1.3 Informational Thresholds (Visual Channel)

We are now in a position to define the effective "informational" thresholds, associated with the visual cues available to the pilot. As we noted earlier, we assume the pilot effectively "inverts" the appropriate equation of equation set (3.4) to obtain an estimate of the vehicular attitude/position change from the visual cues available to him. If we assume that

the effective visual threshold $\gamma$ applies equally to the azimuth $(\psi_{vis})$ and elevation $(\theta_{vis})$ LOS changes, we can then generate an informational threshold table as shown in table 3.2.

The position threshold relations were obtained by inverting the several equations of (3.4), ignoring any sign relations (since the object is to identify magnitude effects), and substituting in the visual threshold $\gamma$ or the discrimination threshold $(\theta_o/30)$, as appropriate. The velocity thresholds were obtained similarly, except that the visual rate threshold $\dot{\gamma}$ was substituted throughout. Note that the roll threshold is divided by a factor of 2 to account for the availability of dual endpoints and the potential resolution enhancement which may exist with a continuous-line horizon.

Since the informational thresholds given in table 3.2 depend on parameters defined by the scene geometry and simulator configuration, we will defer presenting specific threshold values until we discuss the hover task in more detail in chapter 4.

### 3.1.4 Visual Model Implementation

Since the perceptual dynamics of the human visual system are relatively wide-band with respect to the system dynamics we are modelling, we chose not to include any dynamic visual effects. This allowed us to implement our visual perception model by simply

Table 3.2: VISUAL SCENE INFORMATIONAL THRESHOLD FUNCTIONS

| AXIS | POSITION | VELOCITY |
|------|----------|----------|
| YAW | $\psi_{TH} = \gamma$ | $\dot{\psi}_{TH} = \dot{\gamma}$ |
| PITCH | $\Theta_{TH} = \gamma$ | $\dot{\Theta}_{TH} = \dot{\gamma}$ |
| ROLL[1] | $\phi_{TH} = \left(\dfrac{1}{2\sin\psi_{FOV}}\right)\gamma$ | $\dot{\phi}_{TH} = \left(\dfrac{1}{2\sin\psi_{FOV}}\right)\dot{\gamma}$ |
| SURGE[2] | $\chi_{TH} = \left(\dfrac{h_o}{\sin^2\Theta_o}\right)\left(\dfrac{\Theta_o}{30}\right)$ | $\dot{\chi}_{TH} = \left(\dfrac{h_o}{\sin^2\Theta_o}\right)\dot{\gamma}$ |
| SWAY[3] | $y_{TH} = \ell_o\gamma$ | $\dot{y}_{TH} = \ell_o\dot{\gamma}$ |
| HEAVE[2] | $z_{TH} = \left(\dfrac{h_o}{\sin\Theta_o\cos\Theta_o}\right)\left(\dfrac{\Theta_o}{30}\right)$ | $\dot{z}_{TH} = \left(\dfrac{h_o}{\sin\Theta_o\cos\Theta_o}\right)\dot{\gamma}$ |

(1) FACTOR OF 2 ACCOUNTS FOR TWO END-POINT HORIZON
(2) POSITION THRESHOLD IS DISCRIMINATION LIMITED
(3) ASSUMES VISUAL TARGET STRAIGHT AHEAD ($\psi_0 = 0$)

thresholding the appropriate system state variables: the linear/angular positions and velocities of the (simulated) vehicle. The thresholds are those given in table 3.2, and are treated within the OCM pilot model context as described earlier in Section 2.2.2.

## 3.2  Vestibular Perception Model

Models of vestibular motion perception have been the subject of study for a number of years and it is beyond the scope of this report to attempt to summarize this work. Instead, we refer the reader to a relatively recent review of motion cue models by Zacharias (1978), in which a number of these models are described and critically reviewed. The basis for the vestibular model used in the current study is to be found in this review, and we summarize its major features here.

Figure 3.3 shows the vestibular model in block diagram form. The upper portion models the semi-circular canals as transducers of angular velocity, while the lower portion models the otoliths as transducers of specific force.
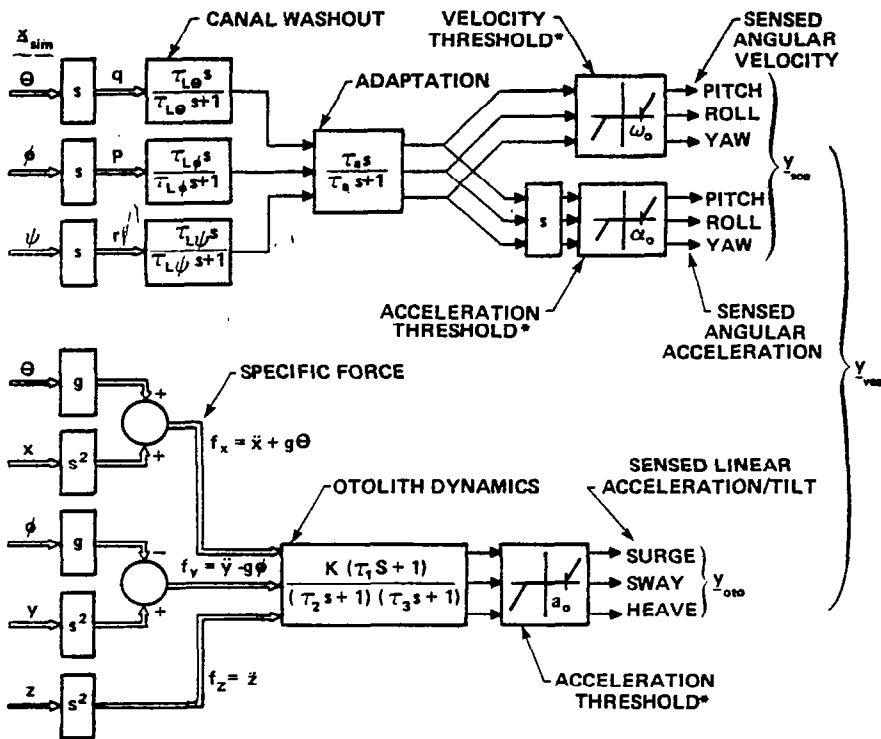
Figure 3.3: Vestibular Model

### 3.2.1 Perception of Angular Velocity (canal model)

The effective canal input is angular velocity of the pilot, which, for simplicity, we assume to be equal to the angular velocity of the vehicle. If p,q, and r represent the conventional roll, pitch, and yaw body rates, then it can be shown that they are related to the conventional Euler angle rates of roll, pitch, and yaw ($\phi, \theta, \psi$) according to:

$$
\begin{bmatrix} p \\ q \\ r \end{bmatrix} = \begin{bmatrix} \dot{\phi} - \dot{\psi}\sin\theta_o \\ \dot{\theta} \\ \dot{\psi}\cos\theta_o \end{bmatrix}
\tag{3.9}
$$

where it is assumed that the vehicle has nominal roll angle of zero, and a nominal pitch angle $\theta_o$. Since our hover problem involves a zero nominal pitch angle ($\theta_o = 0$), the body rates (p,q,r) are simply the derivatives of the Euler angles ($\phi, \theta, \psi$) as shown in the diagram.

The individual body rates are processed by separate channel washout filters, which are used to represent the basic AC transduction characteristics of the canals. The filtered rate signals are passed through an "adaptation" washout, which is used to represent central adaptation to a constant motion stimulus. After thresholding by a velocity threshold $\omega_o$ (one for each axis),

the filtered signals then become the basis for the pilot's (vestibular) sensation of angular velocity. As shown in the diagram, a similar parallel path exists for sensation of angular acceleration.

Specific model parameter values are given in table 3.3, and were taken from table 5 of Zacharias (1978). Note that although the adaptation time constant value $\tau_a$ is the same for all three axes, the other parameter values ($\tau_L$, $\omega_o$, and $\alpha_o$) differ on an axis-by-axis basis.

3.2.2 Perception of Linear Acceleration and Tilt (otolith model)

The effective otolith input is specific force, defined as linear minus gravitational acceleration:

$$\underline{f} = \underline{\ddot{r}} - \underline{g} \tag{3.10}$$

For simplicity, we assume that the specific force acting on the otoliths to be equal to the specific force acting on the vehicle center-of-gravity. As before, if we assume a nominal roll angle of zero and a nominal pitch angle $\theta_o$, then it can be shown that the above equation can be expressed in body-axis coordinates as follows:

$$\begin{bmatrix} f_x \\ f_y \\ f_z \end{bmatrix} = \begin{bmatrix} \ddot{x} \cos \theta_o - \ddot{z} \sin \theta_o + g\theta \cos \theta_o \\ \ddot{y} \qquad\qquad - g\phi \cos \theta_o \\ \ddot{x} \sin \theta_o + \ddot{z} \cos \theta_o + g\theta \sin \theta_o \end{bmatrix} \tag{3.11}$$

With the nominal pitch angle $\theta_o$ set to zero in our hover problem, this relation simplifies to that illustrated in the bottom half of figure 3.3.

These individual components of specific force are processed by a second-order filter representing both the otolith dynamics and any associated central processing. The filtered signals are then passed through an acceleration threshold, and serve as the basis for the pilot's (vestibular) sensation of linear acceleration and tilt away from the vertical. No provision is made for an explicit output which signals "jerk", or rate of change of acceleration.

Specific model parameter values are given in table 3.3. Filter parameter values were based on the model proposed by Young and Meiry (1968). The acceleration threshold was set by assuming an effective velocity threshold $v_o$ of 0.7 ft/sec, and computing $a_o$ according to:

$$a_o = v_o/\tau_1$$

A detailed justification of this approach is given in the review cited above. Note that, in contrast to the rotational sensation model discussed above, the parameter values associated with translation/tilt sensation are the same for all three body axes.

Table 3.3:  PARAMETER VALUES FOR VESTIBULAR PERCEPTION MODEL

| Axis | $\tau_L$ (sec) | $\tau_a$ (sec) | $\omega_o$ (o/sec) | $\alpha_o$ (1/sec$^2$) |
|------|------|------|------|------|
| Pitch | 5.3 | 30 | 3.6 | 0.67 |
| Roll | 6.1 | 30 | 2.5 | 0.41 |
| Yaw | 10.2 | 30 | 4.2 | 0.41 |

Otolith Parameters (all axes)

$$(\tau_1, \tau_2, \tau_3,) = (13.2s,\ 5.33s,\ 0.66s)$$

$$(K, a_o) = (0.4,\ 0.053\ ft/s^2)$$

## 3.2.3  Vestibular Model Implementation

As described, the vestibular model involves a linear transformation of the system state (to obtain specific force),

dynamic processing of these transformed state variables, and appropriate thresholding on the outputs. In implementing this model, we simply expressed the dynamics of figure 3.3 in state-variable form (accounting for the input linear transformation) and augmented the basic system state equation (2.1) introduced earlier in section 2.1. The velocity and acceleration thresholds were treated within the OCM pilot model context as described earlier in section 2.2.2.

To reduce computational requirements imposed by the vestibular model, we performed an analysis of the power spectrum of the vestibular signals. By comparing the power spectra of incoming vestibular signals to that of their filtered outputs, pass-bands were identified which accounted for the majority of the correlated power. Utilizing this information allowed the elimination of any lead or lag elements having break frequencies not in the pass-bands. Table 3.4 outlines the resulting simplifications and Appendix A presents their numerical realization. Although many of the vestibular dynamics were simplified or eliminated, the vestibular thresholds given in table 3.3 were still implemented.

Table 3.4  Simplifications to the Vestibular Model

| Axis | Simplification |
|------|----------------|
| Pitch ($\theta$) | Eliminate canal washout and adaptation filters |
| Roll ($\phi$) | Eliminate adaptation filter |
| Yaw ($\psi$) | Eliminate canal washout and adaptation filters |
| Surge ($f_x$) | No simplification |
| Heave ($f_z$) | Set $\tau_1 = \tau_2 = 0$ |
| Sway ($f_z$) | No simplification |

## 3.3  Attention-Sharing Model

The general features and method of implementation of the attention-sharing model have already been discussed in section 2.2.2. Here, we wish to describe features of the model which are specific to the particular helicopter hover task under consideration.

In our modelling of the hover task, we assumed that "full attention" corresponds to an overall noise/signal ratio of -20 dB, a level which is consistent with the finding of many earlier manual control studies (see, for example, Kleinman et al (1970)). This choice sets the value of $P_o$ in our attention-sharing model of (2.8).

To find the fraction of attention $f_i$ associated with the $i^{th}$ display variable, we first assumed that the pilot need not share attention between modalities. Thus, if $f_{TOT}^{VIS}$ and $f_{TOT}^{VES}$ are the attention levels assigned to the visual and vestibular modalities, we set the two levels equal to unity:

$$f_{TOT}^{VIS} = f_{TOT}^{VES} = 1 \qquad (3.12)$$

We made the additional assumption that, within a modality, the pilot would share attention equally between the (decoupled) longitudinal and lateral control tasks. With $f_{LONG}^{VIS}$ and $f_{LAT}^{VIS}$ representing the visual attention allocation between cues, we then have

$$f_{LONG}^{VIS} = f_{LAT}^{VIS} = 0.5 \qquad (3.13a)$$

with the two summing to $f_{TOT}^{VIS}$. An identical relation holds for the vestibular modality:

$$f_{LONG}^{VES} = f_{LAT}^{VES} = 0.5 \qquad (3.13b)$$

The final breakdown of the pilot's attention-allocation policy was obtained by assuming that attention-sharing was required among the display variables associated with a given control axis (longitudinal or lateral) and a given modality (visual or vestibular). Thus, if $\theta^{VIS}$, $x^{VIS}$, and $z^{VIS}$ represent the visual display variables associated with longitudinal control, it was required that

$$f^{VIS}_{\theta} + f^{VIS}_{x} + f^{VIS}_{z} = f^{VIS}_{LONG}$$

Similar expressions apply to the lateral channel and the vestibular modality.*

Specific values for these individual display-associated attention levels were found by an optimization routine which set the values to ensure optimum hover performance (Levison et al (1971), Kleinman (1976)). The values themselves are presented later in chapter 5, after the system and task are described in more detail.

As a final note on the attention-sharing model, it was assumed that the pilot was not required to share attention between a display variable and the time derivative of that variable. Thus, if $\theta^{VIS}$ and $\dot{\theta}^{VIS}$ represent the visually-obtained pitch and pitch rate information, then the associated attention levels are constrained to equal one another according to:

$$f^{VIS}_{\dot{\theta}} = f^{VIS}_{\theta}$$

with the understanding that $f^{VIS}_{\theta}$ is chosen to optimize performance. (see Levison (1971) for additional discussion).

---

* Although one might argue that this attention-sharing requirement is inconsistent with the "integrated" nature of the out-the-window visual display, we chose to impose this constraint to emphasize the "cue-sharing" which is implicit in our geometric model of visual cue processing (recall discussion of section 3.1.1).

# 4.   TASK/SYSTEM DESCRIPTION

This chapter defines the important helicopter and simulator characteristics, as well as the pilot's task objectives as they relate to our implementation of the optimal control model.  Section 4.1 describes the flight task and vehicle dynamics, while section 4.2 describes the simulator characteristics.  Section 4.3 concludes the chapter with a description of how the simulator characteristics are modelled within the context of the OCM pilot/vehicle model.

## 4.1  Description of Flight Task

The hovering flight control task has been linearized and decoupled into longitudinal and lateral control tasks.  The linearized equations of motion for each control task can be expressed in state variable form as :

$$\dot{\underline{x}} = A\underline{x} + B\underline{u} + E\underline{w} \tag{4.1}$$

where $\underline{x}$ is an $n_x$-vector of vehicle and disturbance states, $\underline{u}$ is an $n_u$-vector of control inputs, and $\underline{w}$ is an $n_w$-vector of white noise disturbance inputs.  For the problems considered here the state, control, and noise variables are defined as follows:

a)  Longitudinal Dynamics

$$\underline{x} = [u_g, w_{g1}, w_g, q_g, x, \dot{x}, z, \dot{z}, \theta, \dot{\theta}]^T$$

$$\underline{u} = [\delta_e, \delta_c]^T$$

$$\underline{w} = [n_u, n_w]^T$$

where

$u_g$ = translational gust, longitudinal

$w_g, w_{g1}$ = translational gust, vertical

$q_g$ = rotational gust, pitch

$x, \dot{x}$ = longitudinal hover error, error rate

$z, \dot{z}$ = vertical hover error, error rate

$\theta, \dot{\theta}$ = pitch angle error, error rate

$\delta_e$ = differential collective (elevator) control

$\delta_c$ = gang collective control

$n_u, n_w$ = white noise inputs to gust states

b)  Lateral Dynamics

$$\underline{x} = [v_g, v_{g1}, p_g, r_g, y, \dot{y}, \phi, \dot{\phi}, \psi, \dot{\psi}]^T$$

$$\underline{u} = [\delta_a, \delta_r]^T$$

$$\underline{w} = [n_v, n_p]^T$$

where

$v_g, v_{g1}$ = translational gust, lateral

$p_g$ = rotational gust, roll

$r_g$ = rotational gust, yaw

$y, \dot{y}$ = lateral  hover error, error rate

$\phi, \dot{\phi}$ = roll angle error, error rate

$\psi, \dot{\psi}$ = yaw angle error, error rate

$\delta_a$ = roll cyclic (aileron) control

$\delta_r$ = yaw cyclic (rudder) control

$n_v, n_p$ = white noise inputs to gust states

Notice that the first four states comprise the gust model and are simply appended to the vehicle's state equations. The gust model used has the Dryden form with parameters appropriate to MILSPEC 8785B for low altitude hover.* Values for the entries of the $\underline{A}, \underline{B}$ and $\underline{E}$ matrices corresponding to CH-47 unaugmented and augmented control dynamics were obtained from Hoffman et al (1976), and are given for reference in Appendix A.  A more detailed derivation of these equations can be found in the original reference.

The hovering task is a disturbance regulation task.  As is standard procedure for application of the OCM, it is assumed that the objective of the task may be characterized

---

* The gust model used does not include the consequences of hovering in ground-effect.

as minimization of the following cost functional (see Kleinman (1976)):

$$J = E \left\{ (y_i / y_{i_{max}})^2 + r_j u_j^2 \right\} \tag{4.2}$$

where $y_{i_{max}}$ is a performance tolerance on the corresponding variable. The values for $y_{i_{max}}$ were chosen to be 5 ft and 1 ft/sec for position (x,y,z) and velocity (x,y,z) variables and 1 deg and .05 deg/sec for attitude ($\psi, \theta, \phi$) and attitude rate ($\dot{\psi}, \dot{\theta}, \dot{\phi}$) variables; these values were taken from Hoffman et al (1976). As noted earlier, the weightings on control rate activity, $r_j$, were chosen by means of an error-control tradeoff analysis. This resulted in the following values for $T_N$:

    a)   longitudinal axis:   $T_N = [.15, .18]$     (4.3a)

    b)   lateral axis:   $T_N = [.1, .1]$     (4.3b)

It should be noted that hover control of the unaugmented CH-47 is not an easy task. The results of the reference cited above suggest that the task cannot be performed to within acceptable tolerances under IFR conditions.

## 4.2 Simulator Configuration

In this section, we provide brief functional descriptions of the three major components of the simulator facility: the main-frame computer, the CGI, and the VMS.

### 4.2.1 Main-Frame Computer

For our study we assumed the vehicle equations of motion were implemented on a digital computer, operating at a nominal update rate of 30 Hz. Based on results from the analytic study by Baron et al (1978), we assumed for simplicity that the integration routine introduced no "distortion" in the continuous vehicle dynamics being modelled, and that the only effect of digitization was the introduction of a sample and hold delay associated with the base cycle time of the main-frame computer.

### 4.2.2 CGI Characteristics

Nominal CGI characteristics were chosen from the range of specifications provided in the original statement-of-work. Table 4.1 summarizes the parameter set used to define nominal CGI configuration used in the analytic studies described later in chapter 5. The nominal field-of-view specification is illustrated in figure 4.1 as screen configuration B.

Off-nominal CGI characteristics were also considered. These included variations in the refresh rate, the effective sample rate, the field-of-view (illustrated as alternate screen configurations A and C in figure 4.1), and the display resolution. The impact of these variations on performance will be discussed later in chapter 5.

Table 4.1:  Nominal CGI Characteristics

Picture Refresh Rate                    30 frames/s

Display Compute Time                    66 msec

Effective Sample Rate/Delay             15 Hz/99 msec

Scene Content                           6000 edges/frame

Field-of-View          3 screens across ($144^O$ horiz, $36^O$ vert)

Display Resolution        1024 lines/frame x 1024 pixels/line

No CGI Lag Compensation

## 4.2.2  VMS Characteristics

Nominal VMS characteristics were set according to the specifications provided in the original statement-of-work.  Figure 4.2 is a block diagram of a single-axis of the six degree-of-freedom system, incorporating both a second-order dynamic model and appropriate position/rate/acceleration servo limits. Table 4.2 defines the nominal parameter values associated with each motion axis.

## 4.3  Model Implementation of Simulator Characteristics

To use the OCM for predicting pilot performance in the simulator environment, it is first necessary to express the above simulator characteristics in terms of relevant OCM parameters. This section provides a brief description of the method for mapping
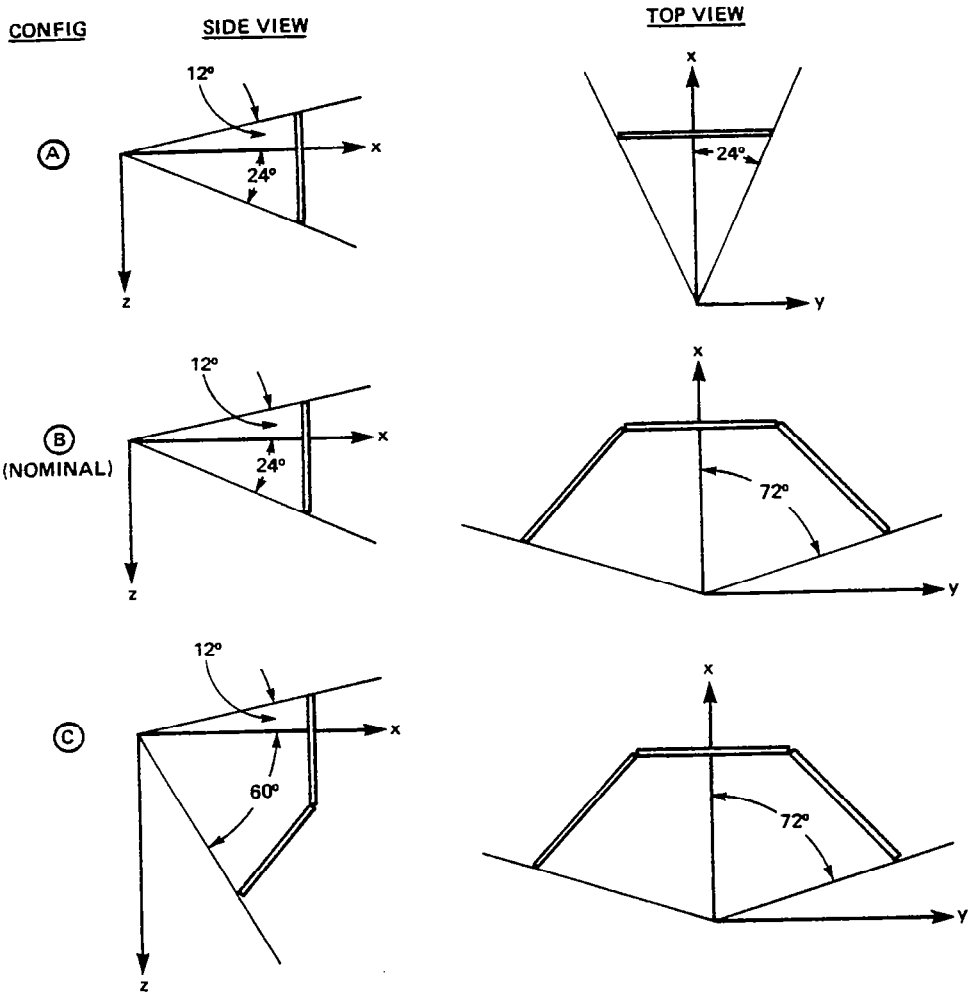
Figure 4.1:  CGI Screen Configuration

Figure 4.2:  VMS MODEL
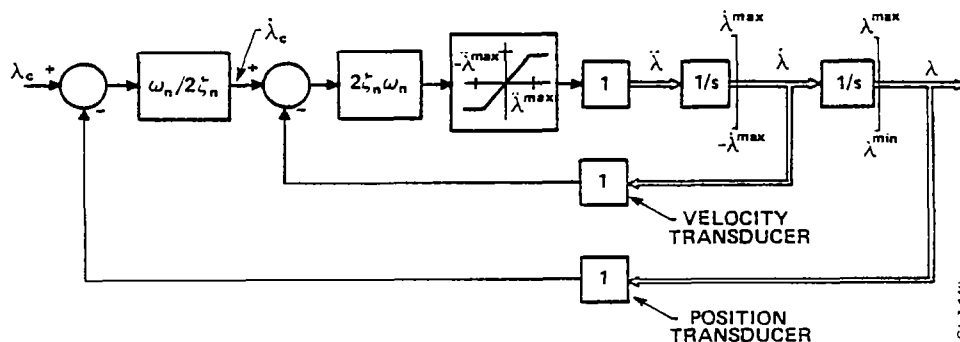


LINEARIZED TRANSFER FUNCTION:  $\dfrac{\lambda}{\lambda_c} = \dfrac{\omega_n^2}{s^2 + 2 f_n \omega_n S + \omega_n^2}$

Table 4.2:  VMS Model Parameters

| | AXIS | $\omega_n^*$ | $f_n$ | $\ddot{\lambda}^{max}$ | $\dot{\lambda}^{max}$ | $\lambda^{min}$ | $\lambda^{max}$ |
|---|---|---|---|---|---|---|---|
| ROLL | ($\phi$) | 9.4 | 0.7 | $50\,°/s^2$ | $15\,°/s$ | $-22°$ | $22°$ |
| PITCH | ($\Theta$) | 9.4 | 0.7 | $50\,°/s^2$ | $15\,°/s$ | $-24°$ | $26°$ |
| YAW | ($\Psi$) | 9.4 | 0.7 | $50\,°/s^2$ | $15\,°/s$ | $-29°$ | $29°$ |
| SURGE | (X) | 9.4 | 0.7 | $16\,FT/s^2$ | $2\,FT/s$ | $-2.5\,FT$ | $2.5\,FT$ |
| SWAY | (Y) | 18.8 | 0.7 | $24\,FT/s^2$ | $10\,FT/s$ | $-20\,FT$ | $20\,FT$ |
| HEAVE | (Z) | 18.8 | 0.7 | $32\,FT/s^2$ | $20\,FT/s$ | $-30\,FT$ | $30\,FT$ |

* RAD/S

-61-

from simulator to OCM parameters, and summarizes the specific OCM ,
parameter values associated with the nominal simulator
configuration.

4.3.1  Main-Frame Computer and CGI Parameters

Figure 4.3 illustrates the general mapping from the computer-
and CGI-associated parameters set to the OCM-associated parameter
set.  Solid lines are used to represent the three basic mappings
used in this study.* As shown, the OCM parameter associated with
visual path delay is impacted both by the main-frame computer rate
and by the CGI-associated parameters specifying the display delay,
refresh rate, and update rate.  The OCM parameter associated with
motion path delay depends solely on the main-frame computer delay.
Finally, the OCM parameters associated with the visual scene
thresholds are impacted by three CGI parameter sets:  those
specifying the scene geometry, the CGI resolution, and the screen
field-of-view.  We discuss these mappings in more detail in the
following paragraphs.

---

* Dashed lines represent more speculative mappings which were
considered but not implemented during the course of the study.

CGI
PARAMETERS

OCM
PARAMETERS

COMPUTER
PARAMETERS

DISPLAY DELAY

REFRESH RATE

UPDATE RATE

RESOLUTION

SCENE GEOMETRY

FIELD-OF-VIEW

VISUAL DELAY

MOTION DELAY

VISUAL THRESHOLDS

OBSERVATION NOISE

ATTENTION SHARING

UPDATE RATE
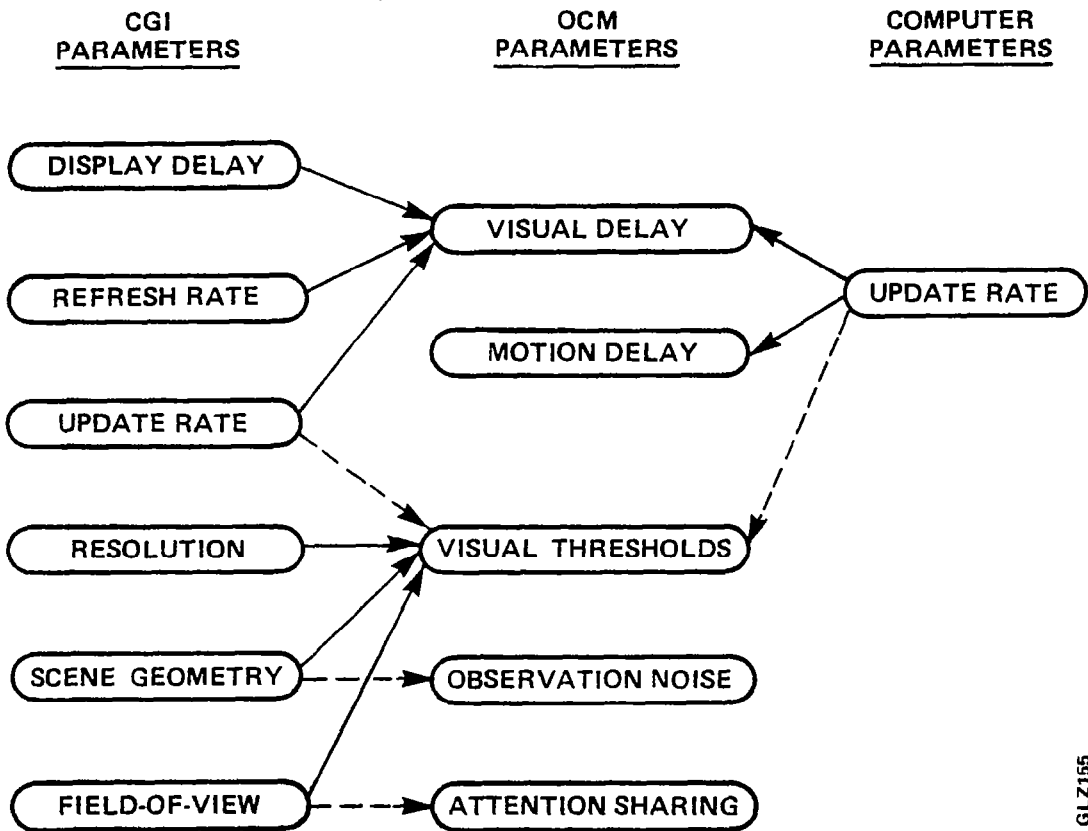
GLZ155

Figure 4.3:  Simulator Mappings for OCM Analysis

## Visual and Motion Delays

Figure 4.4 illustrates how the main computer and CGI characteristics determine both the visual and motion path delays. The main computer is modelled as an ideal sampler acting on the pilot's continuous control signal, followed by a dead-time, a synchronous sampler, and a zero-order hold. The dead-time is assumed to be equal to the sample period $T_C$, which, in turn is assumed to be an integral multiple of a base period $T_O$.

The output of the hold drives the VMS. Thus, the delay between the pilot's stick input and the output to the VMS is obtained by summing the dead-time delay $T_C$ with the effective dead-time generated by the hold, to yield the motion path delay:

$$\tau_{mot} = T_C + \frac{1}{2f_C} = (3/2)T_C \tag{4.4}$$

The output of the main-frame hold also drives the CGI, which, as shown in the figure, is also modelled as a dead-time, two synchronous samplers, and a zero-order hold. The samplers and output hold circuit model the refresh characteristics of the CGI ($T_R$ is the refresh period), while the dead-time models the computational time $T_D$ required to generate the visual scene from the signal generated by the main-frame computer. Both can be independently specified, although, as shown in the figure, we assume both to be integral multiples of a base period $T_O$.
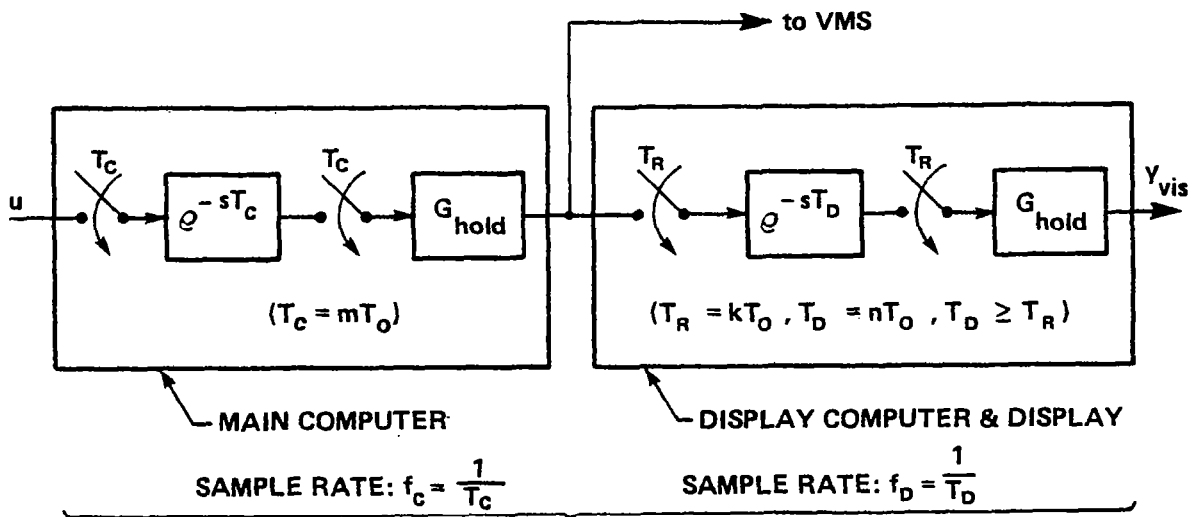
Figure 4.4:  Visual and Motion Path Delays

The sample rate $f_C$ of the main computer is simply $1/T_C$. We assume, for all CGI configurations considered, that the refresh period $T_R$ will be less than or equal to the computational time $T_D$. Thus, the effective sample rate $f_D$ through the CGI is $1/T_D$. With a main-frame computer rate of $f_C$, this implies that the overall effective sample rate associated with the visual path is given by

$$f_{eff} = MIN(f_C, f_D) \qquad (4.5)$$

This, in turn, determines the overall visual path delay, $\tau_d$, since it is obtained by simply summing the main-frame delay $T_C$, the CGI dead-time $T_D$, and the effective dead-time generated by the CGI hold, $1/(2f_{eff})$, to yield:

$$\tau_{VIS} = T_C + T_D + (1/2f_{eff}) \qquad (4.6)$$

This expression takes advantage of the fact that the delay contributed by the main-frame hold is negated by the CGI's input sampler.

The nominal simulator configuration has a CGI refresh rate of 30 Hz ($T_R$ = 33 msec) and a CGI computation time of 66 msec, so that the effective CGI display rate $f_C$ is 15 Hz. With a nominal main-frame rate of 30 Hz, (4.5) implies an effective visual path sample rate of 15 Hz, leading to a visual path delay of 132 msec, based on (4.6). The motion path delay is $(3/2)T_C$, or 50 msec

(based on (4.4)).  A similar computation of the visual and motion delays is equally straightforward using (4.4) through (4.6), for other choices of simulator parameter values.

In modelling these delay paths, we chose to increment the pilot's delay $\tau$ (which delays all display variables) by the smaller of the two delays, in this case, the motion delay of 50 msec.* The visual delay was then implemented by passing each visual display variable through a first-order Pade filter, with the effective delay of the filter set equal to the difference between the visual and motion delays.  In this way, the filter delay sums with the incremental pilot delay, to yield the desired effective visual delay.

## Visual Thresholds

In section 3.1 we discussed how visual resolution and discrimination thresholds led to informational thresholds associated with visually-obtained display variables.  Table 3.2 of that section demonstrated how these thresholds are dependent on both the effective resolution threshold and the scene geometry.  In this section we determine nominal values for these visual parameters, and specify the informational threshold levels.

---

* Due to an early change in the nominal configuration, the motion delay was inadvertently set to 33 msec, rather than the desired 50 msec.  This 17 msec difference makes little difference in overall hover performance, however, as the results of chapter 5 will show.

The angular resolution threshold imposed by the CGI is dependent on the screen frame size, the number of lines per frame, and the number of pixels per line. Taking the frame size as given in table 4.1, and assuming, for simplicity, that the line/pixel density is N lines/frame and N pixels/line, then the horizontal and vertical resolution limits will be:

$$\beta_H = 48^O/N, \qquad \beta_V = 36^O/N \tag{4.7}$$

An approximate (directionless) CGI resolution threshold can then be obtained by averaging the horizontal and vertical limits:

$$\beta = (\beta_H + \beta_V)/2 \tag{4.8}$$

For the nominal configuration of 1024 lines/frame and 1024 pixels/line this yields a CGI-imposed angular resolution limit of about 0.042 deg, smaller than the human operator threshold of 0.05 deg specified by (3.5a). In accordance with (3.7), the effective resolution threshold is thus set by the pilot's limitations:

$$\gamma = 0.05 \text{ deg} \tag{4.9a}$$

This, in conjunction with (3.8), defines the angular rate threshold for the nominal CGI configuration:

$$\dot{\gamma} = 0.20 \text{ deg/sec} \tag{4.9b}$$

One of the geometric factors determining the visual scene informational thresholds is the lateral field-of-view, $\psi_{FOV}$. Reference to table 3.2 of section 3.1.3 shows that the roll threshold $\phi_{TH}$ is inversely proportional to $\psi_{FOV}$, so that the minimum threshold is obtained with the maximum field-of-view. In the simulator environment, this is determined by the CGI screen configuration, and, as can be seen from figure 4.1, the nominal configuration has a $72^O$ half field, so that:

$$\psi_{FOV} = 72^O \qquad (4.10)$$

For screen configurations A and B, this figure would be $24^O$ and $72^O$, respectively.

A second geometric factor impacting the thresholds is the line-of-sight (LOS) depression angle $\theta_o$ for surge (x) axis information. Reference to table 3.2 shows that

$$x_{TH} \sim \theta_o / \sin^2 \theta_o \qquad (4.11a)$$
$$\dot{x}_{TH} \sim 1 / \sin^2 \theta_o \qquad (4.11b)$$

so that $x_{TH}$ and $\dot{x}_{TH}$ are minimized when $\theta_o$ is selected to be $67^O$ and $90^O$, respectively. Since figure 4.1 shows that the allowable maximum $\theta_o$ is $24^O$ for the nominal screen configuration, we can minimize the surge thresholds by choosing $\theta_o$ according to:

$$\theta_O = 24^O \qquad \text{(x-axis)} \qquad (4.12)$$

For screen configurations A and C, this figure would be $24^O$ and $60^O$, respectively.

The LOS depression angle $\theta_O$ for heave (z) axis information also impacts the threshold values. From table 3.2, we have

$$z_{TH} \sim \theta_O / \sin\theta_O \cos\theta_O \qquad (4.13a)$$
$$\dot{z}_{TH} \sim 1 / \sin\theta_O \cos\theta_O \qquad (4.13b)$$

so that $z_{TH}$ and $\dot{z}_{TH}$ are minimized when $\theta_O$ is selected to be $0^O$ and $45^O$, respectively. Since these thresholds are only moderately sensitive to $\theta_O$, we chose to select a single compromise value for both position and rate display variables:

$$\theta_O = 22.5^O \qquad \text{(z-axis)} \qquad (4.14)$$

Reference to the screen geometry of figure 4.1 shows this LOS angle to be unconstrained by the CGI configuration, and thus applicable to all three configurations.

With the hover attitude $h_O$ and visual reference range $l_O$ specified earlier by (3.6), the resolution thresholds specified by (4.9), and the geometric LOS factors specified by (4.10), (4.12) and (4.14), it is then a direct matter to calculate the visual scene informational threshold levels for the nominal configuration.

This is done in table 4.3, which shows values for not only the nominal (configuration B with 1024 lines/frame), but also for off-nominal screen geometries with finer and coarser resolution levels.

This then completes our discussion of the main-frame computer and CGI parameter mappings into specific OCM-associated parameter values. We now turn briefly to a discussion of VMS-associated parameter values.

## 4.3.2 VMS Parameters

As illustrated earlier in figure 4.2, the VMS model incorporates both second-order dynamics and appropriate position/rate/acceleration servo limits. Since no effective motion thresholds were assumed to be introduced by the VMS (e.g., those due to stiction or hysteresis), there is no necessity for the type of informational threshold mapping discussed in the previous section. The dynamics, however, must be accounted for, and this was done simply by specifying an appropriate set of state equations for each VMS axis, and augmenting the system state equation (2.1) to account for the low-pass filtering introduced by the VMS. With a second-order filter associated with each of the six motion axes, this resulted in an increase of the overall system order by 12 states.

Table 4.3:  VISUAL SCENE INFORMATIONAL THRESHOLD VALUES

VISUAL SCENE INFORMATIONAL THRESHOLD VALUES

| THRESHOLD* | RESOLUTION | 500 LINES/FRAME | | | 1000/2000 LINES/FRAME | | |
|---|---|---|---|---|---|---|---|
| | CONFIG. | A | B | C | A | B** | C |
| **ROTATION** | | | | | | | |
| LONG. $\Theta_{TH}$ | | .08 | .08 | .08 | .05 | .05 | .05 |
| LONG. $\dot{\Theta}_{TH}$ | | .34 | .34 | .34 | .20 | .20 | .20 |
| LAT. $\Psi_{TH}$ | | .08 | .08 | .08 | .05 | .05 | .05 |
| LAT. $\dot{\Psi}_{TH}$ | | .34 | .34 | .34 | .20 | .20 | .20 |
| LAT. $\phi_{TH}$ | | .10 | .04 | .04 | .06 | .02 | .02 |
| LAT. $\dot{\phi}_{TH}$ | | .42 | .16 | .16 | .25 | .09 | .09 |
| **TRANSLATION** | | | | | | | |
| LONG. $x_{TH}$ | | .84 | .84 | .47 | .84 | .84 | .47 |
| LONG. $\dot{x}_{TH}$ | | .36 | .36 | .08 | .21 | .21 | .05 |
| LONG. $z_{TH}$ | | .37 | .37 | .37 | .37 | .37 | .37 |
| LONG. $\dot{z}_{TH}$ | | .17 | .17 | .17 | .10 | .10 | .10 |
| LAT. $y_{TH}$ | | .07 | .07 | .07 | .04 | .04 | .04 |
| LAT. $\dot{y}_{TH}$ | | .30 | .30 | .30 | .17 | .17 | .17 |

\* ROTATION THRESHOLD VALUES IN DEG & DEG/SEC
  TRANSLATION THRESHOLD VALUES IN FT & FT/SEC

\*\* NOMINAL CONFIGURATION

# 5. CLOSED-LOOP ANALYSIS OF CGI AND VMS EFFECTS

In this chapter, the optimal control model with the expanded perceptual model is used to analyze the effects of CGI and VMS limitations on closed-loop performance. The flight task considered is low altitude hover in turbulence of a CH-47 helicopter. Performance decrements from ideal or perfect simulations (i.e., flight) are computed for nominal CGI and VMS configurations. The effects of individual simulation parameters are also considered.

## 5.1 Simulator Configurations

The goal of this analysis is to determine the effects of CGI and VMS characteristics on simulator fidelity (more precisely, performance and workload). To this end, a "perfect" or ideal simulator is defined in which there are no simulation time delays, no motion system dynamics, and an infinite resolution imagery system. This simulator configuration corresponds essentially to flight* and provides a benchmark against which to measure simulator deficiencies.

---

* Through an oversight, the assumptions for the perfect configuration included a field-of-view constraint relevant to the nominal CGI configuration. This degraded performance only slightly from what would have been obtained without the constraint.

Realistic or nominal CGI and VMS configurations were defined in section 4.3. For convenient reference, we have summarized the pertinent nominal simulator characteristics in table 5.1. Included in the realistic configuration is a main-frame digital computer delay of 33 msec, corresponding to a 30 Hz computation rate.

The nominal motion system did not include washout filters as all predicted motions except the surge (x) motion were well within their respective simulator limits. A surge motion washout filter was designed for the task and its effects evaluated; this will be discussed later. In addition to the nominal and perfect motion conditions, results were also obtained for a "no-motion" or fixed-base simulator configuration.

Thus, there were six basic simulator configurations to be analyzed so as to evaluate the effects of the visual and motion systems, separately and together. These configurations are listed in Table 5.2.

## 5.2  Pilot Model Parameters

The parameters of the optimal control model pertaining to information processing limitations were set on the basis of previous studies and the perceptual analyses described in Chapter 3. The numerical values and basic assumptions are summarized in Table 5.3.

Table 5.1   REALISTIC (NOMINAL) SIMULATOR CONFIGURATION


CGI CHARACTERISTICS

| | |
|---|---|
| Picture refresh rate | 30 Frames/s |
| Display compute time | 66 msec |
| Effective Sample rate/delay | 15 Hz/99 msec |
| Scene content | 6000 edges/frame |
| Field-of-view | 3 screens across ($144^O$ horiz, $36^O$ vert) |
| Display resolution | 1024 lines/frame x 1024 pixels/line |


VMS CHARACTERISTICS*

2nd order dynamics (all axes)

Position, rate, & acceleration limits (all axes)

No washout filters


*see Table 4.2 for specific parameter values

Table 5.2    SIMULATOR CONFIGURATIONS

| CONFIGURATION | DESCRIPTION |
|---|---|
| Perfect (Flight) | No simulator delays, nominal field of view, human operator thresholds, no VMS dynamics |
| Perfect CGI-Realistic VMS | Includes main frame computer delays and VMS platform dynamics |
| Realistic CGI-Perfect VMS | Includes main frame and display computer delays, CGI imposed visual thresholds, no platform dynamics |
| Realistic CGI-Realistic VMS | Includes all simulator nominal characteristics (see Table 5.1) |
| Perfect CGI-Fixed Base | Includes main frame computer delays in visual cues, no motion cues |
| Realistic CGI-Fixed Base | Includes CGI limitations, no motion cues |

## Table 5.3: NOMINAL PILOT MODEL

- **TASK OBJECTIVE**

  Maintain following RMS hover errors:

  |  |  |
  |---|---|
  | ATTITUDE | 1 DEG |
  | ATTITUDE RATE | 0.5 DEG/S |
  | POSITION | 5 FT |
  | VELOCITY | 1 FT/S |

- **INFORMATION-PROCESSING/CONTROL-BANDWIDTH LIMITATIONS**

  |  |  |
  |---|---|
  | OBSERVATION NOISE/SIGNAL RATIO | -20 DB |
  | INTERNAL TIME DELAY | 0.20 S |
  | MOTOR TIME CONSTANT | 0.15 S |

- **VISUAL PERCEPTION MODEL**

  PERSPECTIVE/GEOMETRIC CUES
  NO SENSORY DYNAMICS
  RESOLUTION/DISCRIMINATION THRESHOLDS

- **MOTION PERCEPTION MODEL**

  ROTATIONAL AND SPECIFIC FORCE CUES
  VESTIBULAR DYNAMICS (CANALS & OTOLITHS)
  RESOLUTION THRESHOLDS

- **ATTENTION-SHARING MODEL**

  SHARED ATTENTION BETWEEN LONGITUDINAL AND LATERAL AXES
  NO INTERFERENCE BETWEEN MODALITIES
  OPTIMUM SHARING WITHIN MODALITIES

## 5.3 Results and Discussion

The effects of CGI and motion system characteristics will be examined largely in terms of relative performance in the hovering task. For each axis, relative performance is defined as

$$\text{Performance (in \%)} = 100 \times (J - J_{FLT})/J_{FLT} \qquad (5.1)$$

where $J$ is the value of the cost functional of (4.2) and $J_{FLT}$ corresponds to the value of $J$ obtained for flight or the "perfect" simulator. Thus, relative performance is a normalized metric of performance that measures the percent deviation from "flight" performance introduced by the simulator characteristics. In this sense, relative performance is a measure of simulator fidelity.

The results will be presented in terms of $J$ (rather than individual error and control scores) because this quantity is a scalar metric of overall performance and, therefore, provides a concise description of the simulator effects. In addition, Hess (1977) has shown that the value of $J$ may be correlated with vehicle flying qualities, so increases in $J$ owing to simulator deficiencies may be related to degraded flying qualities for the simulator. Nonetheless, individual error and control scores may also be of interest and these are presented later in table 5.5 for the six simulator configurations.

Table 5.4 summarizes the optimal attention split found for the nominal fixed and moving base simulator configurations. As discussed in Kleinman (1976), the attention paid to a variable indicates its relative importance to the task. Table 5.4 shows that pitch and pitch rate information is the single most important visually obtained variable for the longitudinal axis, while roll and roll rate are most useful for lateral control. Of the vestibular cues, pitch, pitch rate, and z-axis specific force are all important for longitudinal control, while y-axis specific force is the most useful cue for lateral control.

## 5.3.1  Overall CGI and Motion System Effects

Figure 5.1 presents the model performance predictions for the five simulator configurations, relative to that expected from the "perfect" simulator (which, by definition, has a relative performance of zero). With respect to longitudinal performance (figure 5.1a), it can be seen that the effect of the CGI is much more significant ( 35%) than that of the motion system ( 10%). Indeed, performance is better with a perfect CGI and no motion than with perfect motion and a realistic CGI. However, motion is still important, particularly if the realistic CGI deficiencies are accounted for. This is shown by the prediction of approximately twice the relative performance for the realistic CGI-fixed base configuration as for the realistic CGI-realistic VMS configuration.

Table 5.4:  ATTENTION ALLOCATION FOR NOMINAL CONFIGURATIONS

| | | VARIABLE | MOVING BASE | FIXED BASE |
|---|---|---|---|---|
| LONGITUDINAL AXIS | VISUAL | $X,\dot{X}$ | 0.047 | 0.045 |
| | | $Z,\dot{Z}$ | 0.087 | 0.053 |
| | | $\Theta,\dot{\Theta}$ | 0.366 | 0.402 |
| | | | 0.500 | 0.500 |
| | VESTIBULAR | FX | 0.021 | |
| | | FZ | 0.137 | |
| | | $\dot{\Theta},\ddot{\Theta}$ | 0.291 | |
| | | | 0.500 | |
| LATERAL AXIS | VISUAL | $Y,\dot{Y}$ | 0.105 | 0.088 |
| | | $\phi,\dot{\phi}$ | 0.366 | 0.386 |
| | | $\psi,\dot{\psi}$ | 0.029 | 0.026 |
| | | | 0.500 | 0.500 |
| | VESTIBULAR | FY | 0.339 | |
| | | $\dot{\phi},\ddot{\phi}$ | 0.141 | |
| | | $\dot{\psi},\ddot{\psi}$ | 0.020 | |
| | | | 0.500 | |

742
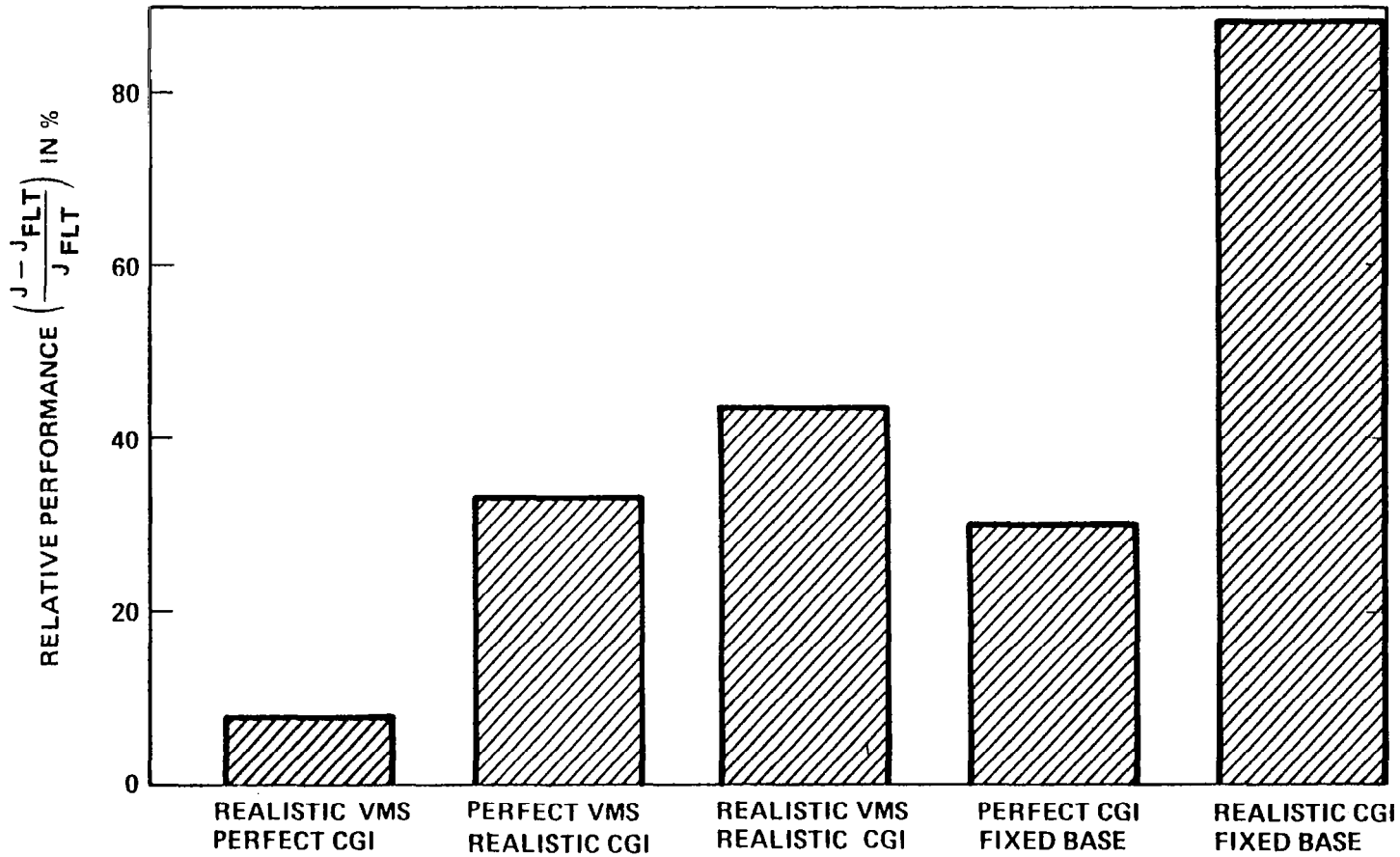
Figure 5.1a:   Relative Performance Vs. Simulator Configuration
(CH-47 Longitudinal Axis)
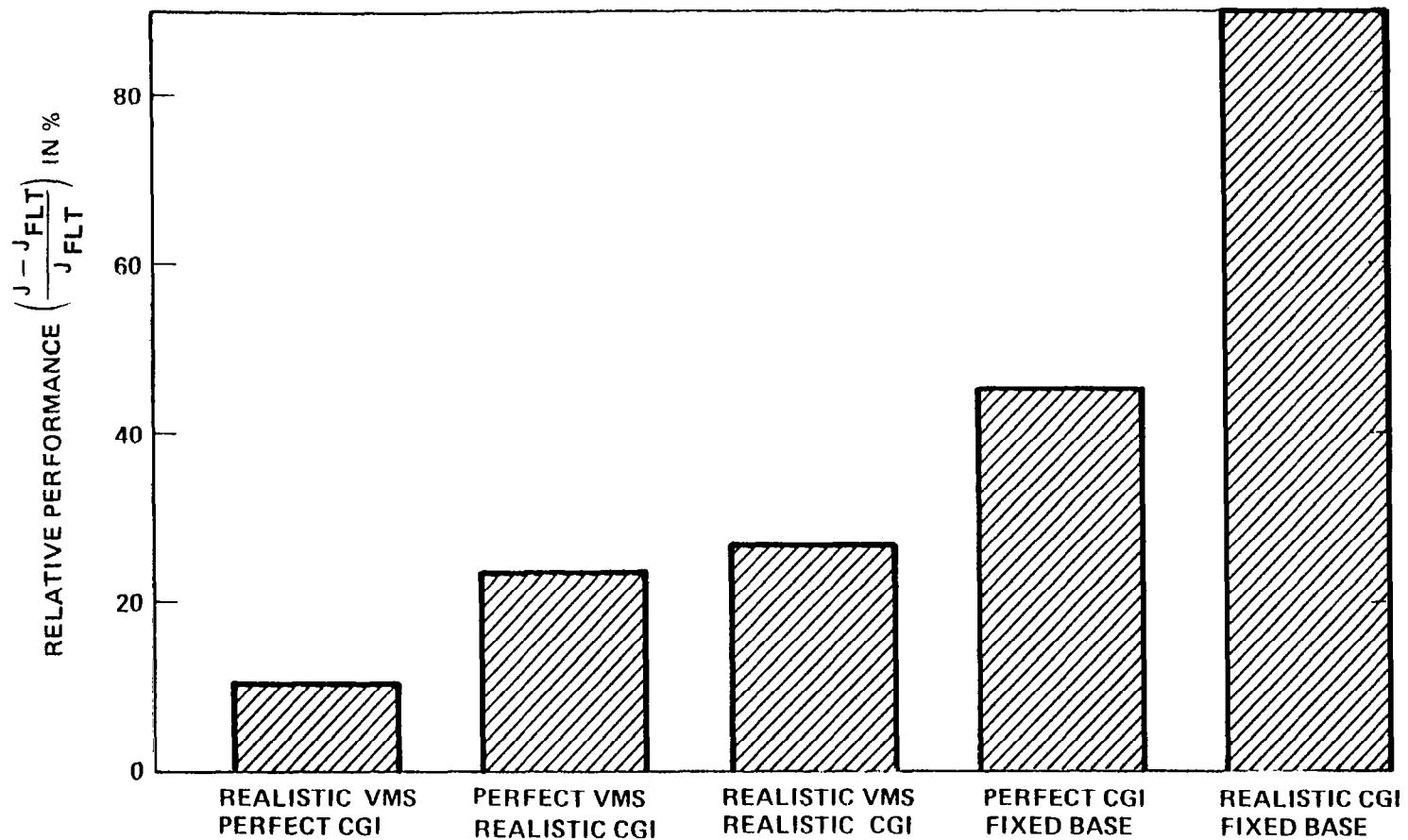
Figure 5.1b:   Relative Performance Vs. Simulator Configuration

(CH-47   Lateral Axis)

The results for the lateral control task (figure 5.1b) are similar to those for the longitudinal task, but motion is even more important. In this case, having a perfect CGI does not compensate for lack of motion, since the fixed base configurations are worse than any other motion configuration. Compared to the longitudinal task, going from perfect to realistic motion introduces less performance degradation. Also, motion ameliorates the consequences of any visual deficiencies.

For either longitudinal or lateral control, the performance change (10-15%) due to introducing the realistic motion system alone is probably within the inter- and intra-pilot variations that might be expected. However, once realistic CGI effects are considered, or motion is removed entirely, this is no longer likely to be true for skilled pilots inasmuch as the deviations predicted can be substantially greater than 20%.

Table 5.5 gives the effects of simulator configurations on individual rms error scores. These scores generally tend to parallel the effects shown for relative performance, as would be expected. However, it is interesting to note that predicted control scores are less affected by simulator changes than are output variables. Indeed, the control scores remain fairly

| Variable | Units | Unaugmented CH-47 Dynamics | | | | | | Augmented CH-47 Dynamics | | |
|---|---|---|---|---|---|---|---|---|---|---|
| | | Simulator Configuration | | | | | | | | |
| | | P Sim | R VMS P CGI | P VMS R CGI | R VMS R CGI | F B P CGI | F B R CGI | P Sim * | R VMS R CGI | F B R CGI |
| $\sigma_x$ | ft | 4.85 | 5.14 | 5.72 | 5.93 | 5.49 | 6.87 | 2.76 | 3.05 | 3.32 |
| $\sigma_{\dot{x}}$ | ft/sec | 0.92 | 0.80 | 1.09 | 1.13 | 1.04 | 1.30 | 0.55 | 0.60 | 6.50 |
| $\sigma_z$ | ft | 1.77 | 1.91 | 2.06 | 2.11 | 2.11 | 2.47 | 0.99 | 1.12 | 1.31 |
| $\sigma_{\dot{z}}$ | ft/sec | 0.60 | 0.66 | 0.67 | 0.70 | 0.78 | 0.87 | 0.39 | 0.42 | 0.56 |
| $\sigma_\theta$ | deg | 0.82 | 0.87 | 0.96 | 1.00 | 0.92 | 1.13 | 0.5 | 0.54 | 0.56 |
| $\sigma_{\dot{\theta}}$ | deg/sec | 0.85 | 0.92 | 0.99 | 1.03 | 0.97 | 1.17 | 0.43 | 0.46 | 0.45 |
| $\sigma_y$ | ft | 6.50 | 6.91 | 7.46 | 7.52 | 8.37 | 9.72 | 4.31 | 4.56 | 5.63 |
| $\sigma_{\dot{y}}$ | ft/sec | 1.27 | 1.35 | 1.44 | 1.46 | 1.65 | 1.91 | 0.88 | 0.93 | 1.15 |
| $\sigma_\phi$ | deg | 1.72 | 1.76 | 1.81 | 1.82 | 1.90 | 2.06 | 1.53 | 1.54 | 1.62 |
| $\sigma_{\dot{\phi}}$ | deg/sec | 1.05 | 1.1 | 1.18 | 1.20 | 1.27 | 1.46 | 0.65 | 0.67 | 0.73 |
| $\sigma_\psi$ | deg | 0.42 | 0.44 | 0.37 | 0.47 | 0.46 | 0.62 | 0.06 | 0.06 | 0.07 |
| $\sigma_{\dot{\psi}}$ | deg/sec | 0.15 | 0.16 | 0.15 | 0.17 | 0.20 | 0.24 | 0.04 | 0.05 | 0.05 |
| $\sigma_{\delta_e}$ | inches | 0.23 | 0.23 | 0.23 | 0.24 | 0.23 | 0.24 | 0.24 | 0.24 | 0.24 |
| $\sigma_{\delta_c}$ | inches | 0.14 | 0.15 | 0.15 | 0.15 | 0.15 | 0.16 | 0.12 | 0.12 | 0.13 |
| $\sigma_{\delta_a}$ | inches | 0.16 | 0.16 | 0.17 | 0.17 | 0.17 | 0.19 | 0.27 | 0.27 | 0.28 |
| $\sigma_{\delta_r}$ | inches | 0.03 | 0.03 | 0.03 | 0.03 | 0.03 | 0.04 | 0.04 | 0.04 | 0.04 |

*P    Perfect
R    Realistic
F B    Fixed Base

Table 5.5   RMS PERFORMANCE SCORES

constant over the various conditions.*

The above model predictions are based on the assumption that the pilot will maintain a fixed level of attention for the longitudinal and lateral control tasks regardless of simulator configuration. However, in actuality, the pilot may choose to devote more (or less) attention to the control tasks, based on simulator configuration. To explore the effects of such a change in strategy, model predictions were obtained for various attention levels. The results are presented in figure 5.2. It can be seen that the relative ordering of simulator configurations is maintained at all levels of attention. At high levels of attention, the performance with the realistic CGI-perfect VMS configuration approaches that for the realistic VMS-perfect CGI configuration. Apparently, if the noise/signal ratio is lowered sufficiently on the motion cues, it can offset some of the visual deficiencies associated with the nominal CGI.

If it is assumed that the pilot adapts his behavior and increases attention levels to achieve performance equivalent to that in flight, then the incremental attention required may be considered a workload penalty associated with the simulator. The curves of figure 5.2 can be used to determine this workload penalty

---

\* As a result, inner loop variables ($\theta$ and $\phi$) are somewhat less affected than outer loop quantities ($x,y,z$ and $\psi$).
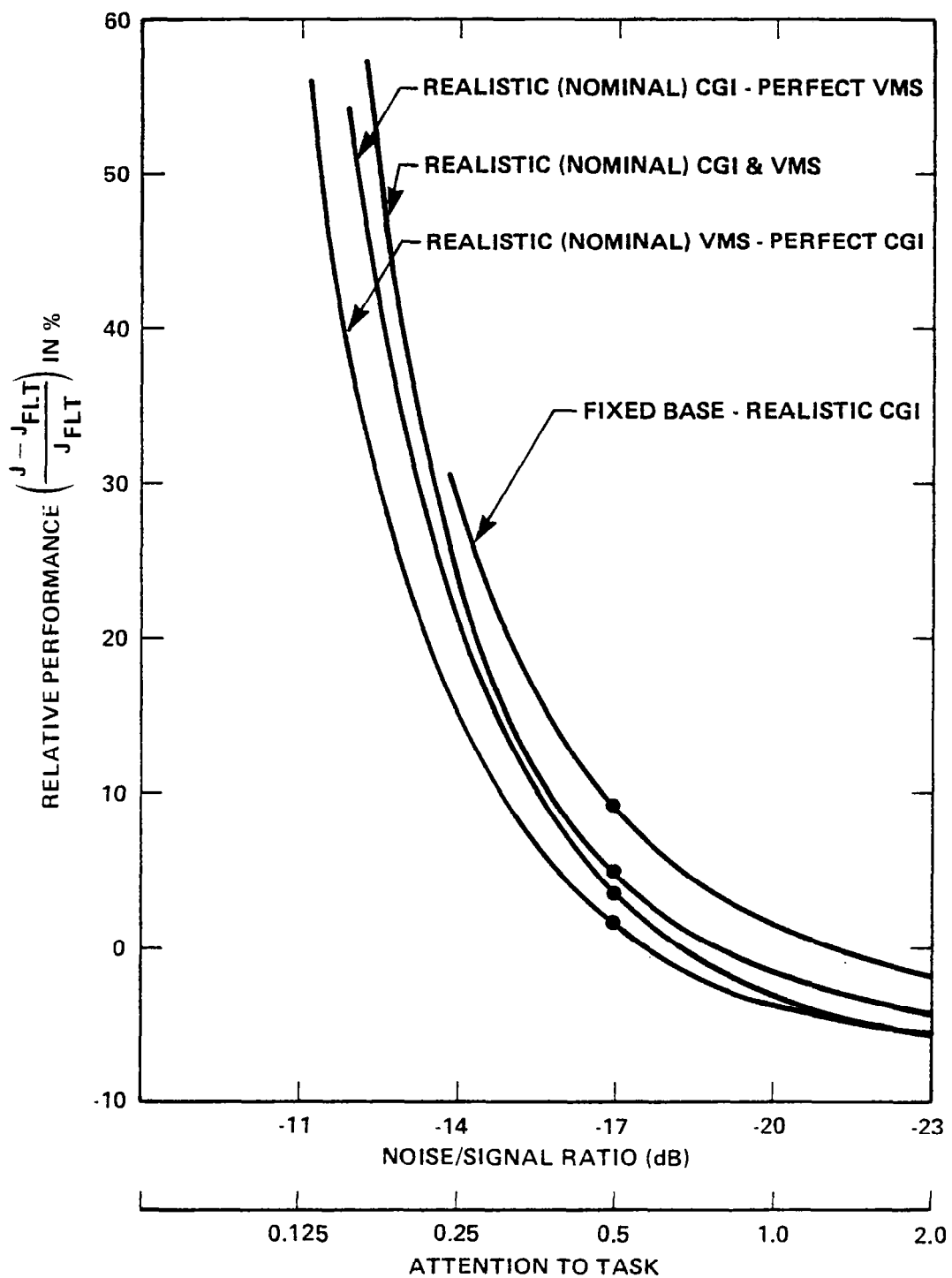
Figure 5.2a: Effect of Workload (CH-47 Longitudinal Axis)
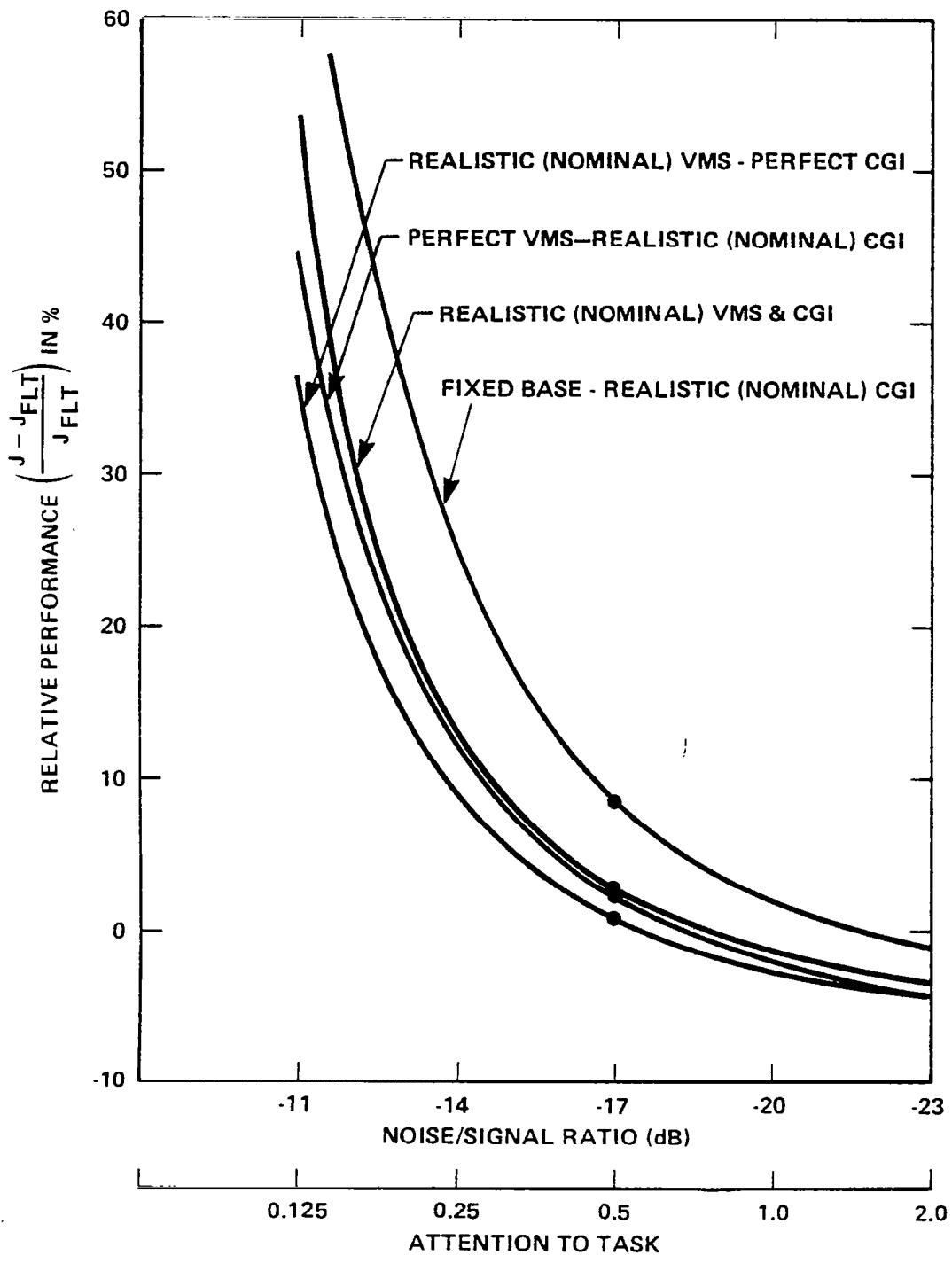
Figure 5.2b:  Effect of Workload (CH-47 Lateral Axis)

for maintaining flight level performance in the simulator; one simply determines the intersection of the particular sensitivity curve with the line of zero relative performance. The computed attention or workload penalties for the various configurations analyzed in Figure 5.2 are given in table 5.6. For the nominal CGI and motion system, the pilot would have to increase attention by 50% over that needed in flight in order to achieve the same performance, whereas almost three times as much attention is required for a fixed base simulation.

Table 5.6   SIMULATOR WORKLOAD PENALTIES

| Condition | - Attention - | | |
|-----------|-------|------|-------|
| | Long. | Lat. | Total |
| | .5 | .5 | 1.00 |
| R. VMS, P. CGI | .55 | .58 | 1.13 |
| P. VMS, R. CGI | .66 | .69 | 1.35 |
| R. VMS, R. CGI | .76 | .76 | 1.52 |
| R. CGI - F. B. | 1.25 | 1.5 | 2.75 |

## 5.3.2 Effects of CGI Parameters

The results of the previous section suggest that the visual processing limitations introduced by a nominal CGI configuration could result in significant deteriorations of closed-loop hover performance. Here, we examine the effects of variations in individual, design-related CGI parameters. In these analyses, a single parameter is varied while all other CGI parameters are kept at their nominal or realistic values. Results will be presented for both realistic motion base and fixed base configurations.

Figures 5.3 and 5.4 show the effect of incremental delays on relative performance for motion-base and fixed-base simulators, respectively. Results are presented as a function of CGI display computer delay, for three values of main-frame computer delay ($T_c$). Recall, the nominal display delay is 99 msec (~.1 sec). For the range of delays considered, relative performance appears to degrade linearly as a function of either display delay or main-frame delay, when motion is present. Comparison of figures 5.3 and 5.4 (note the difference in scale) reveals that the absence of motion cues will accentuate the deterioration of performance for a given delay. Moreover, for a fixed base configuration, performance degrades more rapidly than linearly. It can also be seen from these figures that the longitudinal control task is more sensitive to increases in delay than is the lateral task, particularly to increases in display delays.
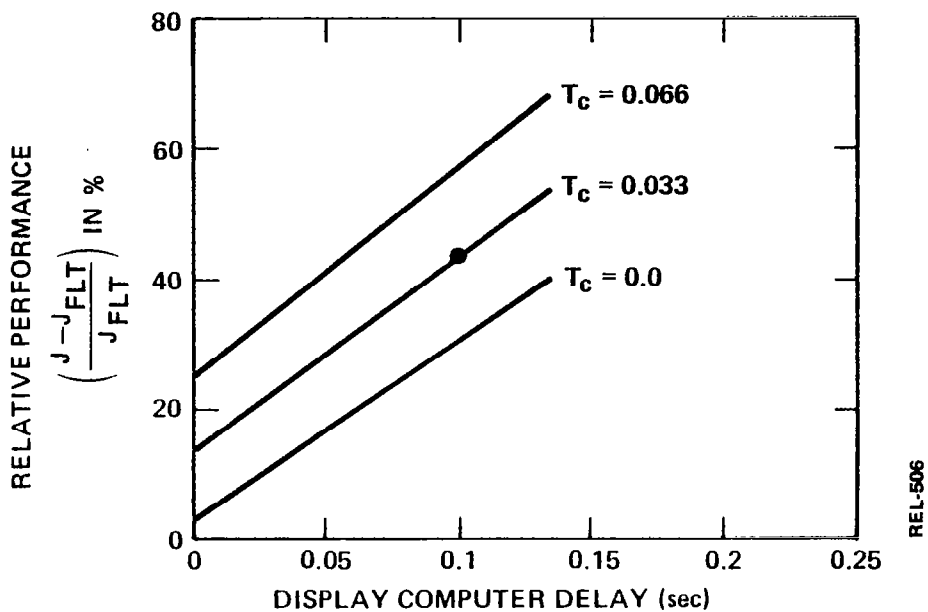
Figure 5.3a:   Relative Performance vs. Time Delay
                (Longitudinal Axis - Moving Base)
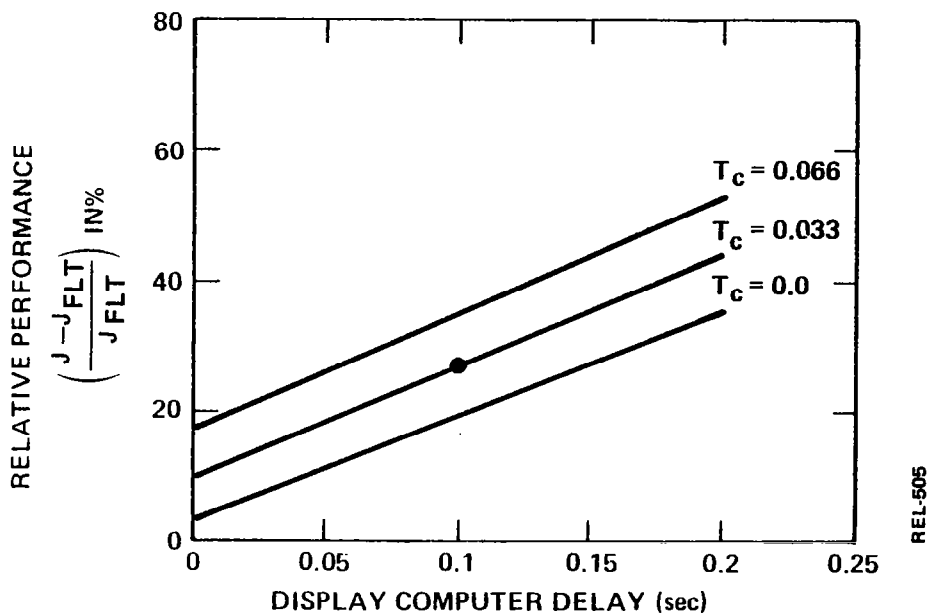


Figure 5.3b:   Relative Performance vs. Time Delay
                (Lateral Axis - Moving Base)
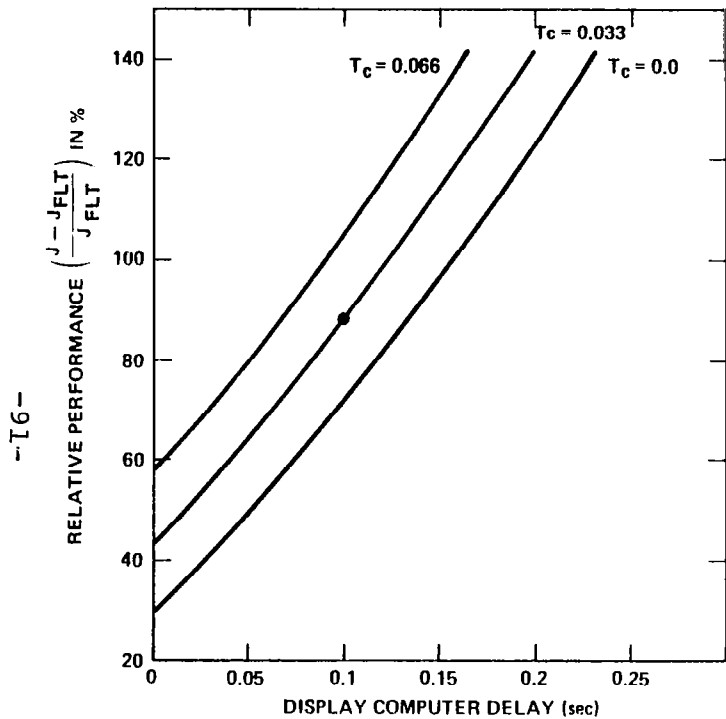
Figure 5.4a: Relative Performance Vs.
Time Delay (Longitudinal
Axis - Fixed Base)
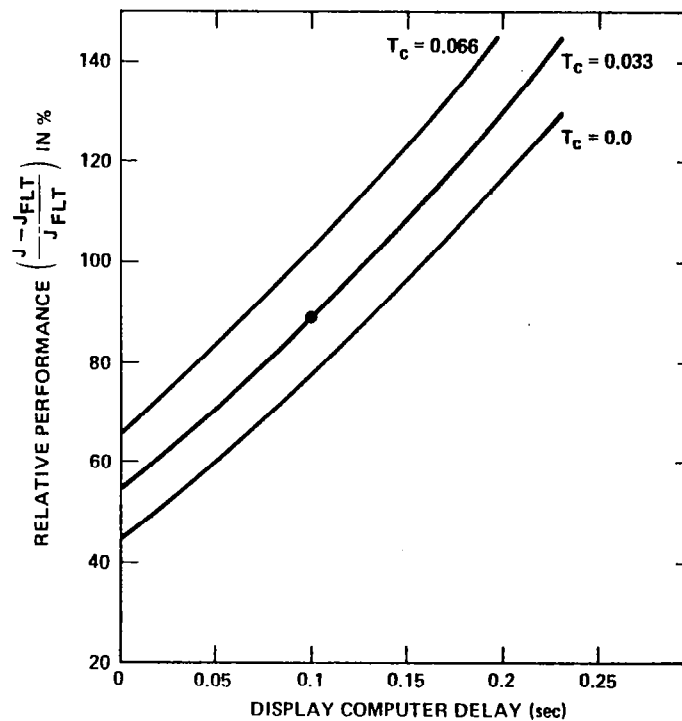


Figure 5.4b: Relative Performance Vs.
Time Delay (Lateral Axis -
Fixed Base)

In general, the magnitude of the effects of display delay are quite significant. Increasing display delay from zero to the nominal, but reasonably conservative, value of 99 msec, causes an increase in relative performance of approximately 20-30% for the motion-base simulation and about 40-50% for the fixed-base case. An examination of the relative performance values for zero display and computer delay shows that the effects of other CGI or motion system limitations are much less significant (at nominal values) than are the effects due to delays.

The effects of field-of-view and display resolution are presented in figure 5.5. Recall that screen configuration B is the nominal configuration corresponding to a $144^{\circ}$ horizontal, $36^{\circ}$ vertical field of view. Configurations A and C provide $48^{\circ}$ by $36^{\circ}$ and $144^{\circ}$ by $72^{\circ}$ fields of view, respectively. The nominal display resolution is 1024 lines. Both field of view and display resolution are assumed to affect observational thresholds as discussed in Section 3.3 and summarized in Table 4.3.

It can be seen from figure 5.5 that decreasing the horizontal field of view (configuration A) does not affect longitudinal performance and increasing the vertical field-of-view has no effect on lateral performance. This is expected because of the assumed
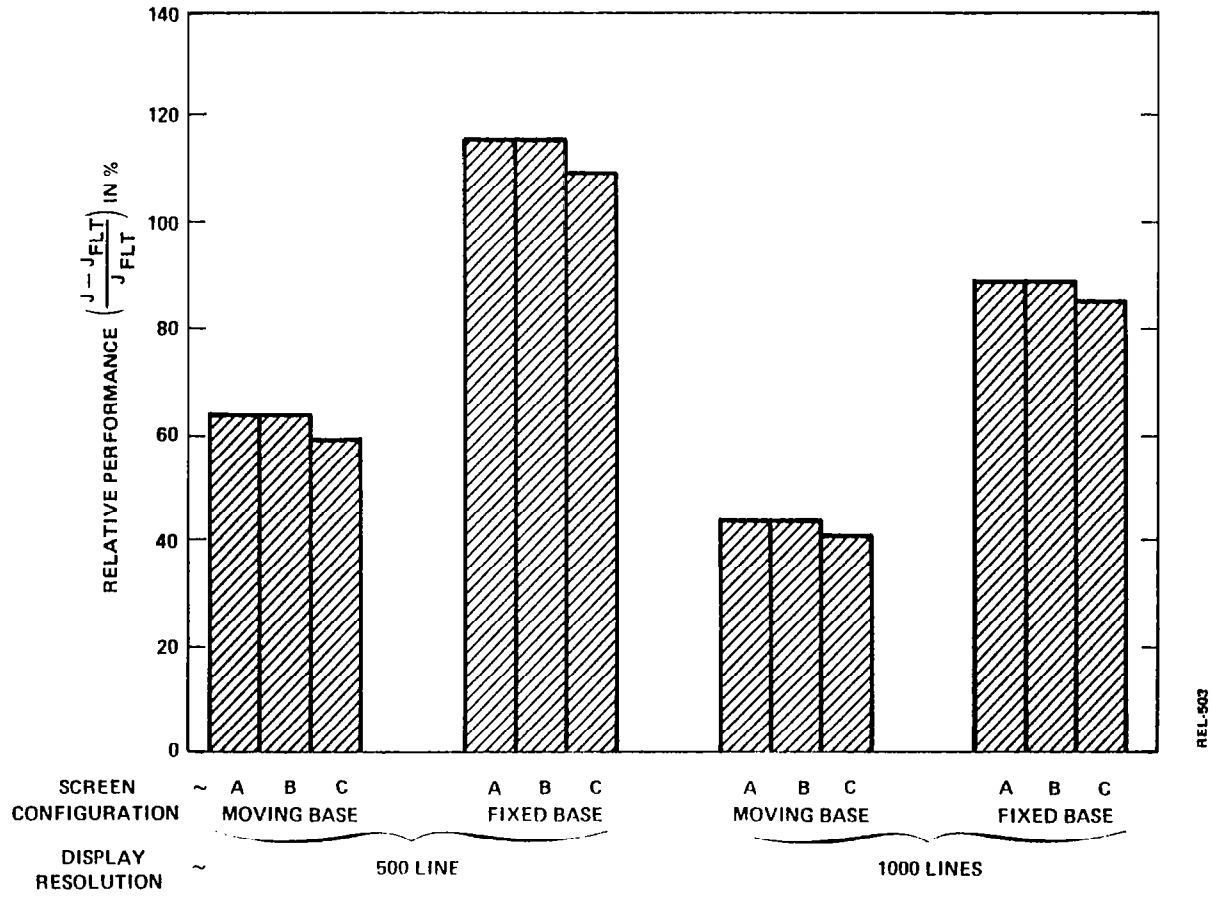
Figure 5.5a: Relative Performance Vs. Field of View and Display Resolution
(CH-47 Longitudinal Axis)
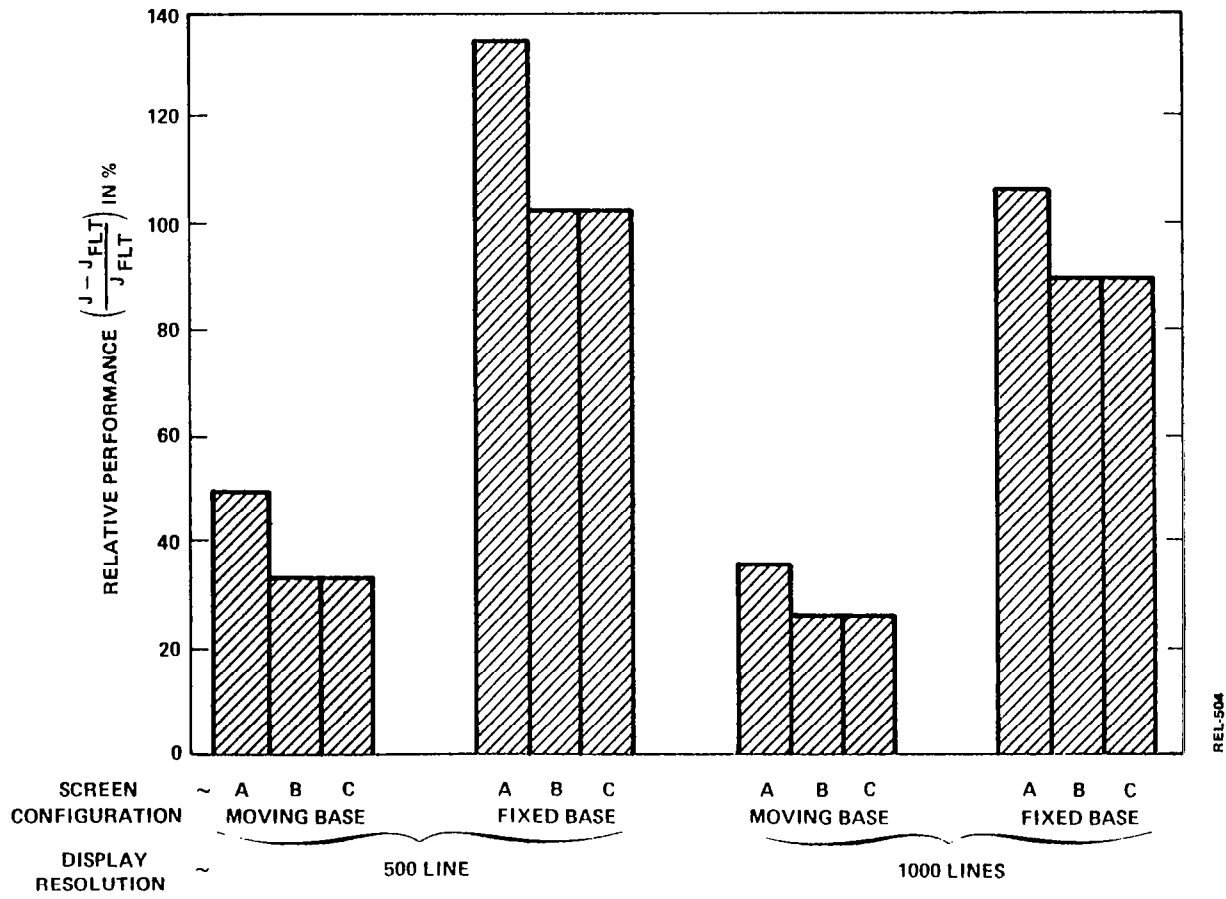
Figure 5.5b: Relative Performance Vs. Field of View and Display Resolution
(CH-47 Lateral Axis)

decoupling between longitudinal and lateral control tasks.* Figure 5.5 also suggests that increasing vertical field-of-view has very little performance payoff and probably would not be justified on the basis of these results.  On the other hand, the improvement in performance with increased lateral field-of-view appears to be significant, especially if the cue presentation is degraded in other ways, such as poorer resolution or no motion.  For the 500 line display, fixed base configuration, reduction of the horizontal field-of-view from $144^{O}$ to $48^{O}$ degrades relative performance by more than 30%.

The effects of display resolution are somewhat different than for field-of-view in that a greater effect is observed for the longitudinal task than the lateral task.  With motion, longitudinal performance is about 20% poorer for the 500 line display as compared to about a 5% degradation in the lateral case; for the fixed-base configurations, these effects are increased to about 25-30% and 10%, respectively.

In order to determine whether the results obtained were highly dependent on the particular values assumed for thresholds as a function of CGI configuration, a sensitivity analysis was

* The possible effects of increased field of view providing useful peripheral information on vehicle rates have not been examined here.

performed. In this analysis, thresholds associated with state variables (and their corresponding rates) were varied, individually or covaried based on the display threshold modelling described in section 3.1. At the same time other thresholds remained fixed, so that relative sensitivity to variations in each could be determined. The results are plotted in figure 5.6. Points corresponding to the nominal threshold values are displayed on the curves. These results show that errors in the assumptions about thresholds on positional variables (or their derivatives) would not change the overall predictions very much, with the possible exception of the threshold on lateral deviation, y. The performance predictions are more sensitive to variations in attitude thresholds, particularly the pitch threshold. For pitch, halving the threshold improves relative performance by about 25%, whereas doubling the threshold degrades performance by about 75%.

In general, it seems likely that the predictions of the effects of threshold are reasonably robust with respect to variations in the values used. Moreover, if thresholds on pitch are not estimated correctly, the results will be changed much more if the nominal value is less than the true value than if the converse is true. Given that either type of error in estimating the pitch threshold is equally probable, the predictions corresponding to the nominal value are conservative; i.e., the relative performance is more likely to be worse than predicted than
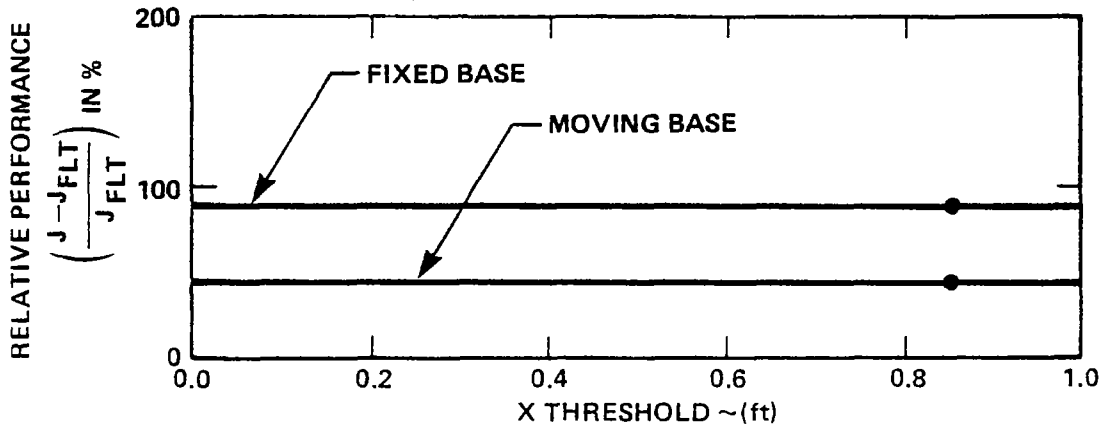
Figure 5.6a:    Relative Performance Vs. X Threshold
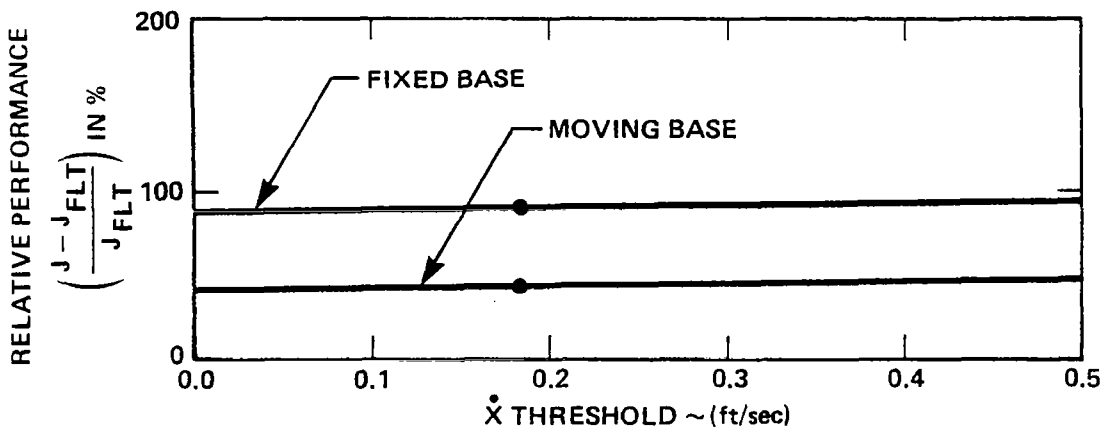


Figure 5.6b:    Relative Performance Vs. $\dot{X}$ Threshold
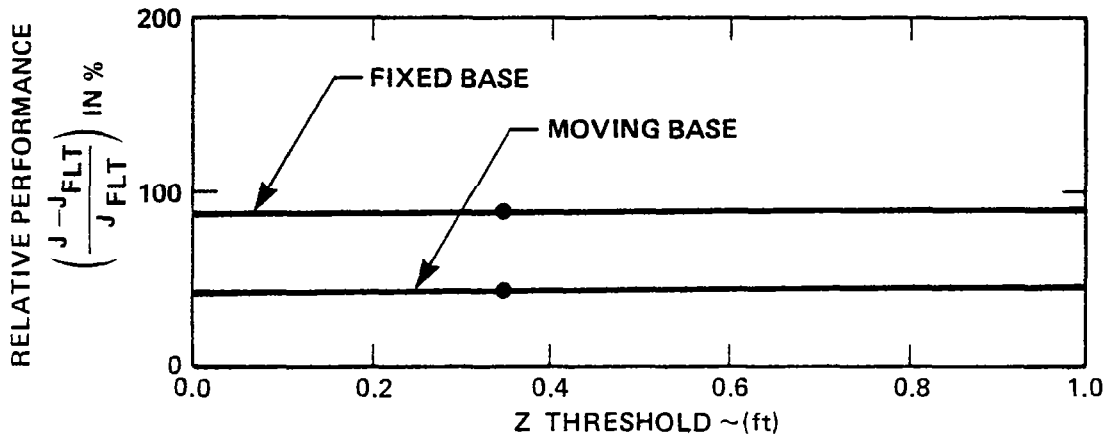
Figure 5.6c:  Relative Performance Vs. Z Threshold
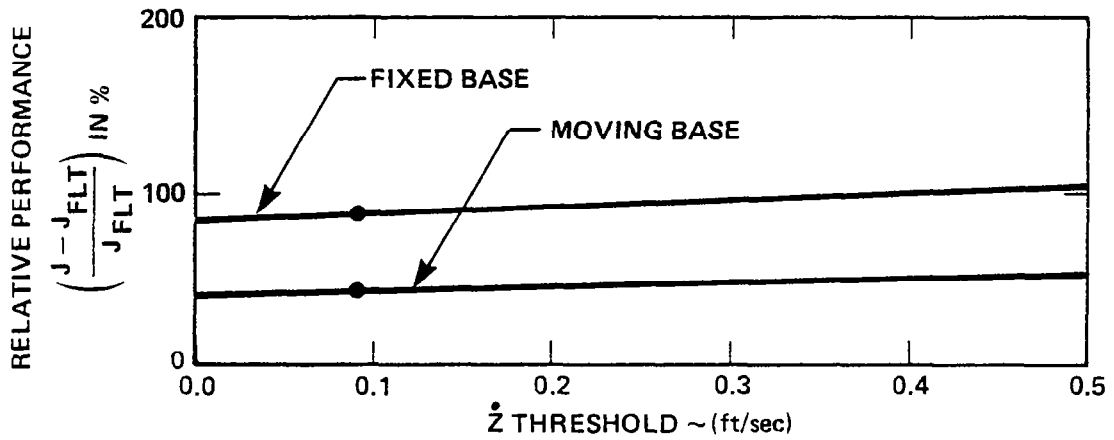


Figure 5.6d:  Relative Performance Vs. Ż Threshold
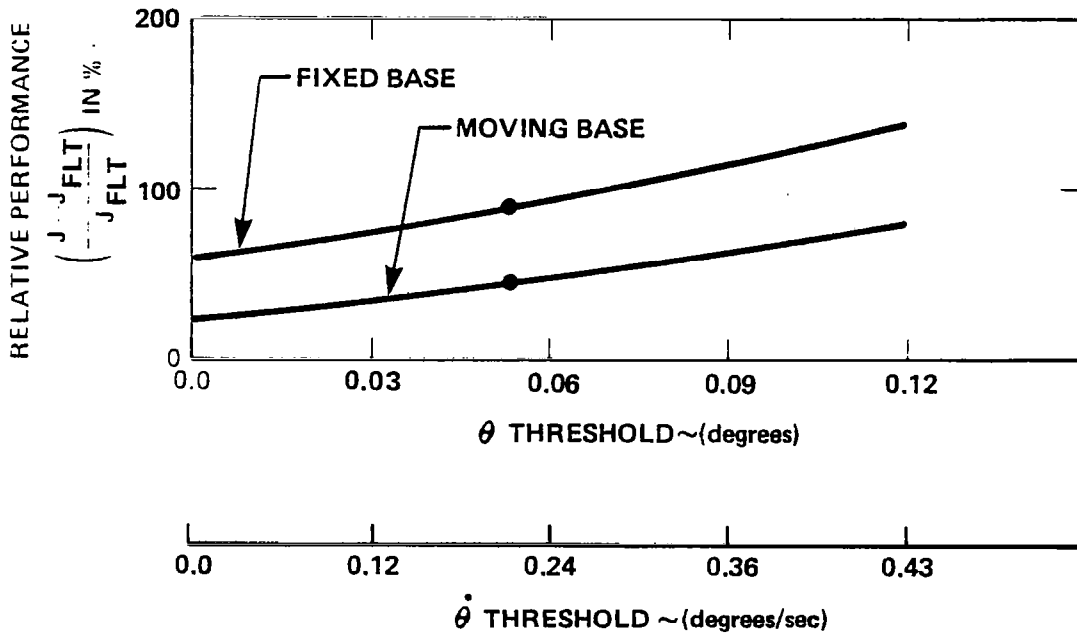
Figure 5.6e:   Relative Performance Vs. $\theta$ And $\dot{\theta}$ Thresholds
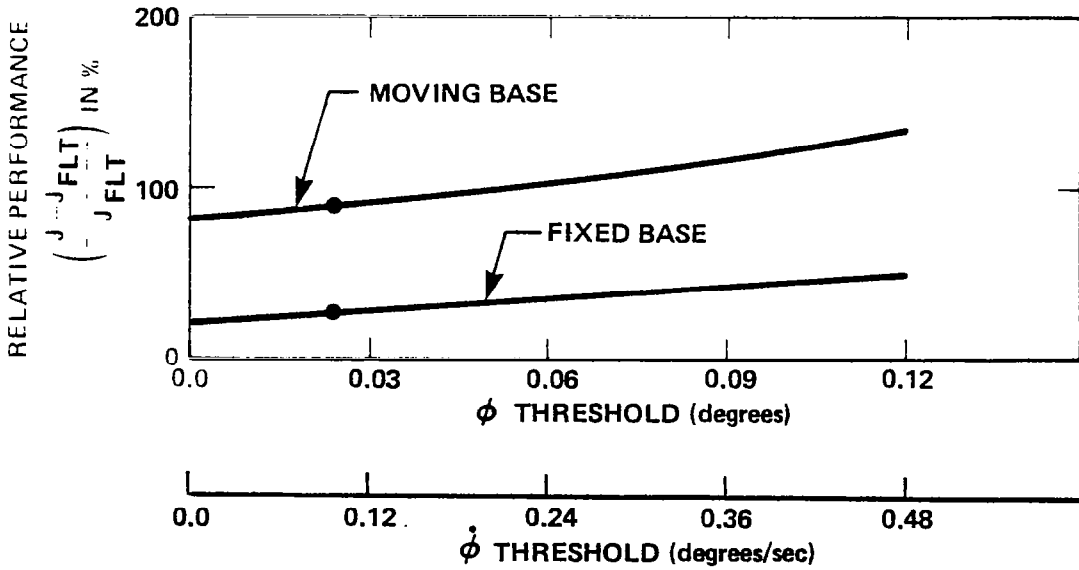


Figure 5.6f:   Relative Performance Vs. $\phi$ And $\dot{\phi}$ Thresholds
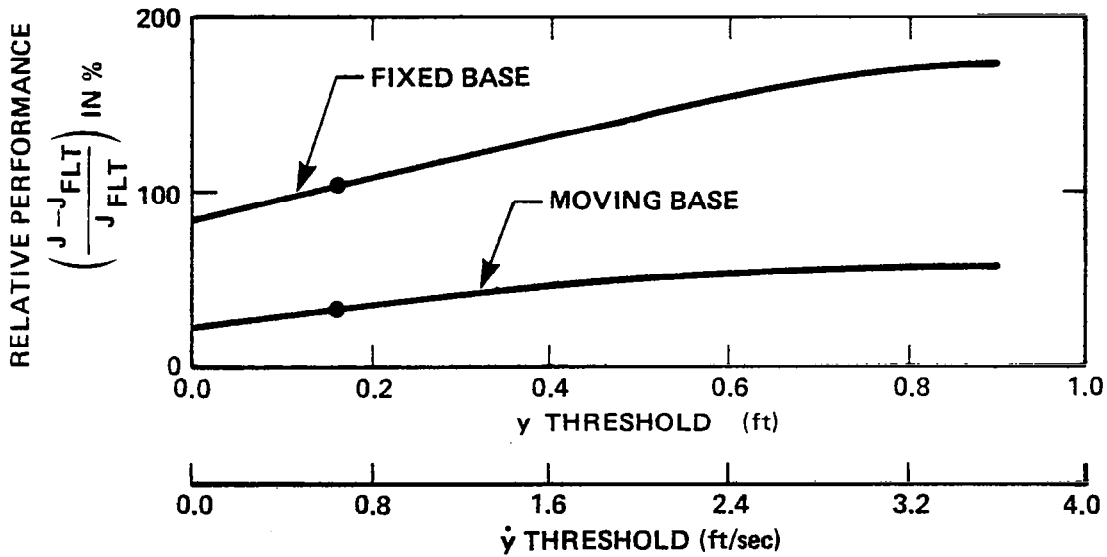
Figure 5.6g:   Relative Performance Vs. Y And Ẏ Thresholds
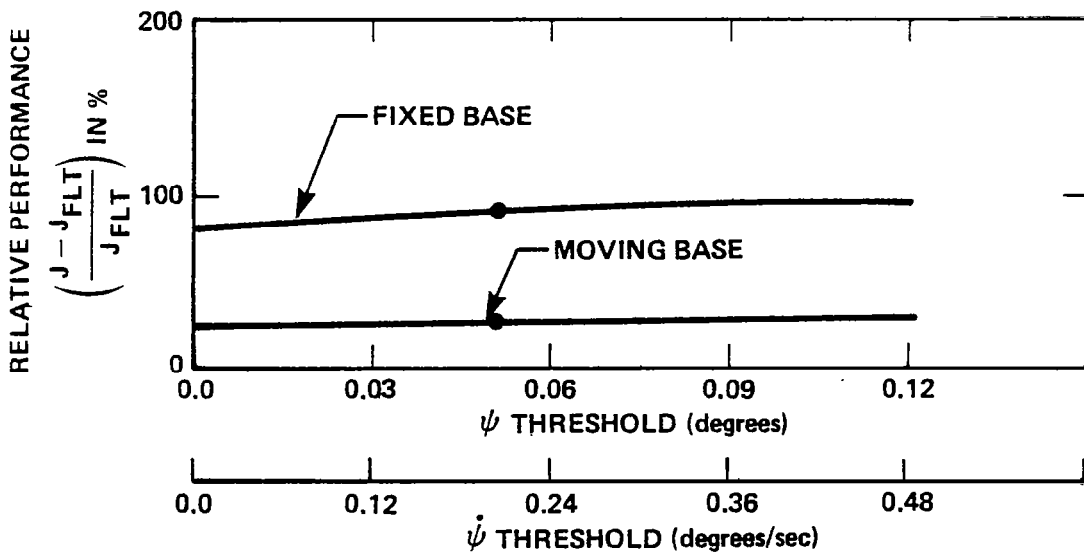


Figure 5.6h:   Relative Performance Vs. $\psi$  And $\dot{\psi}$  Thresholds

better than predicted. It should be noted however, if many of the thresholds are in error their composite effect may be significant.

Figure 5.7 shows the sensitivity of relative performance to changes in observation noise ratio, with all other parameters fixed at their nominal values. It is reasonable to conjecture that observation noise/signal ratio is affected by the scene content--the more realistic and compelling the scene, the greater the motivation and attention and the lower the noise ratio.* It can be seen from the plots of figure 5.7 that the "knees" of the sensitivity curves are approximately at the nominal noise/signal ratios Thus, lower increased noise rates would not result in performance predictions much better than those for the nominal value, but larger noise ratios could degrade performance substantially. The nominal value of noise/signal ratio (-20 dB for full attention to the combined longitudinal, lateral task) is typical of the values measured in laboratory tracking tasks with symbolic displays. One might expect a real world scene to increase pilot motivation leading to a lower noise ratio and marginally better performance than predicted by the nominal. However, if the computer generated scene is impoverished in any significant way, it

---

* Alternatively, the finer the detail of the scene, the less necessary it is to share attention among different parts of the scene in order to obtain the same quality of information--thus, effectively, reducing the overall noise ratio.
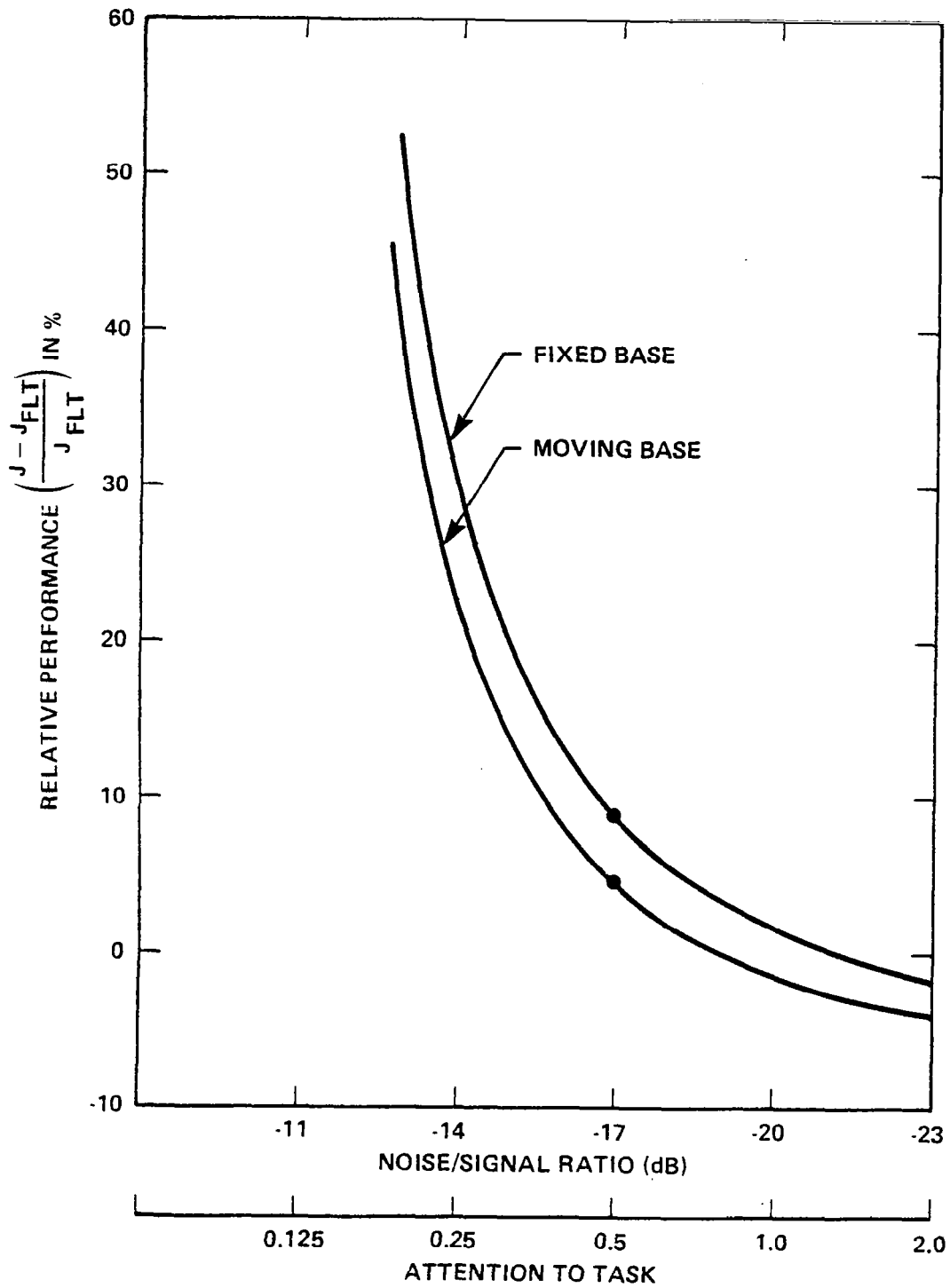
Figure 5.7a: Relative Performance Vs. Observation Noise Ratio
(CH-47 Longitudinal Axis)
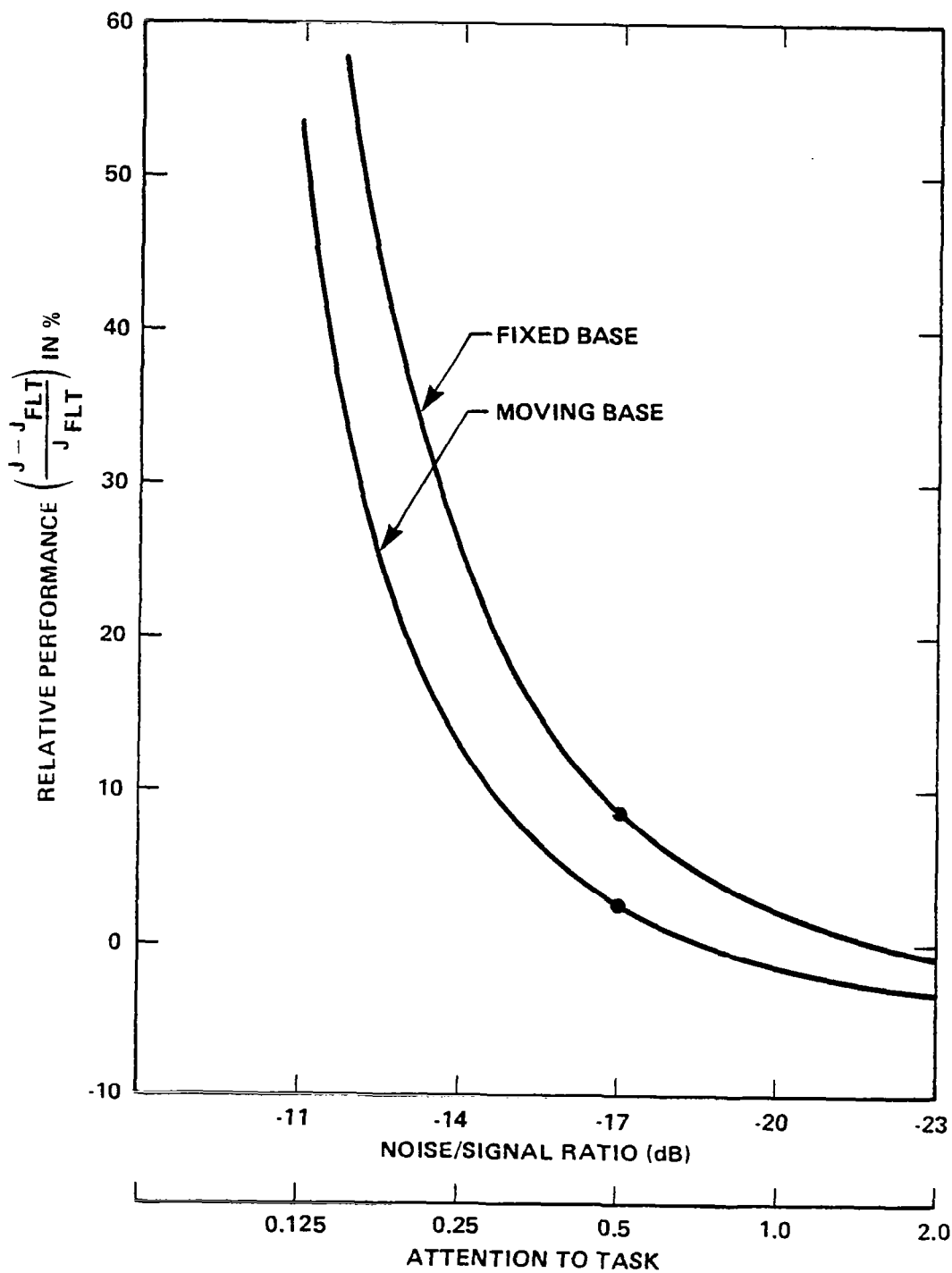
-102-

Figure 5.7b: Relative Performance Vs. Observation Noise Ratio
(CH-47 Lateral Axis)

may not provide the required control information in a more precise, integrated or attention-getting fashion than a symbolic display; if this were the case, relative performance could be affected severely.

Before leaving this discussion of the effects of individual CGI parameters, it should be noted, as a caution, that the assumption of a one-to-one correspondence with model parameters is made for simplicity. In reality, design changes can alter several factors related to information processing and tradeoffs are often the result. For example, improved scene content may lower noise/signal ratios but may require more computation and, hence, increase delay.

## 5.3.3  Effects of VMS Parameters

Only two aspects of the motion system were examined independently, VMS platform bandwidth and the presence or absence of a surge motion washout filter. Relative performance is plotted as a function of platform bandwidth and control task in figure 5.8. A bandwidth of zero corresponds to a fixed base configuration and an infinite bandwidth corresponds to flight motion. It can be seen that changing the bandwidth does not have an appreciable effect on relative performance, so long as a reasonable degree of motion fidelity is maintained. The effects of bandwidth are somewhat more
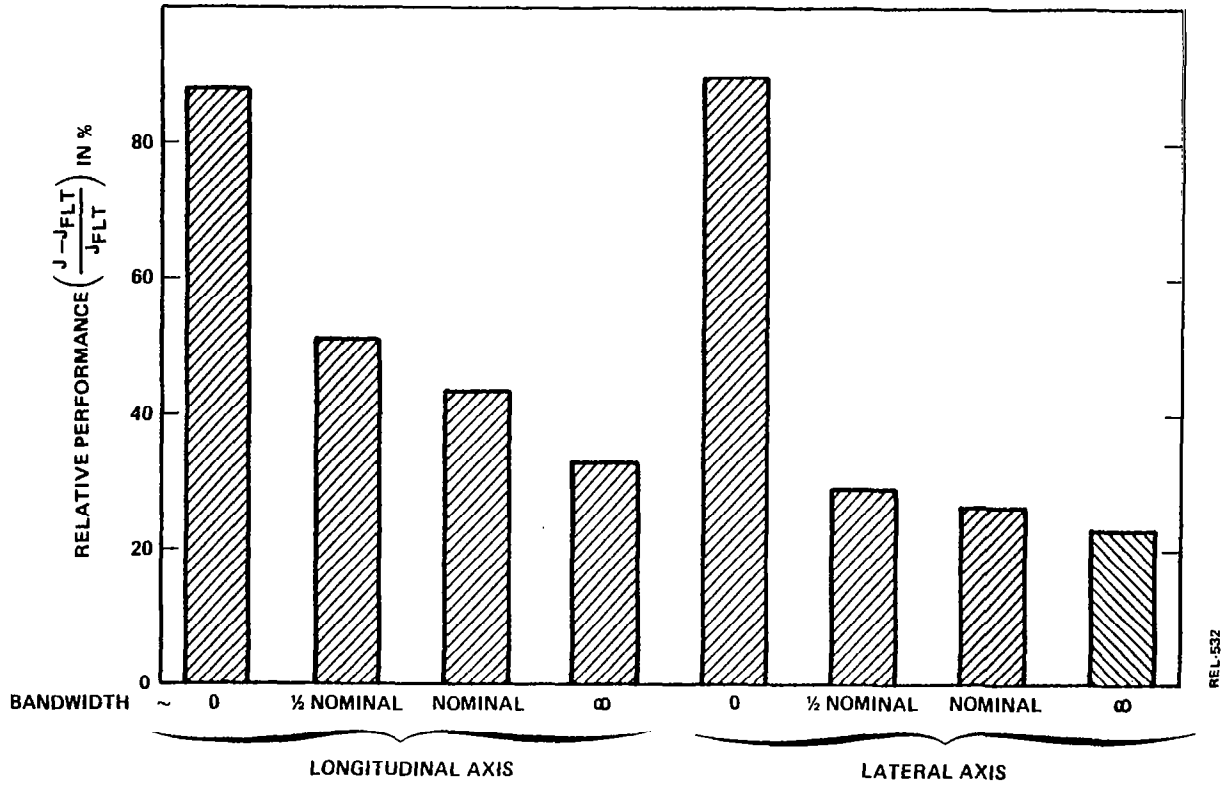
Figure 5.8:   Relative Performance Vs. VMS Platform Bandwidth

pronounced for the longitudinal control task than for the lateral.

It was desired to explore the possibility of using the optimal control model to design a washout filter for the VMS and to examine the effect of such a filter. An examination of the rms hover errors for the nominal conditions showed that only the VMS limits in surge would be exceeded a reasonable fraction of the time. Thus, only a surge washout filter was designed using the model. The design methodology used and the resulting filter are described in Appendix B.

Performance predictions with and without a surge washout filter are presented in table 5.7. The scores correspond to measures at the output of the motion system. The washout filter keeps the motion system essentially fixed in surge in this case. However, all other platform motions are within 10% of those that would have been obtained without a washout filter. The effect of the washout filter on overall performance is to introduce about a 3% degradation in J. Thus, the washout filter appears to have satisfied reasonable design objectives for such a filter (see discussion in Appendix B).

5.3.4 Effects of Vehicle Dynamics

The effects of simulator parameters will depend on the specifics of the task, including the vehicle dynamics. This has

Table 5.7  EFFECT OF SURGE WASHOUT ON
RMS PLATFORM MOTION (CH-47 LONGITUDINAL AXIS)

| | | | PREDICTED RMS MOTION | |
|---|---|---|---|---|
| VARIABLE | UNITS | VMS LIMITS | WITH WASHOUT | W/O WASHOUT |
| J | | | 7.987 | 7.73 |
| X | FT | $\pm 2.5$ | 0.0 | 5.14 |
| $\dot{X}$ | FT/SEC | $\pm 2.0$ | 0.0 | 0.98 |
| Z | FT | $\pm 30.0$ | 1.92 | 1.91 |
| $\dot{Z}$ | FT/SEC | $\pm 20.0$ | 0.636 | 0.66 |
| $\theta$ | DEG | $\pm 26.0$ | 0.801 | 0.87 |
| $\dot{\theta}$ | DEG/SEC | $\pm 15.0$ | 0.913 | 0.91 |
| $\delta_e$ | INCHES | -- | 0.23 | 0.23 |
| $\delta_c$ | INCHES | -- | 0.14 | 0.15 |

already been illustrated in differences between predicted
longitudinal and lateral performance.  To explore further the
effects of vehicle dynamics, results were obtained for the CH-47

with a velocity command control augmentation system, as specified in Hoffman et al (1976). The augmented vehicle presents a significantly less difficult control task. Figure 5.9 gives relative performance as a function of control augmentation for the nominal simulator configuration (and for the nominal fixed-base configuration). The effect of simulator characteristics is substantially less for the augmented vehicle. However, the effect is still significant for longitudinal control and for fixed-base simulation of lateral (augmented) control.

It is interesting to ask how simulator characteristics might bias the results of an investigation into the effectiveness of the control augmentation design. This can be examined by comparing the ratio of augmented to unaugmented performance predicted for flight with that predicted for various simulator configurations. An unbiased evaluation would yield the same ratio for a simulator as for flight. The predicted ratios for flight, nominal moving-base and nominal fixed-base configurations are shown in figure 5.10. It can be seen that the simulators tend to predict a greater advantage for control augmentation than is predicted for flight. However, the differences in this case are small, and results suggest the overall improvement from augmentation would be apparent in either a motion-base or fixed-base simulator.
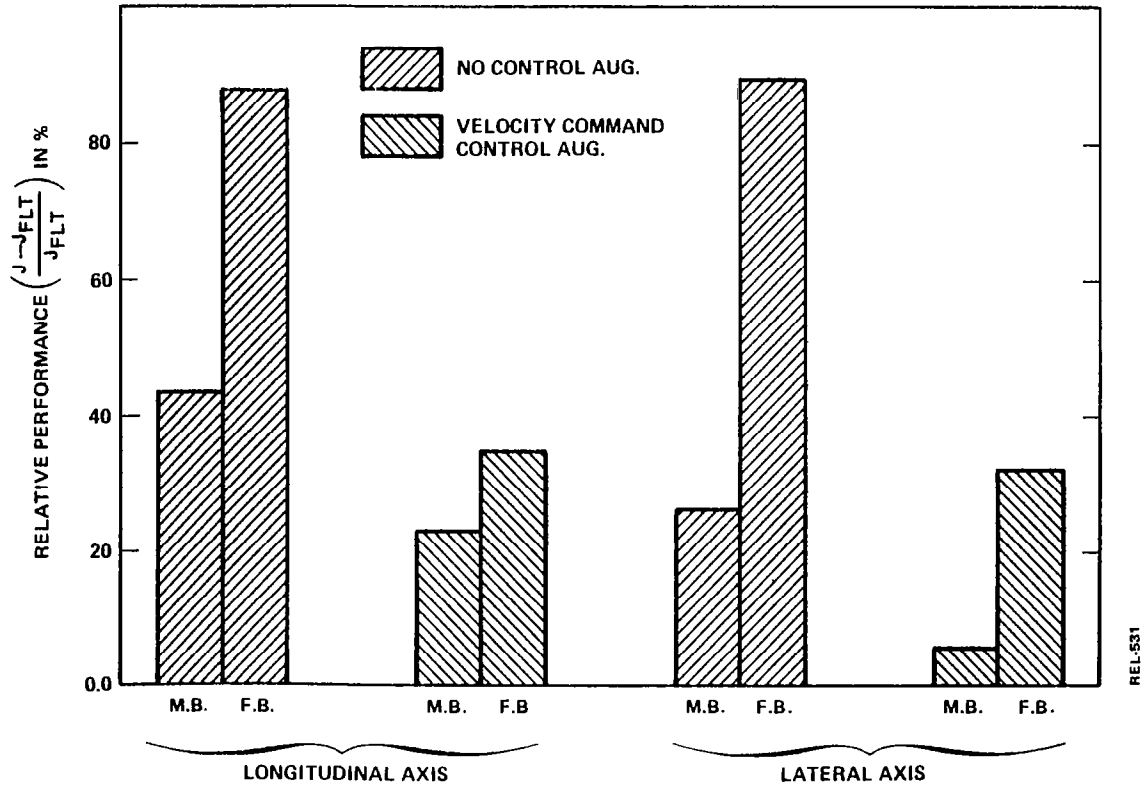
Figure 5.9:   Relative Performance Vs. Control Augmentation
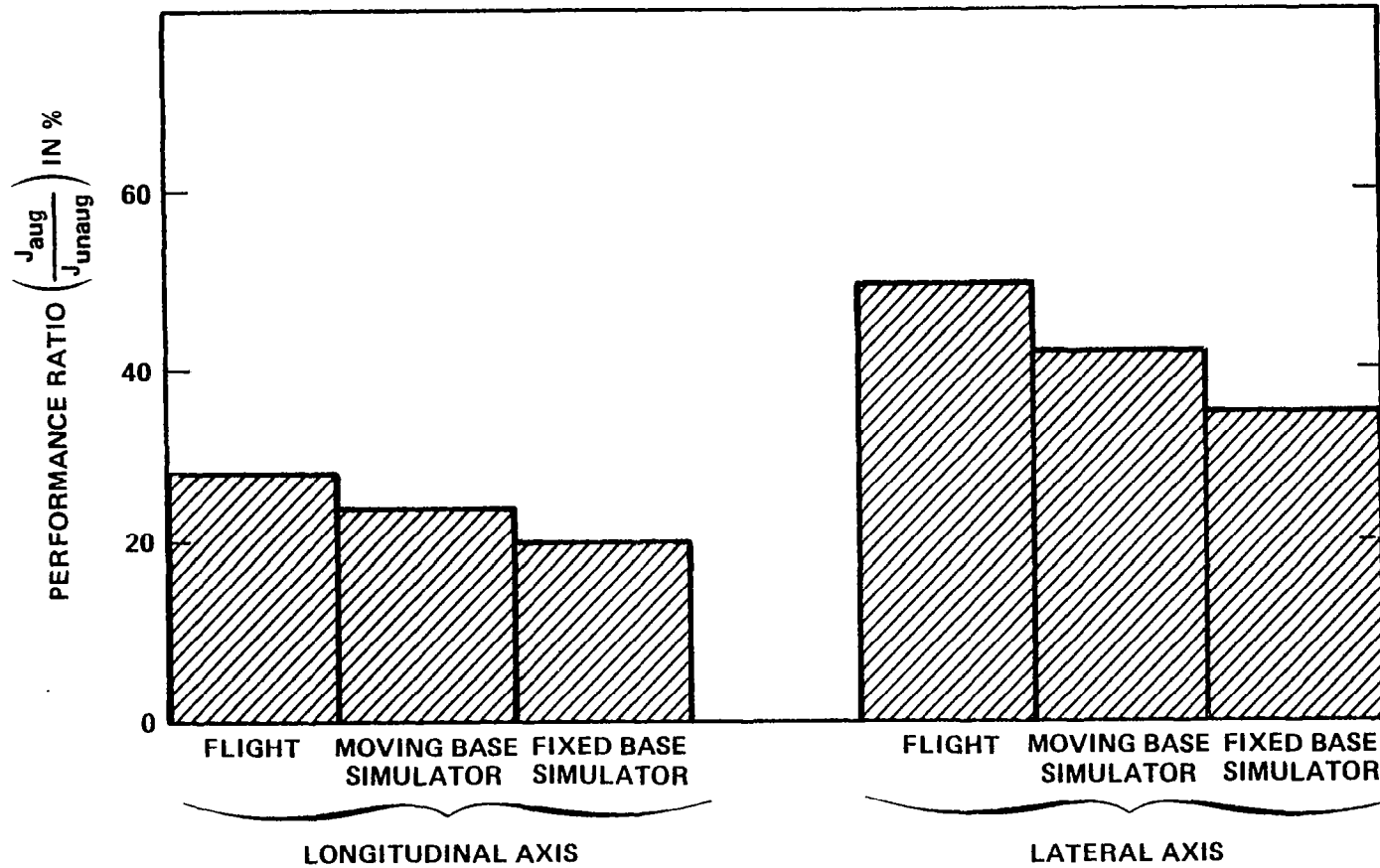
Figure 5.10:  Performance Ratio Vs. Simulator Configuration

## 6. SUMMARY AND CONCLUSIONS

The optimal control model for pilot/vehicle analysis has been used to explore the effects of a CGI visual system and motion system dynamics on helicopter hover simulation fidelity. This was accomplished by expanding the perceptual aspects of the model to include motion sensing and by relating CGI parameters to information processing parameters of the model. Simulator fidelity was examined by comparing predicted performance and workload for flight with that predicted for various simulator configurations.

The results of the analysis suggest that simulator deficiencies of a reasonable nature (by current standards) can result in substantial performance and/or workload infidelity. Both CGI and motion system effects are significant for this task. There is an interaction between the two sources of pilot cues. In particular, the presence of motion reduces the sensitivity to CGI limitations.

With respect to the CGI system, the most important parameter in terms of its effect on performance was display delay. This was followed in order of importance by display resolution and field-of-view.

The main effect associated with motion system bandwidth was introduced by going to a fixed-base configuration. Halving the VMS

platform bandwidth or going to full flight motion made only a marginal change in the performance predicted for the nominal VMS bandwidths. The task considered violated motion system limits only in the surge-axis, and a washout filter was designed for this axis using the model. The filter achieved its design objectives by keeping surge motions within limits while maintaining other motions and overall performance close to their original values.

The trends of the results are fairly consistent although there were some differences between lateral and longitudinal control tasks. The magnitude of the effects and relative importance of various parameters are clearly dependent on the task as exemplified here by longitudinal vs. lateral and unaugmented vs. augmented vehicle dynamics. It is, of course, for this reason that models of the pilot/vehicle system are needed to evaluate the importance of simulator parameters for a given situation.

Several areas for further research suggest themselves. First, it would be desirable to validate some of these results empirically. In this regard it should be noted that model predictions of other simulator effects have been borne out by experimental data (see, for example, Junker and Levison (1978)) as, of course, has the basic optimal control model. Nonetheless, certain assumptions were necessary concerning the relationship of model parameters to CGI parameters and the sharing (or non-sharing)

of attention between visual and motion modalities and these assumptions have not been verified. Indeed, a fundamental study of these relationships would probably be more valuable in the long run than empirical validation of the specific results obtained here. Along similar lines, it would be desirable to incorporate in the model mechanisms related to other simulator cueing systems such as g-suits and g-seats, control loaders, etc.

Finally, the use of the model to aid in the design of compensation for simulator deficiencies is a promising area for research. The design of washout filters discussed herein is one possibility that seems worthy of further study. Perhaps more important would be the development of a model-based methodology for designing compensators for simulator delays.

# 7. REFERENCES

1. Baron, S. and J. E. Berliner, "MANMOD 1975: Human Internal Models and Scene-Perception Models", Technical Report No. RD-CR-76-3, U.S. Army Missile Command, Redstone Arsenal, Alabama, September 1975.

2. Baron, S. and Kleinman, D. L., "The Human as an Optimal Controller and Information Processor", NASA-CR-1151, September 1968. (Also IEEE Trans. Man-Machine Systems: MMS-10, 1969.)

3. Baron- S. and Levison, W. H., "A Manual Control Theory Analysis of Vertical Situation Displays for STOL Aircraft," NASA CR-114620, April 1973.

4. Baron, S., Muralidharan R. and Kleinman, D. L., "Closed Loop Models for Analyzing the Effects of Simulator Characteristics", AIAA Flight Simulation Tech. Conf., Arlington, TX, September 1978.

5. Brown, J. L., "Visual Elements in Flight Simulation", University of Rochester, TR-73-2, December 1973.

6. Gibson, J. J., The Perception of the Visual World, Riverside Press, Cambridge, Mass., 1950.

7.  Gibson, J. J., et al., "Parallax and Perspective During Aircraft Landings", American J. of Psych., 68, 1955.

8.  Graham, C. H., "Perception of Movement", in Vision and Visual Perception, C. H Graham (editor), John Wiley and Sons, N.Y., 1965.

9.  Gum, D. R. and Albery, W. B., "Time Delay Problems Encountered in Integrating the Advanced Simulator for Undergraduate Pilot Training", J. of Aircraft, 4, 1977.

10.  Hess, R., "Prediction of Pilot Opinion Ratings Using an Optimal Pilot Model", Human Factors, 19, 1977.

11.  Hoffman, W. C., Kleinman, D., and Young, L., "Display/Control Requirements for Automated VTOL Aircraft", ASI-TR-76-39, October 1976.

12.  Junker, A. M. and Levison, W. H., "Recent Advances in Modelling the Effects of Roll Motion on the Human Operator", Aviation Space and Environmental Medicine, 49, 1978.

13.  Kleinman, D. L., "Solving the Optimal Attention Allocation Problem in Manual Control", IEEE Trans. on Automatic Control, AC-21, 1976.

14. Kleinman, D. L., Baron, S., and Levison, W. H., "An Optimal Control Model of Human Response, Part 1: Theory and Validation", Automatica, 6, 1970.

15. Kleinman, D. L., Baron, S. and Levison, W. H., "A Control Theoretic Approach to Manned-Vehicle Systems Analysis", IEEE Trans. on Auto. Control, AC-16 1971.

16. Levison, W. H., "The Effects of Display Gain and Signal Bandwidth on Human Controller Remnant", AMRL-TR-70-93, Wright-Patterson Air Force Base, Ohio, March 1971.

17. Levison, W. H., Baron S., and Kleinman, D. L., "A Model for Human Controller Remnant", IEEE Trans. on Man-Machine Systems, MMS-10, 1969.

18. Levison, W. H., Elkind, J. I., and Ward, J. L., "Studies of Multivariable Manual Control Systems: A Model for Task Interference", NASA-Ames Research Center, NASA CR-1746, May 1971.

19. Levison, W. H. et al, "Proposal for Research in Manual Control Techniques Applied to Military ACFT Display Design", BBN Proposal P73-BSC-3, Bolt Beranek and Newman, Inc., Cambridge, Mass., 1972.

20. Luce, R. D. and Galanter, E., "Discrimination", in Handbook of
    Mathematical Psychology, R. D. Luce, R. R. Bush, and E.
    Galanter (editors), vol. 1, John Wiley and Sons, Inc., New
    York, 1963.

21. Matheny, W. G., et al., "An Investigation of Visual, Aural,
    Motion and Control Movement Cues", Naval Training Device
    Center, Technical Report NAVTRADEVCEN 69-C-0304-1, April 1971.

22. Quiejo, M. J. and Riley, D. R., "Fixed-Base Simulator Study of
    the Effect of Time Delays in Visual Cues on Pilot Tracking
    Performance", NASA TN D-8001, October 1975.

23. Riggs, L. A., "Visual Acuity", in Vision and Visual
    Perception, C. H. Graham (editor), John Wiley and Sons, NY,
    1965.

24. Staples, K. J., "Motion, Visual, and Aural Cues in Piloted
    Flight Simulation", AGARD Conference Proceedings No. 79 on
    Simulation, AGARD CP-79-70, March 1970.

25. Thielges, J. R., Matheny, W., "Analysis of Visual
    Discriminations in Helicopter Control", HumRRO Technical
    Report 71-13, June 1971.

26. Wewerinke, P. H., "Visual Scene Perception Process Involved in
    the Manual Approach", NLR-TR-78130U, 1978.

27. Wewerinke, P. H., "A Theoretical and Experimental Analysis of the Outside World Perception Process", _Proceedings of the Fourteenth Annual Conference on Manual Control_, NASA conf. Pub. 2060, November 1978.

28. Young, L. R. and Meiry, J. L., "A Revised Dynamic Otolith Model", _Aerospace Medicine_, _39_, 1968.

29. Zacharias, G. L., "Motion Cue Models for Pilot-Vehicle Analysis", AMRL-TR-78-2, Wright-Patterson Air Force Base, Ohio, May 1978.

SYSTEM MATRICES FOR THE SIMULATED CH-47 HOVER TASK

As noted in the main text, dynamics associated with the vehicle, gust environment, control tasks, simulator, and human sensory systems are augmented together into a single A,B,C,D,E equation set for use in the OCM. This appendix presents the numerical values of these matrices as used in our analysis. However, rather than display them in augmented form, the ABCDE description of each system element corresponding to the blocks in Figure 2.2 will be given on the following pages. For reference, Figure A.1 and A.2 show, in a more stream-lined fashion, the name of the dynamics set and the interconnections of each set for the unaugmented control, realistic VMS-realistic CGI simulator configuration. Notice that any other configuration investigated can be recreated by either shunting out sets of dynamics (for example, removing PADE3 elements to form the realistic VMS-perfect CGI case), or by replacing one set with another (for example replacing C47LOB with C47LOF to form the augmented control case).
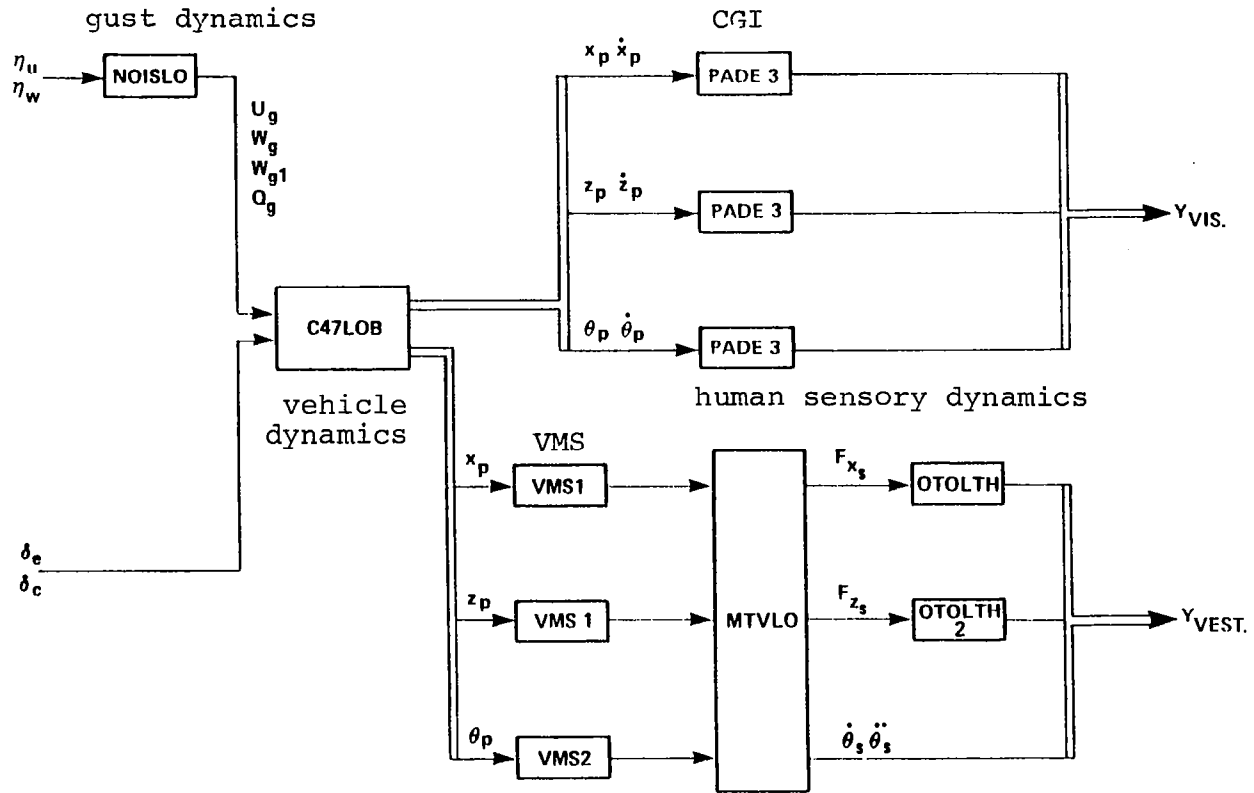
Figure A.1:  Linking Diagram for Nominal Simulator Configuration
(Longitudinal Axis)

gust dynamics

CGI

$\eta_v$
$\eta_p$ → NOISLA

$\gamma_p, \dot{\gamma}_p$ → PADE 3

$V_g$
$V_{g1}$
$P_g$
$R_g$

$\phi_p, \dot{\phi}_p$ → PADE 3 → $Y_{VIS.}$

C47LAB

$\psi_p, \dot{\psi}_p$ → PADE 3

vehicle
dynamics

human sensory dynamics

VMS

$\delta_a$
$\delta_r$

$\gamma_p$ → VMS 2 → $F_{Y_s}$ → OTOLTH

$\phi_p$ → VMS 1 → MTVLA → $\dot{\phi}_s, \ddot{\phi}_s$ → CNALR 2 → $Y_{VEST.}$

$\psi_p$ → VMS1 → $\dot{\psi}_s, \ddot{\psi}_s$

REL-528
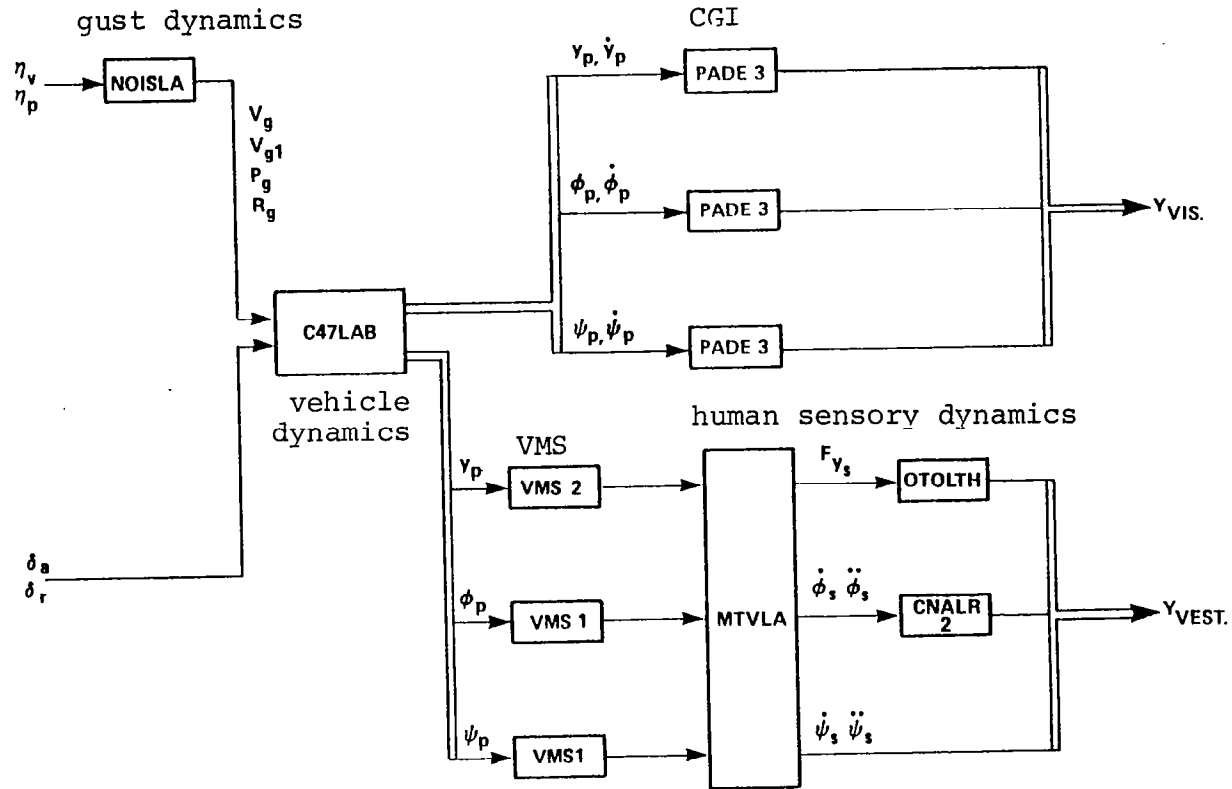
Figure A.2:  Linking Diagram for Nominal Simulator Configuration
(Lateral Axis)

NOISLO.DNL

Dryden gust model for CH-47 longitudinal axis.

TOTAL NO. NOISE STATES =   4

A    MATRIX:
   -4.740E-02    0.            0.            0.
    0.          -5.060E-01     2.530E-01     0.
    0.          -2.530E-01     0.            0.
    0.          -4.000E-03     2.000E-03    -2.010E-01

B    MATRIX:
    1.926E+00    0.
    0.           2.358E+00
    0.           1.362E+00
    0.           1.870E-02


NO NOISE INPUTS

C    MATRIX:
    1.000E+00    0.            0.            0.
    0.           1.000E+00     0.            0.
    0.           0.            1.000E+00     0.
    0.           0.            0.            1.000E+00

D    MATRIX:
    0.           0.
    0.           0.
    0.           0.
    0.           0.


EIGENVALUES
         REAL         IMAG          FREQ          DMPG
    1   -4.740E-02    0.000E+00     4.740E-02     1.000E+00
    2   -2.530E-01    0.000E+00     2.530E-01     1.000E+00
    3   -2.530E-01    0.000E+00     2.530E-01     1.000E+00
    4   -2.010E-01    0.000E+00     2.010E-01     1.000E+00

NOISLA.DNL

Dryden gust model for CH-47 lateral axis.

TOTAL NO. NOISE STATES =   0

    A    MATRIX:
      -9.480E-02     4.740E-02     0.            0.
      -4.740E-02     0.            0.            0.
       0.            0.           -2.000E-01     0.
       1.000E-03    -5.000E-04     0.           -2.680E-01

    B    MATRIX:
       2.360E+00     0.
       1.360E+00     0.
       0.            1.650E-02
      -2.480E-02     0.


NO NOISE INPUTS

    C    MATRIX:
       1.000E+00     0.            0.            0.
       0.            1.000E+00     0.            0.
       0.            0.            1.000E+00     0.
       0.            0.            0.            1.000E+00

    D    MATRIX:
       0.            0.
       0.            0.
       0.            0.
       0.            0.


EIGENVALUES
          REAL          IMAG          FREQ          DMPG
      1  -4.740E-02     9.344E-06     4.740E-02     1.000E+00
      2  -4.740E-02    -9.344E-06     4.740E-02     1.000E+00
      3  -2.680E-01     0.000E+00     2.680E-01     1.000E+00
      4  -2.000E-01     0.000E+00     2.000E-01     1.000E+00

C47LOB.DNL

CH-47 longitudinal vehicle dynamics for the unaugmented
control case.

SYSTEM UNSTABLE


TOTAL NO. NOISE STATES =   0

   A    MATRIX:
       0.            1.000E+00    0.            0.            0.
       0.

       0.           -1.820E-02    0.            4.000E-04    -3.220E+01
       2.620E+00

       0.            0.           0.            1.000E+00    0.
       0.

       0.           -7.300E-03    0.           -2.990E-01    0.
       1.350E-01

       0.            0.           0.            0.            0.
       1.000E+00

       0.            9.500E-03    0.            1.300E-03    0.
      -1.230E+00


   B    MATRIX:
       0.            0.           0.            0.            0.
       0.

       1.820E-02    -4.000E-04    0.           -2.620E+00    1.170E-01
       4.400E-03

       0.            0.           0.            0.            0.
       0.

       7.300E-03     2.990E-01    0.           -1.350E-01    1.700E-02
      -8.120E+00

       0.            0.           0.            0.            0.
       0.

      -9.500E-03    -1.300E-03    0.            1.230E+00    3.290E-01
       1.910E-02

NO NOISE INPUTS

C. MATRIX:

| 1.000E+00 | 0. | 0. | 0. | 0. |
| 0. | | | | |
| 0. | 1.000E+00 | 0. | 0. | 0. |
| 0. | | . | | |
| 0. | 0. | 1.000E+00 | 0. | 0. |
| 0. | | | | |
| 0. | 0. | 0. | 1.000E+00 | 0. |
| 0. | | | | |
| 0. | 0. | 0. | 0. | 5.730E+01 |
| 0. | | | | |
| 0. | 0. | 0. | 0. | 0. |
| 5.730E+01 | | | | |
| 0. | -1.820E-02 | 0. | 4.000E-04 | 0. |
| 2.620E+00 | | | | |
| 0. | -7.300E-03 | 0. | -2.990E-01 | 0. |
| 1.350E-01 | | | | |
| 0. | 0. | 0. | 0. | 0. |
| 5.730E+01 | | | | |
| 0. | 5.443E-01 | 0. | 7.449E-02 | 0. |
| -7.048E+01 | | | | |

D   MATRIX:
        0.              0.              0.              0.              0.
        0.

        0.              0.              0.              0.              0.
        0.

        0.              0.              0.              0.              0.
        0.

        0.              0.              0.              0.              0.
        0.

        0.              0.              0.              0.              0.
        0.

        0.              0.              0.              0.              0.
        0.

        1.820E-02      -4.000E-04       0.             -2.620E+00       1.170E-01
        4.400E-03

        7.300E-03       2.990E-01       0.             -1.350E-01       1.700E-02
       -8.120E+00

        0.              0.              0.              0.              0.
        0.

       -5.444E-01      -7.449E-02       0.              7.048E+01       1.885E+01
        1.094E+00


EIGENVALUES
         REAL            IMAG           FREQ            DMPG
   1    0.000E+00       0.000E+00       0.000E+00       1.701E+38
   2   -1.405E+00       0.000E+00       1.405E+00       1.000E+00
   3    7.809E-02       4.599E-01       4.664E-01      -1.674E-01
   4    7.809E-02      -4.599E-01       4.664E-01      -1.674E-01
   5   -2.982E-01       0.000E+00       2.982E-01       1.000E+00
   6   -6.927E-09       0.000E+00       6.927E-09       1.000E+00

C47LAB.DNL

CH-47 lateral vehicle dynamics for the unaugmented
control case.

SYSTEM UNSTABLE


TOTAL NO. NOISE STATES =   0

A    MATRIX:

| | | | | |
|---|---|---|---|---|
| 0. | 1.000E+00 | 0. | 0. | 0. |
| 0. | | | | |
| 0. | -1.370E-01 | 3.200E+01 | -1.490E+00 | 0. |
| 8.600E-03 | | | | |
| 0. | 0. | 0. | 1.000E+00 | 0. |
| 0. | | | | |
| 0. | -6.700E-03 | 0. | -7.230E-01 | 0. |
| 7.500E-03 | | | | |
| 0. | 0. | 0. | 0. | 0. |
| 1.000E+00 | | | | |
| 0. | -1.100E-03 | 0. | -5.470E-02 | 0. |
| -4.090E-02 | | | | |


B    MATRIX:

| | | | | |
|---|---|---|---|---|
| 0. | 0. | 0. | 0. | 0. |
| 0. | | | | |
| 1.370E-01 | 0. | 1.490E+00 | -8.600E-03 | 1.160E+00 |
| -5.040E-02 | | | | |
| 0. | 0. | 0. | 0. | 0. |
| 0. | | | | |
| 6.700E-03 | 0. | 7.230E-01 | -7.500E-03 | 4.370E-01 |
| -3.750E-02 | | | | |
| 0. | 0. | 0. | 0. | 0. |
| 0. | | | | |
| 1.100E-03 | 0. | 5.470E-02 | 4.090E-02 | 4.270E-02 |
| 2.000E-01 | | | | |

NO NOISE INPUTS

C    MATRIX:

| | | | | | |
|---|---|---|---|---|---|
| 1.000E+00 | 0. | 0. | 0. | 0. | 0. |
| 0. | 1.000E+00 | 0. | 0. | 0. | 0. |
| 0. | 0. | 5.730E+01 | 0. | 0. | 0. |
| 0. | 0. | 0. | 5.730E+01 | 0. | 0. |
| 0. | 0. | 0. | 0. | 5.730E+01 | 0. |
| 0. | 0. | 0. | 0. | 0. | 5.730E+01 |
| 0. | -1.370E-01 | 0. | -1.490E+00 | 0. | 8.600E-03 |
| 0. | 0. | 0. | 5.730E+01 | 0. | 0. |
| 0. | -3.839E-01 | 0. | -4.143E+01 | 0. | 4.298E-01 |
| 0. | 0. | 0. | 0. | 0. | 5.730E+01 |
| 0. | -6.303E-02 | 0. | -3.134E+00 | 0. | -2.344E+00 |

```
D   MATRIX:
    0.              0.              0.              0.              0.
    0.

    0.              0.              0.              0.              0.
    0.

    0.              0.              0.              0.              0.
    0.

    0.              0.              0.              0.              0.
    0.

    0.              0.              0.              0.              0.
    0.

    0.              0.              0.              0.              0.
    0.

    1.370E-01       0.              1.490E+00       -8.600E-03      1.160E+00
   -5.040E-02

    0.              0.              0.              0.              0.
    0.

    3.839E-01       0.              4.143E+01       -4.298E-01      2.504E+01
   -2.149E+00

    0.              0.              0.              0.              0.
    0.

    6.303E-02       0.              3.134E+00       2.344E+00       2.447E+00
    1.146E+01
```

EIGENVALUES

|   | REAL | IMAG | FREQ | DMPG |
|---|---|---|---|---|
| 1 | 0.000E+00 | 0.000E+00 | 0.000E+00 | 1.701E+38 |
| 2 | -9.886E-01 | 0.000E+00 | 9.886E-01 | 1.000E+00 |
| 3 | 6.492E-02 | 4.611E-01 | 4.657E-01 | -1.394E-01 |
| 4 | 6.492E-02 | -4.611E-01 | 4.657E-01 | -1.394E-01 |
| 5 | -4.214E-02 | 0.000E+00 | 4.214E-02 | 1.000E+00 |
| 6 | -7.910E-09 | 0.000E+00 | 7.910E-09 | 1.000E+00 |

C47LOF.DNL

CH-47 longitudinal vehicle dynamics for the
(system f) augmented control case.

SYSTEM NEUTRALLY STABLE


TOTAL NO. NOISE STATES =   0

A    MATRIX:
     0.              1.000E+00       0.              0.              0.
     0.

     8.900E-06      -1.070E-02      -1.200E-06      -4.000E-04      -3.337E+01
     1.825E+00

     0.              0.              0.              1.000E+00       0.
     0.

    -3.700E-06      -4.900E-03.     -5.000E-04      -5.030E-01      -1.211E-01
     5.970E-02

     0.              0.              0.              0.              0.
     1.000E+00

     2.500E-05       3.070E-02      -2.800E-06      -1.000E-03      -3.278E+00
    -3.464E+00


B    MATRIX:
     0.              0.              0.              0.              0.
     0.

     1.820E-02      -4.000E-04       0.             -2.620E+00       1.170E-01
     4.400E-03

     0.              0.              0.              0.              0.
     0.

     7.300E-03       2.990E-01       0.             -1.350E-01       1.700E-02
    -8.120E+00

     0.              0.              0.              0.              0.
     0.

    -9.500E-03      -1.300E-03       0.              1.230E+00       3.290E-01
     1.910E-02


-130-

NO NOISE INPUTS

C    MATRIX:

| 1.000E+00 | 0. | 0. | 0. | 0. |
| 0. | | | | |
| 0. | 1.000E+00 | 0. | 0. | 0. |
| 0. | | | | |
| 0. | 0. | 1.000E+00 | 0. | 0. |
| 0. | | | | |
| 0. | 0. | 0. | 1.000E+00 | 0. |
| 0. | | | | |
| 0. | 0. | 0. | 0. | 5.730E+01 |
| 0. | | | | |
| 0. | 0. | 0. | 0. | 0. |
| 5.730E+01 | | | | |
| 8.900E-06 | -1.070E-02 | -1.200E-06 | -4.000E-04 | -1.170E+00 |
| 1.825E+00 | | | | |
| -3.700E-06 | -4.900E-03 | -5.000E-04 | -5.030E-01 | -1.211E-01 |
| 5.970E-02 | | | | |
| 0. | 0. | 0. | 0. | 0. |
| 5.730E+01 | | | | |
| 1.433E-03 | 1.759E+00 | -1.604E-04 | -5.730E-02 | -1.878E+02 |
| -1.985E+02 | | | | |

D    MATRIX:

| | | | | |
|---|---|---|---|---|
| 0. | 0. | 0. | 0. | 0. |
| 0. | | | | |
| 0. | 0. | 0. | 0. | 0. |
| 0. | | | | |
| 0. | 0. | 0. | 0. | 0. |
| 0. | | | | |
| 0. | 0. | 0. | 0. | 0. |
| 0. | | | | |
| 0. | 0. | 0. | 0. | 0. |
| 0. | | | | |
| 0. | 0. | 0. | 0. | 0. |
| 0. | | | | |
| 1.820E-02 | -4.000E-04 | 0. | -2.620E+00 | 1.170E-01 |
| 4.400E-03 | | | | |
| 7.300E-03 | 2.990E-01 | 0. | -1.350E-01 | 1.700E-02 |
| -8.120E+00 | | | | |
| 0. | 0. | 0. | 0. | 0. |
| 0. | | | | |
| -5.444E-01 | -7.449E-02 | 0. | 7.048E+01 | 1.885E+01 |
| 1.094E+00 | | | | |

EIGENVALUES

| | REAL | IMAG | FREQ | DMPG |
|---|---|---|---|---|
| 1 | -2.223E+00 | 0.000E+00 | 2.223E+00 | 1.000E+00 |
| 2 | -6.249E-01 | 2.896E-01 | 6.887E-01 | 9.073E-01 |
| 3 | -6.249E-01 | -2.896E-01 | 6.887E-01 | 9.073E-01 |
| 4 | -7.613E-04 | 0.000E+00 | 7.613E-04 | 1.000E+00 |
| 5 | -5.034E-01 | 0.000E+00 | 5.034E-01 | 1.000E+00 |
| 6 | -9.966E-04 | 0.000E+00 | 9.966E-04 | 1.000E+00 |

C47LAF.DNL

CH-47 lateral vehicle dynamics for the
(system f) augmented control case.

SYSTEM NEUTRALLY STABLE


TOTAL NO. NOISE STATES =   0

  A    MATRIX:
     0.            1.000E+00     0.            0.            0.
     0.

    -1.000E-04    -1.819E-01     2.401E+01    -8.206E+00    -2.170E-01
    -3.487E-01

     0.            0.            0.            1.000E+00     0.
     0.

    -5.000E-05    -2.390E-02    -3.042E+00    -3.283E+00     9.850E-02
     1.246E-01

     0.            0.            0.            0.            0.
     1.000E+00

     9.600E-07     5.000E-04     6.120E-02     2.780E-02    -1.972E+00
    -2.799E+00


  B    MATRIX:
     0.            0.            0.            0.            0.
     0.

     1.370E-01     0.            1.490E+00    -8.600E-03     1.160E+00
    -5.040E-02

     0.            0.            0.            0.            0.
     0.

     6.700E-03     0.            7.230E-01    -7.500E-03     4.370E-01
    -3.750E-02

     0.            0.            0.            0.            0.
     0.

     1.100E-03     0.            5.470E-02     4.090E-02     4.270E-02
     2.000E-01

NO NOISE INPUTS

C    MATRIX:

| 1.000E+00 | 0. | 0. | 0. | 0. |
| 0. | | | | |
| 0. | 1.000E+00 | 0. | 0. | 0. |
| 0. | | | | |
| 0. | 0. | 5.730E+01 | 0. | 0. |
| 0. | | | | |
| 0. | 0. | 0. | 5.730E+01 | 0. |
| 0. | | | | |
| 0. | 0. | 0. | 0. | 5.730E+01 |
| 0. | | | | |
| 0. | 0. | 0. | 0. | 0. |
| 5.730E+01 | | | | |
| -1.000E-04 | -1.819E-01 | -8.200E+00 | -8.206E+00 | -2.170E-01 |
| -3.487E-01 | | | | |
| 0. | 0. | 0. | 5.730E+01 | 0. |
| 0. | | | | |
| -2.865E-03 | -1.369E+00 | -1.743E+02 | -1.881E+02 | 5.644E+00 |
| 7.140E+00 | | | | |
| 0. | 0. | 0. | 0. | 0. |
| 5.730E+01 | | | | |
| 5.501E-05 | 2.865E-02 | 3.507E+00 | 1.593E+00 | -1.130E+02 |
| -1.604E+02 | | | | |

D   MATRIX:

```
     0.              0.              0.              0.              0.
     0.

     0.              0.              0.              0.              0.
     0.

     0.              0.              0.              0.              0.
     0.

     0.              0.              0.              0.              0.
     0.

     0.              0.              0.              0.              0.
     0.

     0.              0.              0.              0.              0.
     0.

  1.370E-01          0.           1.490E+00      -8.600E-03       1.160E+00
 -5.040E-02

     0.              0.              0.              0.              0.
     0.

  3.839E-01          0.           4.143E+01      -4.298E-01       2.504E+01
 -2.149E+00

     0.              0.              0.              0.              0.
     0.

  6.303E-02          0.           3.134E+00       2.344E+00       2.447E+00
  1.146E+01
```

EIGENVALUES

| | REAL | IMAG | FREQ | DMPG |
|---|---|---|---|---|
| 1 | -1.339E-03 | 0.000E+00 | 1.339E-03 | 1 000E+00 |
| 2 | -7.028E-01 | 2 273E-01 | 7.387E-01 | 9.515E-01 |
| 3 | -7.028E-01 | -2.273E-01 | 7.387E-01 | 9.515E-01 |
| 4 | -2.060E+00 | 0.000E+00 | 2.060E+00 | 1.000E+00 |
| 5 | -1.399E+00 | 1.076E-01 | 1.403E+00 | 9.971E-01 |
| 6 | -1.399E+00 | -1.076E-01 | 1.403E+00 | 9.971E-01 |

PADE3.DNL

99 msec. pade´ delay dynamics.

TOTAL NO. NOISE STATES =   0

A    MATRIX:
-2.020E+01

B    MATRIX:
2.020E+01    -1.000E+00


NO NOISE INPUTS

C    MATRIX:
1.000E+00
-2.020E+01

D    MATRIX:
0.              0.
2.020E+01    -1.000E+00


EIGENVALUES
       REAL         IMAG         FREQ         DMPG
1   -2.020E+01    0.000E+00    2.020E+01    1.000E+00

VMS1.DNL

VMS platform dynamics for use in the rotational and surge axis.
Second order approximation with BW = 1.5 hz., and DR = .7 .

TOTAL NO. NOISE STATES =   0

  A    MATRIX:
    0.             1.000E+00
   -8.836E+01   -1.316E+01

  B    MATRIX:
    0.
    8.836E+01


NO NOISE INPUTS

  C    MATRIX:
    1.000E+00    0.
    0.           1.000E+00
   -8.836E+01   -1.316E+01

  D    MATRIX:
    0.
    0.
    8.836E+01


EIGENVALUES

| | REAL | IMAG | FREQ | DMPG |
|---|---|---|---|---|
| 1 | -6.580E+00 | 6.713E+00 | 9.400E+00 | 7.000E-01 |
| 2 | -6.580E+00 | -6.713E+00 | 9.400E+00 | 7.000E-01 |

VMS2.DNL

VMS platform dynamics for use in the sway and heave axis.
Second order approximation with BW = 3.0 hz., and DR = .7 .

TOTAL NO  NOISE STATES =  0

    A    MATRIX:
        0.              1.000E+00
       -3.534E+02      -2.632E+01

    B    MATRIX:
        0.
        3.534E+02


NO NOISE INPUTS

    C    MATRIX:
        1.000E+00      0.
        0.             1.000E+00
       -3.534E+02     -2.632E+01

    D    MATRIX:
        0
        0.
        3.534E+02


EIGENVALUES
         REAL           IMAG          FREQ          DMPG
    1  -1.316E+01    1.343E+01     1.880E+01     7.000E-01
    2  -1.316E+01   -1.343E+01     1.880E+01     7.000E-01

MTVLO.DNL

Formation of proper vestibular cues from RMS platform
outputs. (longitudinal axis)

TOTAL NO. NOISE STATES =  0


NO STATES


NO NOISE INPUTS

    D    MATRIX:
      0              0              0              5.620E-01    0.
      0.             0.             0.             0.

      0.             0.             0.             0.           0.
      0.             0.             0.             1.000E+00

      0.             0.             0.             0.           1.000E+00
      0.             0.             0.             0.

      0.             0.             0.             0.           0.
      1.000E+00      0.             0.             0.

MTVLA.DNL

Formation of proper vestibular cues from RMS platform
outputs. (lateral axis)

TOTAL NO. NOISE STATES =  0


NO STATES


NO NOISE INPUTS

D    MATRIX:

| 0. | 0. | 1.000E+00 | -5.620E-01 | 0. |
|---|---|---|---|---|
| 0. | 0. | 0. | 0. | |
| 0. | 0. | 0. | 0. | 1.000E+00 |
| 0. | 0. | 0. | 0. | |
| 0. | 0. | 0. | 0. | 0. |
| 1.000E+00 | 0. | 0. | 0. | |
| 0. | 0. | 0. | 0. | 0. |
| 0. | 0. | 1.000E+00 | 0. | |
| 0. | 0. | 0. | 0. | 0. |
| 0. | 0. | 0. | 1.000E+00 | |

```
                 OTOLTH.DNL

             Otolith dynamics.

TOTAL NO  NOISE STATES =  0

   A    MATRIX:
     -1.876E-01     0.
      1.515E+00    -1.515E+00

   B    MATRIX:
      1.876E-01
      0.


NO NOISE INPUTS

   C    MATRIX:
      8.000E+00    -7.600E+00

   D    MATRIX:
      0.


EIGENVALUES
          REAL          IMAG         FREQ         DMPG
     1  -1.876E-01    0.000E+00    1.876E-01    1.000E+00
     2  -1.515E+00    0.000E+00    1.515E+00    1.000E+00
```

OTOLTH2.DNL

Simplified otolith dynamics. Essentially a
low pass filter with break at 1.5152 rad.

TOTAL NO. NOISE STATES = 0

A     MATRIX:
   -1.515E+00

B     MATRIX:
    1.515E+00


NO NOISE INPUTS

C     MATRIX:
    1.000E+00

D     MATRIX:
     0.


EIGENVALUES
         REAL          IMAG          FREQ          DMPG
   1   -1.515E+00    0.000E+00    1.515E+00    1.000E+00

CNALR2.DNL

Simplified canal dynamics for the roll axis.
Filter is T1S/(T1S+1) .

TOTAL NO  NOISE STATES =  0

A    MATRIX:
  -1.639E-01

B    MATRIX:
  1.639E-01    0.


NO NOISE INPUTS

C    MATRIX:
  -1.000E+00
  1.639E-01

D    MATRIX:
  1.000E+00    0.
  -1.639E-01    1.000E+00


EIGENVALUES
        REAL         IMAG         FREQ         DMPG
  1  -1.639E-01    0.000E+00    1.639E-01    1.000E+00

# APPENDIX B:   DESIGN OF SIMULATOR CONTROL LAWS

## B.1  Overview

The following design procedure is intended to provide desired rotational and specific force cues to the simulator pilot through co-ordinated attitudinal and translational motions of a moving-base simulator.  Command-following simulator drive circuits are assumed to have been previously designed and implemented.  The objective of the design procedure, therefore, is to generate a set of simulator commands that best meets the following conflicting objectives:

a.  reproduce perceptual cues related to whole-body motion,

b.  minimize the introduction of "false" cues inherent in ground-based motion simulation, and

c.  minimize the probability of driving the simulator to its physical limits.

The design procedure leads to a fixed-form control law implementation of the general form shown in Figure B.1 for either the pitch-surge or the roll-sway axis.  Inputs to the control law are attitude rate and specific force; outputs are attitude and position commands to the simulator drive circuits.

Each simulator command is implemented as the sum of two commands -- one arising from simulated attitude rate, the other

Figure B.1:   Structure of Fixed-Form Control Laws
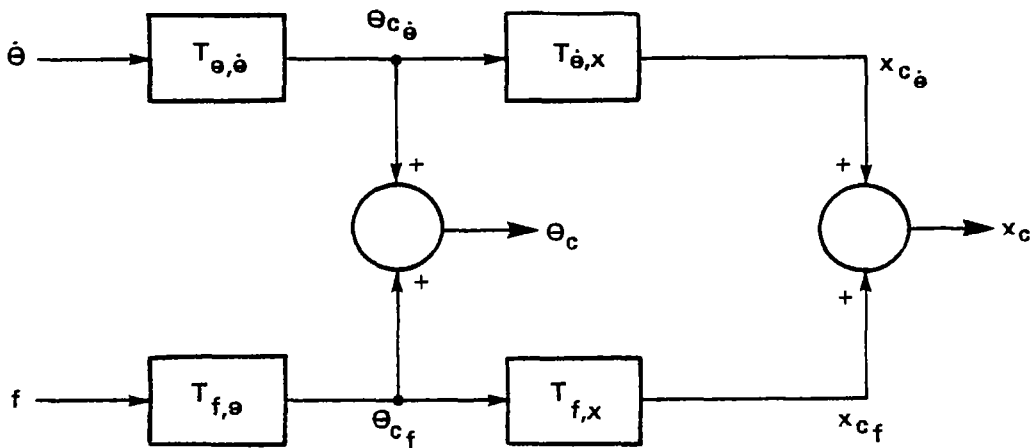
$\dot{\Theta}$ = SIMULATED ATTITUDE RATE
f = SIMULATED SPECIFIC FORCE
$\Theta_c$ = COMMANDED SIMULATOR ATTITUDE
$x_c$ = COMMANDED SIMULATOR TRANSLATION

WHL508

from specific force. The structure of the linear elements of the system shown in Figure B.1 is described later.

B.2   Description of the Design Procedure

The design procedure consists of the following steps:

1.  Analysis of the pilot/vehicle system to determine the characteristics of the motion cues available to the pilot in the actual flight task, as well as the importance of these cues to the task of closed-loop control.

2.  Derivation of low-order analytic approximations to the spectra for attitude-rate and specific force predicted in Step 1.

3.  Initial design of simulator control laws using an appropriate LQG minimization scheme.

4.  Selection of parameters of the fixed-form structure of Figure B.1 to approximate the initial design.

5.  Pilot-vehicle analysis of the simulated flight task using the fixed-form simulator control laws.

These steps are described briefly below.

B.2.1   Model Analysis of the Flight Task

The "actual" flight task is analyzed with the optimal-control model (OCM) to predict rms levels and power spectra for important

system variables, including perceptual variables assumed to be available to the pilot as a result of whole-body motion. This analysis includes the prediction of the pilot's allocation of "attention" to the various perceptual variables; presumably, predicted fractional attention relates directly to the importance of a particular perceptual variable with regard to achieving the closed-loop control objectives.

B.2.2  Low-Order Spectral Approximation

Because of the relatively free-form nature of the pilot response strategy generated by the OCM, the order of the equations of motion of any system variable is equal to the number of state variables required to describe the flight task (including aircraft states, "input states", and possible additional states related to display dynamics and control augmentation). In practice, however, a relatively low-order (say three or four degrees of freedom) approximation will provide an adequate representation of the spectral characteristics of most any signal of interest. To minimize problem complexity, then, a suitable fitting procedure is employed to obtain low-order approximations to the attitude-rate and specific-force spectra predicted in the initial analysis of the flight task.

## B.2.3   Initial Control Law Design

The control-law design problem is diagrammed in Figure B.2. The dashed block (simulator control law) indicates the element to be designed; remaining blocks indicate various dynamic subsystems that constitute the problem description.

The block labeled "approximate pilot/vehicle system" contains low-order analytic approximations to the predicted attitude rate and specific force spectra obtained in Step 2.   Attitude rate and specific force serve as inputs to the control laws and are used for predicting perceptual errors as described below.   The "simulator dynamics" element is assumed to contain dynamical models (second-order or higher) for both attitude and translational response of the simulator.   Outputs of this block include position, velocity, and acceleration of simulator attitude and translation, as well as specific force generated at the pilot's head location.

For purposes of this design procedure, we assume that the pilot's head is located at the center of rotation.   Specific force is thus defined as

$$f_s = \pm 0.562\ \theta_s + \ddot{x}_s$$

where
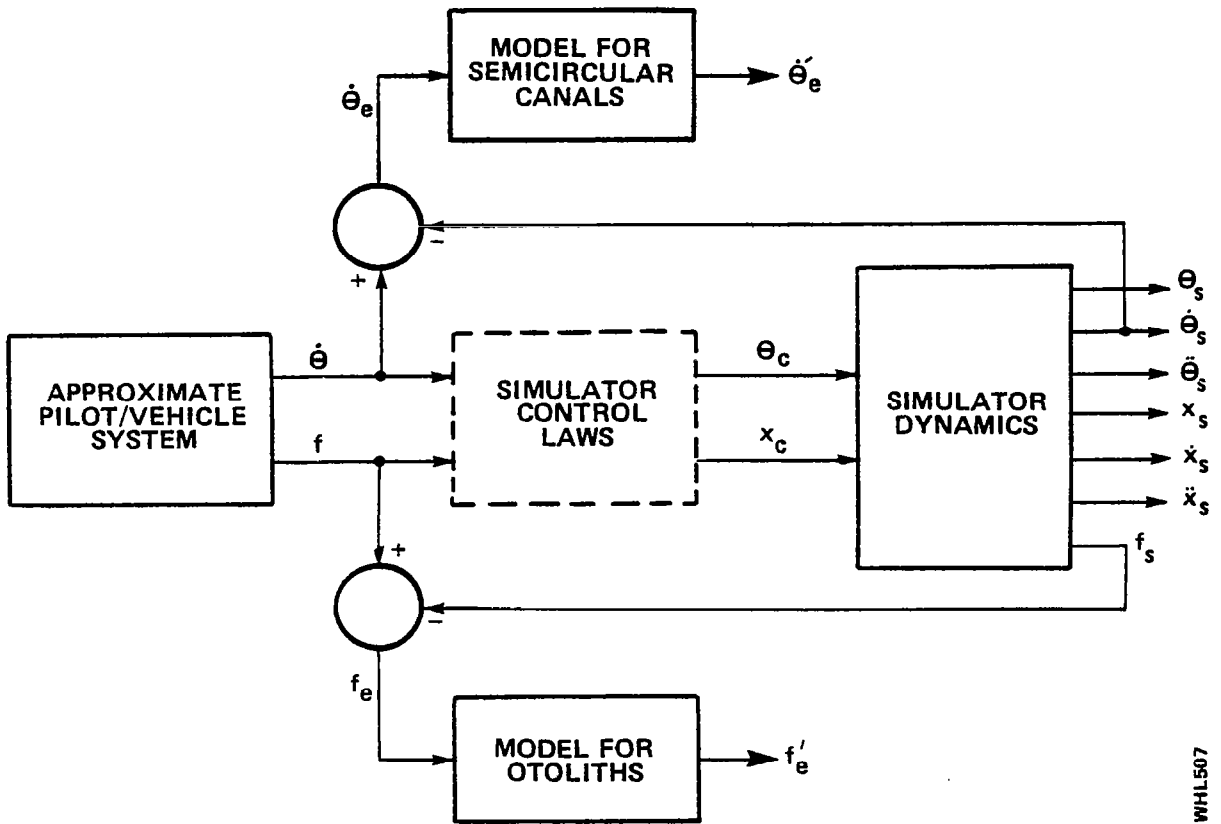
Figure B.2: Design of Control-Law Design Problem

$\theta_s$ = simulator attitude, degrees

$x_s$ = simulator displacement, feet

$f_s$ = simulated specific force, feet/second

The sign preceding the component due to simulator tilt is positive for the pitch-surge axis and negative for the roll-sway axis.

Part of the design objective is to minimize perceptual errors: i.e., the difference between the motion perceptions obtained in flight and those obtained in the simulator. In both actual and simulated flight, motion variables perceived by the pilot through vestibular sensory mechanisms are mediated by the dynamical response characteristics of the semicircular canals and otoliths. Because we are dealing with linear models, we can compute perceptual error as the difference between the perception obtained in flight and the corresponding perception obtained in the simulator, or as the difference between actual and simulated stimulus as mediated by sensory dynamics. As the two approaches are equivalent, we choose the latter in order to minimize the dynamical order of the problem.

Design objectives of the control laws are formulated in terms of the following quadratic performance index:

$$J_c = q_1 , \bar{\theta}_s^2 , + q_2 \bar{\dot{\theta}}_s^2 + q_3 \bar{\ddot{\theta}}_s^2$$

$$+ q_4 \bar{x}_s^2 + q_5 \bar{\dot{x}}_s^2 + q_6 \bar{\ddot{x}}_s^2 \qquad\qquad \text{(B.1)}$$

$$+ q_7 \bar{\dot{\theta}}_e^2 + q_8 \bar{f}_e^2$$

The first six terms reflect the physical limitations of the simulator; the remaining terms reflect the requirement to minimize perceptual error.

It is suggested that weighting coefficients be chosen on the basis of maximum allowable values, or "limits" as follows:

$$q = 1/(\text{Limit}) \qquad\qquad\qquad \text{(B.2)}$$

Limits related to simulator outputs are usually given in the simulator specifications -- these limits may be used for the control-law design procedure.

Two alternative schemes for selecting the appropriate limit on perceptual errors are suggested: (1) set the limit equal to the perceptual threshold, or (2) set the limit equal to the perceptual threshold normalized by the attention devoted to the motion cue as predicted in Step 1. In the latter case, the weighting coefficient is computed as

$$q = (f/\text{threshold})^2 \qquad\qquad \text{(B.3)}$$

where "f" is the fraction of attention devoted to the particular motion cue, and "threshold" refers to the effective perceptual threshold as determined from an experiment in which the subject's only task is to detect the cue under study.

The rationale for these schemes is that there is no need to replicate motion cues to within a tolerance that is lower than the subject's ability to detect a cue discrepancy. The question arises as to whether the "threshold" used in the design procedure should be that associated with a basic perceptual limitation, or an "indifference" threshold that reflects the interfering effects of concurrent tasks (e.g., continuous control). Normalization of the basic perceptual threshold by the attention is a means of accounting for the larger indifference threshold observed when the subject performs combined detection and control tasks.

Once the coefficients of the performance index have been specified, an appropriate LQG minimization scheme is employed to determine the simulator control laws.

The minimization scheme provides solutions to the estimation and control elements of the overall design. These results may then be processed to provide transfer functions relating control-law output variables (commanded attitude and translation) to input variables (simulated attitude rate and specific force).

## B.2.4  Fixed-Form Approximation

Implementation of the specified control laws is aided by approximating the results of the previous step in the design procedure by a suitable fixed-form structure. If the structure of Figure B.1 is adopted, the following procedure is to be followed:

1.  Manipulate the LQG solution to yield Bode plots of the following transfers: $\theta_{c_{\dot{\theta}}}/\dot{\theta}$, $x_{c_{\dot{\theta}}}/\theta_{c_{\dot{\theta}}}$, $\theta_{c_f}/f$, and $x_{c_f}/\theta_{c_f}$, where the quantities appearing in these ratios are defined in Figure B.1.

2.  Select the parameters of the transfer elements of Figure B.1 to provide a best match to the corresponding Bode plots. Various automated matching procedures are available to help at this stage, although "eyeball" fits to the model-predicted curves may be adequate in many cases.

The following structures were adopted for the four linear transfer elements in this study:

$$T_{\dot{\theta},\theta} = \frac{K_1}{s + a_1}$$

$$T_{\dot{\theta},x} = \frac{-.562}{(s + b_1)^2}$$  $\qquad$ (B.4)

$$T_{f,\theta} = \frac{K_2}{.562} \quad \frac{a_2^2}{(s + a_2)^2}$$

$$T_{f,x} = \frac{.562}{a_2^2} \quad \frac{s + 2a_2}{s + b_2}$$

where attitude is in degrees, translation in feet, specific force in g's, and g/57.3 = .562.

With this scheme, attitude command is implemented as a first-order low-pass filter operating on attitude rate (in effect, a first-order washout on attitude) plus a second-order low-pass filter operating on specific force. Commanded translational position is generated by a second-order low-pass filter operating on the attitude-related of the commanded simulator attitude plus a pole-zero filter operating on the specific force-related portion of the attitude command.

The structure described here has the following properties:

1. Attitude rate commands are transmitted without phase errors at high frequencies.

2. False tilt cues induced by attitude-rate following are eliminated at high frequencies.

3. Specific force cues are provided by simulator tilt at low frequencies and by translational acceleration at high frequencies.

4. Phase errors between commanded and theoretical specific force are eliminated asymptotically at low and high frequencies.

5. Attitude rate and specific force cues are not necessarily reproduced with unity gains.

Other models may be constructed to have these properties, and one might choose to implement a second-order washout instead of a first-order washout on attitude commands. This one was selected as the structure of minimum complexity required for simulating hover motions.

B.2.5 Model Analysis of the Simulation

Pilot-in-the loop analysis is performed. This analysis is similar to that performed in the first step, except that the pilot is now assumed to be operating the simulator with the control laws designed as described above.

If predicted performance scores and pilot response parameters are essentially identical to those predicted in step one, the control laws may be assumed to provide the pilot with essentially that same cues that he would obtain and use in actual flight. If predicted performance differs substantially from that predicted earlier, one or more of the following problems may exist: (a) the fixed-form structure of Figure B.1 is inadequate, (b) cost coefficients or other model parameters have been inadequately chosen, or (c) the physical constraints of the moving-base simulator prohibit a faithful presentation of motion cues to the pilot.

Potential inadequacies of the fixed-form control-law structure may be explored by re-analyzing the task with a higher-order implementation of the control-laws obtained in Step 3 (or with a control law obtained from an alternative procedure). In addition, new control-law designs may be obtained with alternative choices for model parameters. Typically, one would vary the weighting coefficients of the performance index to obtain a different trade off between perceptual fidelity and simulator travel. If these procedures do not lead to an overall improvement in predicted performance, one may reasonably conclude that performance degradation imposed by the simulator constraints cannot be entirely overcome.

## B.3  Design of Pitch-Surge Control Law

The design procedure described above was employed to design a control law for the pitch-surge axis for the helicopter hovering task. Two sets of control laws were obtained: one based on perceptual indifference thresholds obtained by dividing perceptual thresholds by predicted attentional levels, the other based on unmodified perceptual thresholds.

Application of the design procedure deviated from that described above in the following respects:

1. The influence of vestibular sensory dynamics was neglected. That is, perceptual errors were assumed to be essentially the same as simulator errors.
2. A ninth term was added to the performance index of (B.1) to include a specific penalty on attitude-acceleration perceptual errors.

The results of analysis performed previously for the assumption of perfect motion cues (described in the main text) were used to obtain low-order spectral representations of simulated pitch attitude and specific force along the x axis. "Limits" on simulator motion obtained from the simulator specifications yielded performance weighting coefficients as defined by (B.2). Table B.1 shows thresholds (limits) assumed for perceptual variables. "Attentions" used in computing indifference thresholds were obtained from the preceding analysis and are also shown in the Table.

Table B.1
Perceptual Thresholds

| Variable | Attention | Effective Threshold | |
| --- | --- | --- | --- |
| | | Perceptual | Indifference |
| $\theta$ (deg/sec) | 0.41 | 3.6 | 8.8 |
| $\dot{\theta}$ (deg/sec$^2$) | 0.37 | 0.67 | 1.8 |
| f (g) | 0.02 | 0.053 | 2.7 |

The "display vector" used in obtaining the model solution consisted of simulated (i.e., theoretical) pitch rate, pitch acceleration, and specific force, plus the six simulator variables included in the performance index of (B.1). (Perceptual error variables, while needed for computing the performance index, were not included in the display vector because they would have represented redundant variables.) Time delay was set to zero, motor time constant and motor noise/signal ratios were made negligibly small, and observation noise/signal ratios were set to −30 dB for all quantities in the display vector.

Values for the parameters of the linear transfer elements as defined in (B.4) are given in Table B.2. Analysis with the larger perceptual thresholds (i.e., perceptual thresholds weighted inversely by attention) yielded x-axis simulator commands that were small enough to be neglected. Accordingly, no values are given for x-axis drive parameters for the control law based on indifference thresholds.

## Table B.2

## X-Axis Simulator Drive Parameters

| Parameter | Effective Threshold | |
| --- | --- | --- |
| | Perceptual | Indifference |
| $K_1$ | 1.0 | 1.0 |
| $a_1$ | 0.3 | 0.3 |
| $b_1$ | 0.1 | --- |
| $K_2$ | 1.0 | 0.75 |
| $a_2$ | 1.0 | 0.62 |
| $b_2$ | 0.7 | --- |

| 1. Report No. NASA CR-3312 | 2. Government Accession No. | 3. Recipient's Catalog No. |
|---|---|---|
| 4. Title and Subtitle Pilot/Vehicle Model Analysis of Visual and Motion Cue Requirements in Flight Simulation | | 5. Report Date **OCTOBER 1980** |
| | | 6. Performing Organization Code |
| 7. Author(s) Sheldon Baron, Roy Lancraft, and Greg Zacharias | | 8. Performing Organization Report No. 4300 |
| 9. Performing Organization Name and Address Bolt, Beranek and Newman, Inc. 50 Moulton Street Cambridge, Massachusetts 02138 | | 10. Work Unit No. 505-09-41 |
| | | 11. Contract or Grant No. NAS2-10145 |
| 12. Sponsoring Agency Name and Address National Aeronautics and Space Administration Washington, D. C. 20546 | | 13. Type of Report and Period Covered Contractor Report |
| | | 14. Sponsoring Agency Code |

16. Abstract

The optimal control model (OCM) of the human operator is used to predict the effect of simulator characteristics on pilot performance and workload. The piloting task studied is helicopter hover. Among the simulator characteristics considered were (computer generated) visual display resolution, field of view and time delay.

| 17. Key Words (Suggested by Author(s)) Flight Simulation, Pilot Modelling | 18. Distribution Statement Unclassified - Unlimited Star Category - 05 |
|---|---|
| 19. Security Classif. (of this report) Unclassified | 20. Security Classif. (of this page) Unclassified | 21. No. of Pages 162 | 22. Price* A08 |